Università
Ca'Foscari
Venezia

JOINT INTERNATIONAL MASTER's DEGREE

in

SUSTAINABLE

DEVELOPMENT

IMPLEMENTING E.O. SYSTEMS TO ASSESS THE RISK OF FAECAL BACTERIA CONTAMINATION IN THE NORTHERN ADRIATIC SHELLFISH-FARMS

Supervisor:
Prof. Dr. Pastres Roberto

Co-Supervisor:
Prof. Dr.

Graduand:
Mattia Andreoletti
Matriculation No – 867747 (Ca' Foscari University)
Matriculation No – 11738783 (K.F. University Graz)
Matriculation No – 6313469 (Utrecht University)

Academic Year:
2018 – 2019

ACKNOWLEDGMENTS

I hereby would like to thank for the great support received from my professor R. Pastres, whose expertise was invaluable in the formulating of the research topic and helped me developing the concepts and methods applied along the whole thesis manuscript. Furthermore, provided me with the chance to experience an internship in his office, at the Department of Environmental Sciences, Informatics and Statistics at Ca' Foscari, developing skills for environmental and remote sensing data analysis.

I would like to acknowledge my colleague Dr. E. M. D. Porporato who supported me through my internship at the Department. Thank you, you have been a key help developing skills in programming with R statistic software and were always available for any necessity or reasoning.

I would also like to thank the whole team of R. Pastres' office, with which I had the chance and opportunity of exchanging ideas and talks. for me personally important through the time I spent in the department.

Finally, I would like to thank Dr. S. M. De Jong from Utrecht University for the inspiring Remote Sensing course, from which I grasped knowledge and ideas developed through this thesis. Furthermore, I would like to thank my co-relator from Utrecht University which spent time and energy judging and evaluating this manuscript.

TABLE OF CONTENTS

ABSTRACT

The present thesis originates from the opportunity of providing an instrument for comprehending and efficiently applying the European regulations in the field of food-safety for shellfish-farming (***Regulation (EU) 2015/2285***). The importance of the above is further explained by continuous expansion of the aquaculture sector. especially in coastal and marine environments, Europe only produced 1.3 million tons of aquatic organisms in 2016, of which 46.6% of the total volume was due to mollusks farming (***Eurostat 2018***). In the light of these consideration. an analysis was conducted over the probability of faecal-bacteria contamination for different shellfish-farms in the northern Adriatic Sea, as a result of extreme events such as heavy rainfall and river runoffs. Intense precipitations are known to be associated to faecal-bacteria proliferation (***Cho et al., 2010***) and when the digestion capacity of wastewater treatment plants is exceeded, river flows transporting bacteria are discharged directly into the sea. Earth Observation, demonstrated to reliably map water quality indicators, has been applied to distinguish and characterize different water masses depending on their origins. Remote sensing technologies were implemented to retrieve environmental variables for water turbidity and surface temperature over the period running from March 2013 to September 2019. Different water masses were characterized to detect river plume diffusion along the current preferential direction and its influence on shellfish-farms in the area of interest. In order to achieve high spatial resolution, Landsat-8 NASA satellite products were used. Time series of the variables were analyzed to determine the relation between water quality in shellfish-farms and river mouths. The stronger the relation, the higher the probability to have fresh river water in the shellfish farms, therefore presence of bacteria is signaled. The comparison between the dates spotted through Earth Observation and to the contamination data of regional authority zonal controls, is used to evaluate the consistency of the method in identifying the contaminations or bacteria presence over all the shellfish farms. Finally, conclusions are drawn upon the capability of developing a trustworthy early-warning system.

1. INTRODUCTION

In the light of the changes in the world climate, causing the exacerbation of extreme weather conditions, and the rapidly growing human population, expected to reach 9.8 billion by 2050 and 11.2 by 2020 (***United Nations, 2019***), food-security and food-safety topics are of major interests and concerns. Especially in the context of the fast-expanding sector of aquaculture, with an annual consumption growth rate that doubles the human population one (***J. G. da Silva, Fao Director General***). Europe only produced 1.3 million tonnes of aquatic organisms in 2016 (***Eurostat, 2018***), of which around three quarters were produced by five members state, nominally: Spain, United Kingdom, France, Italy and Greece. In 2016 the total Italian output of aquaculture sector amounted to around 157 thousand tonnes of which more than a third was accounted for by blue mussel (63 700 tonnes – ***Eurofish, 2019***). For instance, it is understandable how this practice represents a valuable social and economic resource for the country.

Earth Observation is widely applied in aquatic ecosystems. ***Grant et al. 2009***, presented a series of case studies in which remote sensing technologies were key element for the identification of optimal zones for aquaculture, considering nutrients availability and environmental stress factors, for instance potential harmful algal blooms. E.g. ***Radiarta et Al. 2008*** used data of chlorophyll, turbidity and temperature to evaluate the seasonal trends in the spring bloom and related them to scallop production in Funka Bay, Japan. ***Thomas et Al. 2006***, tried to predict the carrying capacity for existing site of mussel cultures, as well as new potential sites, using satellite data to derive chlorophyll, which well relates to mussel growth, in the bay of Mont St. Michel, Along the Northern Adriatic Sea. chlorophyll-a and sea surface temperature satellite data were used in a Spatial Multi Criteria Evaluation method assessing the site suitability for mussel farming (***Brigolin et Al., 2017***). These examples are important for they show how remote sensing deliver a better comprehension of the dynamics that occur in the coastal ecosystems and how this can be used to provide a more efficient management of aquaculture practices worldwide.

Regarding fisheries and aquaculture products a major concern is that of pollutant and bacteria contamination. This is usually referred to the presences of toxic substances or dangerous microorganisms for human health when ingested. The food products may build up these contaminants, if contained in the water environment where production takes place. The recent EU Directive (***EU Regulation 2015/2285***) extends the previous European regulations (***EU Regulations No 854/2004 and No 2073/2005***), layes down, to quote the regulation. "specific rules for the organisation of official controls on products of animal origin intended for human consumption as regards certain requirements for live bivalve molluscs, echinoderms, tunicates and marine gastropods". The aim of the legislation is that of ensuring that areas allocated for mollusks aquaculture are characterized by environmental condition feasible for marketing the food products. The waters allocated for shellfish farming products intended for direct human consumption, needs to respect specific thresholds for the live bivalve mollusks, echinoderms, tunicates and marine gastropods in terms of bacteria that might be harmful for human heath, such as Enterococci and *Escherichia coli*, known as Faecal Bacteria (here on FB). According to the regulation, areas where mussel farming is authorized are classified as A, B or C depending on their water quality. The end use of the shellfish products are defined depending on the zone in which they are grown: A class products may be collected for direct human ingestion, while B products either needs to undergo purification processes or cannot be eaten raw. Areas classified as C requires, as post harvesting treatment, the relaying or cooking by an approved method and cannot be directly consumed (***Cefas, 2014***). This logically results in large differences in the market value of shellfish products. Therefore, it represents a matter of great interest for the shellfish farmer to lay his activity in an area highly

productive with low risk of faecal contamination. The classification of each zone is carried out through a sampling period in which is determined the presence and occurrence of faecal pollutants, such as Enterococci and *E. coli*, in the designed zone. This procedure uses *E. coli* as indicator organism, providing an assessment of the risk of contamination with bacteria and vital pathogens. A description of point and non-point sources is provided for each zone, according to the seasonal variations of both human and animal population. With this whole procedure is also defined the point within the zone that shows to be the most prone to contamination. The controls are said to be carried out by competent authority and therefore a matter of regional interest in the specific case of the Italian country. The specific values not to be exceeded are listed in the table below (see Table 1 – ***EU Regulation 2015/2285***).

Species	**Bacteria Indicator**	**Class A Threshold**	**Class B Threshold**	**Class C Threshold**	**End Use**
Live bivalve molluscs and live echinoderms, tunicates and marine gastropods	*E.coli*	230 MPN/100g of flesh and intravalvular liquid	700 MPN/100g of flesh and intravalvular liquid	46000 MPN/100g of flesh and intravalvular liquid	Products placed on the market during their shelf-life

Table 1: Amount of Faecal Bateria allowed in live bivalve mollusks and live echinoderms, tunicates and marine gastropods.

Zones undergo periodical controls. that are carried out on a monthly basis. as requested by the new EU Directive. When a sample is exceeding 230 Most Probable Number (MPN)/ 100 g of flesh and intravalvular liquid, the farms laying within the corresponding zone are not supposed to harvest the mussels and, quoting the regulation: “at least two consecutive results below the regulatory limit separated at least 48 hours are necessary to re-open it”. If during the sampling period for the definition of the zone allocation. which is performed every three years, the ones that showed samples that were exceeding the *E.coli* limits, are not able to prove that those were outliers, the zone may be reclassified as B. A declassification of a farm leads to increase depuration costs, thus strongly reducing profit margins. *E. coli* is of terrestrial origin: its concentration in coastal water is affected by (***Cho et al., 2010***) river discharges and rainfall events: extreme rainfall may cause malfunctioning in wastewater treatment plants, thus resulting in larger plumes of fresh water coming from inland in the coastal area, transporting bacteria off shore. As a consequence, mussel farms located in areas which are not reached by river plumes under normal meteorological conditions may become contaminated during such events. If the competent authority happens to perform controls over one of these mussel-farms few days within these events, it is probable that standards would not be met. This resulting in the closure of the farm until it meets the standards in the following mandatory controls. Moreover, if the controls are not delivering the results quickly, the farmer could place the product on the market with consequences on the consumers and the public image of the farmer may be compromised.

The delivery of an early warning systems to inform both the competent authority and the farmers of the zone exposed to contamination risk and its magnitude would therefore be extremely relevant for increasing food security. On the other hand, assessing the probability that a given area could be reached by a river plume may also be relevant for site selection and spatial planning.

The availability of different Earth Observation tools to investigate the environmental condition in the context of aquaculture opens up the chance of verifying whether would be possible to relate precipitation, river flows and faecal bacteria contamination. Accordingly, it would be helpful to deliver a tool for an improved supervision by the competent authority and management of the situation which present a concrete risk of contamination by the farmers, in such a way that could

guarantee a valuable and safe product while holding the image of the Italian products in the peninsula and abroad. Method that could be, ideally, extended to different water farming techniques in different coastal areas around the globe, adapting the algorithms implemented in the present study to the different areas of interest.

The present work aims at investigating the potential use of remotely sensed Earth Observation for assessing the risk of faecal bacteria contamination for shellfish farms located in coastal and tidal areas. Environmental variables captured from hyperspectral images are used to distinguish fresh and salty water masses (***Hopkins J. et Al., 2013***). Dates of possible contamination identified though the methodology are confronted with controls dates provided by the Veneto Region. This are carried out by the Istituto Zooprofilattico delle Venezie (ISZVe), which has the laboratories and equipment to perform the analyses. Showing that more than 80% of the dates are matching presence of faecal bacteria.

The main objectives of this paper are:

- To assess the suitability of remote sensing technology to evaluate the risk of feacal contamination in intertidal coastal areas allocated for aquaculture;
- To evaluate the chance of developing an early warning system based on the river flows of the major rivers in the area.

2. MATERIALS & METHODS

In light of the objectives of the present thesis, the methodology used to determine an early-warning system for faecal-bacteria contamination in coastal areas is the following:

1) Definition of the environmental variables feasible to distinguish between different water masses. Hereafter in Table 2 a list of possible variables used to distinguish water masses is presented, with the relative reference. Notably in the case of Sentinel 2, no references for the retrieval of Surface Temperature and Salinity variables were found;

Variable	Resolution [m]	Satellites	References
Sea Surface Temperature [°C]	100	Landsat 8	*Jaleani et al. 2017*
Total Suspended Matter [g/m^3]	30 10	Landsat 8 Sentinel 2	*Shi et al. 2018* *Huizeng et al. 2017*
Coloured Dissolved Organic Matter [g/m^3]	30 10	Landsat 8 Sentinel 2	*Chen et al. 2017* *Zhao et al. 2017*
Chlorophyll-a [mg/m^3]	30 10	Landsat 8 Sentinel 2	*Bresciani et al. 2018* *Ansper et al. 2018*
Salinity [psu]	30	Landsat 8	*Zhao et al. 2017*

Table 2: List of variables that have been used to distinguish between different water masses.

2) Choice of the preferred variables between the alternatives, depending on the capability of defining water quality and on the application site. Here the variables of sea surface temperature (SST) and total suspended matter (TSM), retrieved through Landsat 8 imagery have been chosen. Figure 1 shows TSM concentration in the study area on an event of large river discharge into the coastal area;

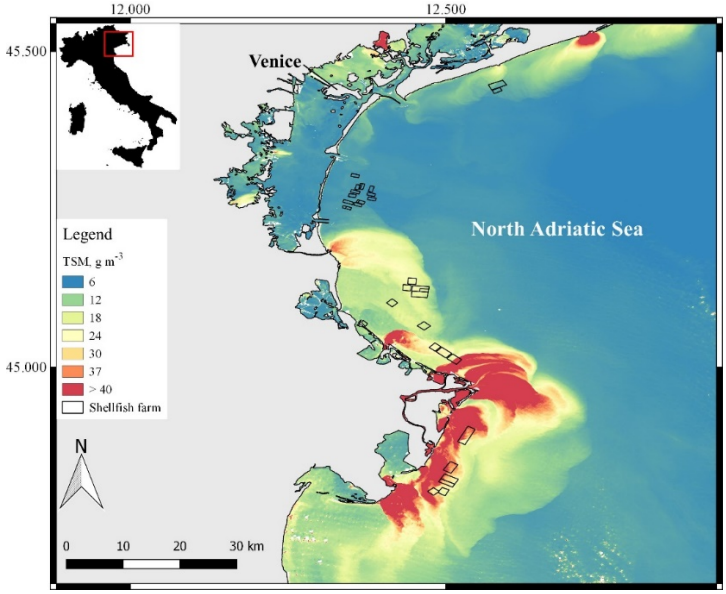

Figure 1: Application of the Total Suspended Matter algorithm in the study area, image collected on 19th November 2014. Meteorological condition of strong precipitation and large river flows discharged into the salty coastal water.

3) Evaluation of the river flow threshold for which a majority of the freshwater is found in the shellfish farms. This is site specific and depends on the river and the farm in analysis. Furthermore, it depends on the minimum flow for which bacteria presence is found (if data available). This process is an iterative process in which different river flows are calculated, since the river flow threshold will be crucial in developing the early warning system;

4) The presence of fresh riverine water inside a shellfish farm is proven through a multiple linear regression model. The model weights the influence of the river mouth against water from the open sea, where anomaly situations are found. If the relation is high and statistically significant, the fresh water from the river mouth has reached the farm. The regression is performed, not only on the events in which river flows are exceeded, also on the other dates. This is to shows that when the situation is normal, dependency on the fresh water unleashed from the river mouth is not found;

5) In order to corroborate the relation, explained in point 4, distances between shellfish farm and open sea, and between river mouth and the open sea, in terms of TSM and SST, are calculated. When large distances are found anomalous situations are defined. If the distances found on the same date (satellite scene) the quality of the water inside of the shellfish farm is comparable to that of the river mouth. The distances are plotted to have a graphical more effective interpretation of these events.

6) Finally, the effectiveness of the methodology in identifying infected water masses is assessed. Early-warning system based on the capability of the method to identify events of bacteria diffusion and presence is developed. The river flow threshold is used as first element to define the meteorological condition linked to bacteria presence in the coastal water. Precipitation analysis and corrivation model can be further applied.

Figure 2 show a schematic representation of the methodology followed.

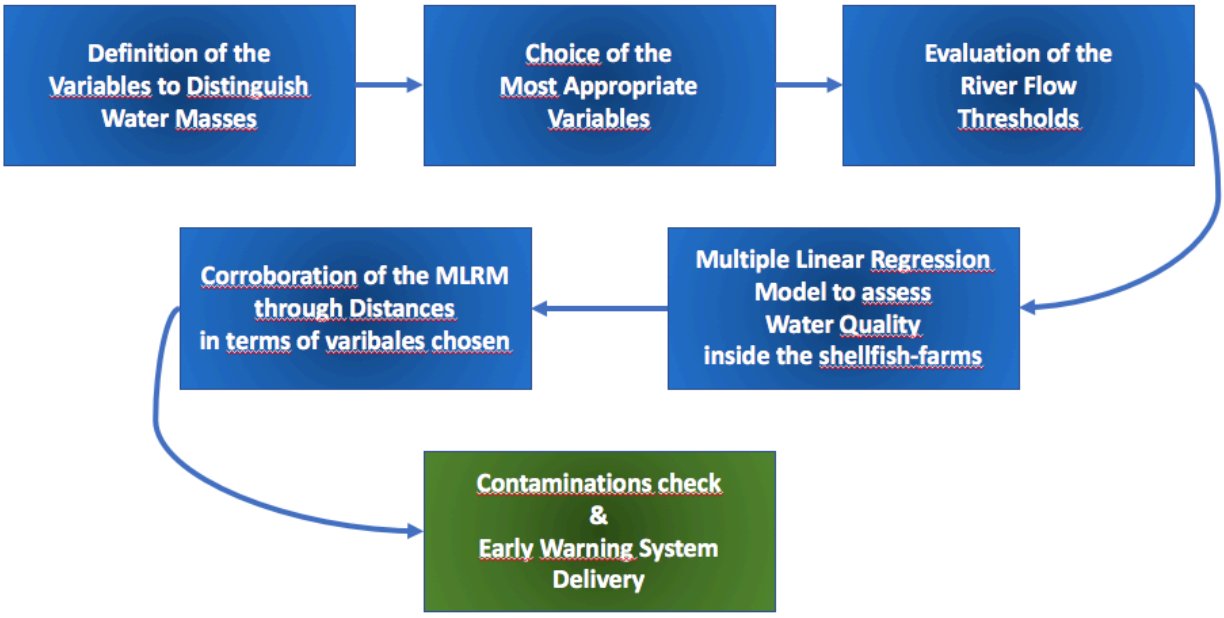

Figure 2: Schematic overview of the methodology.

Following the above scheme the methodology develop as follow.

Environmental variables that can be detected directly from satellite images, through which it is possible to distinguish water masses of different composition and nature, e.g. sweet riverine or salty waters. are water turbidity, temperature, chlorophyll or salinity concentrations. These have been proven to be good indicators for characterizing water and its quality (***Nezlin et al.. 2008. Zhaojun et al.. 2010. Hopkins et al.. 2013. Brando et al.. 2015. Wang et al.. 2017***). Between the different variables Total Suspended Matter (TSM) and Sea Sruface Temperature are chosen as best indicator for the study area.

This is followed by the definition of the Earth Observation system, e.g. Satellite, that present the sensor's characteristics needed for retrieving such variables and the environment which will be used to analyze such images. The time series of the two variables extracted from Landsat 8 imagery, which is the satellite providing the spatial and temporal definition needed for the evaluation of contamination within shellfish farms, which length are usually around tens to hundreds of meters, are extracted and analyzed to explore which are the trends and mean values around the area.

The environmental and weather variables of rain or river flows are collected in order to determine which are the extreme rain events and whether they relate to river flows. Different rivers flow percentiles are calculated to define the thresholds of exceedances that will correlate to the bacteria presence. Dates of exceedance are used to match satellite images. The river flow threshold may be lowered also in the light of a minimum number of dates to perform statistical analysis. In particular the river flows exceeding a certain percentile will be used to filter the satellite images on the same date or up to 3 days later, because of transport lag times. This result in a list of dates in which the river flow percentile is exceeded and a high risk of contamination is found, and a list in which this is not exceeded, and the risk presented is lower.

The presence of riverine water within a shellfish farm, given the availability of Landsat-8 products. is esteemed through a multiple linear regression model. The model correlates TSM and SST values within a shellfish farm with the TSM and SST of the closest river mouth, following the current patterns, and a point in the open sea, which is far enough from coast never to show contaminations. The esteemed coefficients and the goodness of fit of the model are statistically tested through a student t-test. Therefore, the probability of contamination of the different areas in which the farms are distributed is linked to their river dependencies.

In order to compare water quality at a shellfish farm with those of the open sea and riverine ones, the values of the two environmental variables, TSM and SST, of the open sea are used as reference values to calculate the distances of both the shellfish farms and the relative river mouths. These distances, between river farm and open sea, and river mouth and open sea, are then normalized and plotted against each other to see when anomalies appear and how is the correlation between them. Same anomalies will align on a line starting from the origin, very similar to sea water, and outdistancing the center, getting further as the magnitude of the anomaly is increasing.

The output list of events (dates), mentioned above, is compared to monthly controls on the date presented and matches are used to calculate the percentage of success in identifying the location of contamination. This is used to assess the suitability of an early warning method based on the percentile identified of the different river flows.

Hereafter will be presented where and how data have been collected, their availability and the method with which they are analyzed through this paper.

REMOTELY SENSED DATA

Earth Observation systems are developing at a fast rate and the information that can be retrieved through Remote Sensing technologies is very broad and different. The environmental variables considered to detect riverine flows into brackish waters in the area of study, in order to highlight plumes diffusion, are Total Suspended Matter and Sea Surface Temperature. This choice is driven by a series of considerations about the characteristics of different water types. Between riverine water and sea water the first difference usually thought of is the salt content. Hence, salinity could be a good variable to distinguish the two water masses. Since river are usually running thought different kind of land-types with turbulent flow which mixes to the water different kinds of small organic and non-organic particles, the turbidity of the water should be higher compared to that of the salted water in the open sea and could greatly be used to differentiate the waters. Also, from an optical perspective the particles, both organic and inorganic, content in the water alter it composition, which results in a stronger characterization of the reflectance properties observed through satellites imagery. As a matter of fact, Total Suspended Matter have been used in different studies assessing water quality in coastal marine and lacustrine environments the variable uses the reflectance on the red spectrum (0.600 – 0.690 μm) to identify particles within the water (***Son,. K., et Al. 2011***. ***Shi, W., et Al., 2018***). Depending on the season of the period analyzed, changes in average temperature are expected to fluctuate from lower during winter months and higher for the summer ones, but sea water temperature should be less prone to variations, while riverine water, particularly in winter are colder that open sea ones, in such a coastal area characterized by a low bathymetry profile. At least considering the surface temperature. Therefore, Sea Surface Temperature could be a second discriminant for distinguishing the two masses (***Hopkins et Al., 2013. Jaelani et Al., 2017***). The temperatures are observed through specific thermal bands, that needs particular sensor to be captured (10.00 – 12.50 μm). The variables listed above are to be weighed against the availability of the bands. that are needed to retrieve directly such information, collected by the sensor mounted upon the satellite chosen. Therefore, the following consideration to be made is which kind of satellite can provide the sufficient resolution in time and space to detect small changes given the overall area and the kind of analysis that needs to be carried out, this evaluation comes from the interval of light reflectance that is for retrieving the two variables. as previously mentioned, the red band and the thermal band. Here two alternative satellite can provide a high resolution in space, ranging between 15 and 100m depending on the wavelength detected, and an acceptable resolution in time, passing exactly over the same place every 15days: Sentinel-2A and Landsat-8. Landsat-8 products are the one chosen because of a major number of literature findings, applying its imagery for surveys. By reason of the choice of Lansat-8, which carries two different sensor: the OLI sensor, Operational Land Imager, with spatial resolution ranging from 15m (panchromatic) to 30m (rest of the visible spectra, near and short infrared) and the TIRS sensor, Thermal Infrared, with a spatial resolution of 100m, the Total Suspended Matter (TSM), indicator of turbidity and the Sea Surface Temperature (SST) are retrieved (Table 3 presents the resolutions by band).

Landsat-8 OLI and *TIRS* Bands (μm)		
30 m Coastal/Aerosol	0.435 - 0.451	Band 1
30 m Blue	0.452 - 0.512	Band 2
30 m Green	0.533 - 0.590	Band 3
30 m Red	0.636 - 0.673	Band 4
30 m NIR	0.851 - 0.879	Band 5
30 m SWIR-1	1.566 - 1.651	Band 6
100 m TIR-1	*10.60 – 11.19*	Band 10
100 m TIR-2	*11.50 – 12.51*	Band 11
30 m SWIR-2	2.107 - 2.294	Band 7
15 m Pan	0.503 - 0.676	Band 8
30 m Cirrus	1.363 - 1.384	Band 9

Table 3: Landsat-8 bands spectral resolutions.

The environment used to get the Landsat-8 images and analyze them is the Google Earth Engine Code software, an open source software. that offers a wide range of image collections gathered and uploaded from different satellites and ready to be used. The software uses a JAVA-script programming language to perform different kind of operation over the images, the ones used in the following study are about filtering the images, on a cloud presence, area of interest and date basis, masking the land or inter-tidal areas on the base of indexes and creating functions to re-elaborate the bands in order to retrieve the variables needed. The script used are listed at the bottom of this study, but the equations are shown below in this chapter.
The images collections that can be used. present different product levels, depending on the corrections that the scene undergo. In the retrieval of the variables the collections used contained products with either Top of Atmosphere calibrations or Surface Reflectance calibration. Both the collections follow the calibration procedure, and equations, explained in ***Chander, 2009***. The first step in calibrating an image is the conversion of the raw digital number (DN) to at-sensor spectral radiance. This is performed using the following equation:

$$L_\lambda = G_{res} \times Q_{cal} + B_{res}$$

Where:

$$G_{res} = \frac{LMAX_\lambda - LMIN_\lambda}{Q_{calmax} - Q_{calmin}}$$

$$B_{res} = LMIN_\lambda - \left(\frac{LMAX_\lambda - LMIN_\lambda}{Q_{calmax} - Q_{calmin}}\right) Q_{calmin}$$

The terms are:

L_λ = Spectral radiance at the sensor's aperture [W/(m^2 sr μm)]
Q_{cal} = Quantized calibrated pixel value [DN]

Q_{calmin} = Minimum quantized calibrated pixel value corresponding to $LMIN_\lambda$ [DN]
Q_{calmax} = Maximum quantized calibrated pixel value corresponding to $LMAX_\lambda$ [DN]
$LMIN_\lambda$ = Spectral at-sensor radiance that is scaled to Q_{calmin} [W/(m^2 sr μm)]
$LMAX_\lambda$ = Spectral at-sensor radiance that is scaled to Q_{calmax} [W/(m^2 sr μm)]
G_{res} = Band-specific rescaling gain factor [(W/(m^2 sr μm))/DN]
B_{res} = Band-specific rescaling bias factor [W/(m^2 sr μm)]

For the retrieval of the Total Suspended Matter is used the library of Landsat-8 TIER 1 Top of Atmosphere (TOA), while the Sea Surface Temperature uses the Landsat-8 TIER 1 Surface Reflectance (SR). The respective corrections that are done for the two collections are as follow (***Chander, 2009***).

To the first collection is applied the conversion to TOA reflectance, which corrects for the differences in solar zenith angle, compensate for the exoatmospheric solar irradiance and corrects for variations in Earth-Sun distance:

$$\rho_\lambda = \frac{\pi \cdot L_\lambda \cdot d^2}{ESUN_\lambda \cdot cos\theta_s}$$

Where:

ρ_λ = Planetary TOA reflectance [unitless]
π = Mathematical constant [unitless]
L_λ = Spectral radiance at the sensor's aperture [W/(m^2 sr μm)]
d = Earth-Sun distance [astronomical units]
$ESUN_\lambda$ = Mean exoatmospheric solar irradiance [W/(m^2 μm)]
θ_s = Solar zenith angle [degrees]

While the second collection undergo the conversion to at-sensor brightness temperature, which convert the thermal band data (B10, B11) from at-sensor radiance to at-sensor brightness temperature, assuming the Earth's surface as a black body.

$$T = \frac{K2}{\ln\left(\frac{K1}{L_\lambda} + 1\right)}$$

Where:

T = Effective at-sensor brightness temperature [K]
K2 = Calibration constant 2 [K]
K1 = Calibration constant 1 [W/(m^2 sr μm)]

TOTAL SUSPENDED MATTER RETRIEVAL

For the retrieval of the Total Suspended Matter, or Yellow Stuff, a forward Gordon's model is applied (***Gordon, 1998. van Rijn, 2010***). that uses the red reflectance performing a regression against increasing TSM concentrations. The model usually is applied to the SPOT satellite band 2 (the red band) and calibrated for the Schedt estuary, intercoastal area, but is proven to perform well if applied to the Landsat red band (***van Rij,. 2010***). The equation to compute the total suspended matter concentration form the landsat-8 band 4 (the red band) is:

$$TSM = 2.7 \cdot e^{(19.0 * \lambda_{red})}$$

Where:

TSM = Total suspended matter [g m^{-3}]
e = Mathematical constant
λ_{red} = Spectral radiance of the band 4 [unitless]

SEA SURFACE TEMPERATURE RETRIEVAL

The Sea Surface Temperature retrieval is easier given the correction already contained in the collection from Landsat-8 TIER 1 SR, where the band 10 and 11 correspond to the effective temperature on the surface, expressed in Kelvin and rescaled by a factor of 10 for computing and memory issues. Therefore, the equation used is:

$$T = (0.1 \cdot \lambda_{TI}) - 273.15$$

Where:

T = Temperature [Celsius]
λ_{TI} = Effective at sensor brightness of the thermal infrared bands (band 10 and 11)

From the algorithms used to retrieve the environmental variables of TSM and SST, applied, as previously stated, in the GEE Code environment, a total of respectively 246 and 229 images have been collected to be analyzed through the R statistical software, where an ad-hoc script was developed to delete outliers and compare the data between each other and the river flows exceeding the 75th percentile. The images left after the cleaning of the data are on average 68 observations, depending on the location of the point taken into consideration and the river mouth closest.

MULTIPLE LINEAR REGRESSION MODEL

A multiple linear regression model (MLRM) is applied in order to evaluate the correlation between the shellfish farms data of, respectively, the Sea Surface Temperature and the Total Suspended Matter values, to the river mouth that appears to majorly influence the particular farm, and the open ocean. The idea underlying the application of a multiple linear regression model is that of being able to weight different source of water quality to determine their contribution to the water in a precise point (***Lesar et al., 2017***), here the shellfish farm. More precisely different percentiles

were calculated for the river flows, starting from the 99th percentile. in order to obtain the dates in which events exceeding or not that threshold happened. The events are then used to filter the images, therefore SST and TSM data, that are corresponding to either the outpaced percentile dates or the enclosed dates. A minimum of satellite images is needed to be found in order to perform the multiple linear regression model, when this is not found the percentile is lowered. The model is used to define events in which the water found in a shellfish farm is mainly coming from the river mouth correlated, indicating that presence of bacteria is highly probable. The model is structured as follow:

$$y = \alpha_1 x_1 + \alpha_2 x_2 + \beta$$

Where:

y = The response variable. either SST or TSM values at the shellfish farm location
x_1 = The first explanatory variable, either SST or TSM values at the river mouth coordinates
α_1 = The parameter to be estimated, associated to the first variable
x_2 = The second explanatory variable, either SST or TSM values in the open sea
α_2 = The parameter to be estimated, associated to the second variable
β = The intercept coefficient to be estimated, representing the model deviation

As stated in the introduction, the idea underlying the application of the model is that when river flow exceeds a certain percentile, water digestion plant may fail, and riverine water is freed into the brackish water leading to possible shellfish contamination. Therefore, if the polluted riverine water reaches the farm, the values of α_1 should be higher compared to that of α_2, highlighting a stronger correlation with the values of either SST or TSM of the river mouth taken into account. On the other hand, during normal fiver flows situation, the water inside the shellfish farm should be similar to that of the open ocean, with some case to case variation given the position relatively close to the coast. Therefore, the values of α_1 here should be lower to that of α_2, proving the stronger correlation with the open sea water.

This procedure is accompanied by the calculation of the distances between river mouth and open sea, and the distances between shellfish-farm and open sea, in the two variables space (SST and TSM). In bidimensional plot distances, after normalization process, of the farm and the river mouth from the sea are set as axis. When large distance occurs, an anomaly situation if identified. Furthermore, if the points corresponding to this situation both for river mouth and shellfish farm are showing similar distances form the sea, they are expected to align on the diagonal. It can be stated that the water within the shellfish farm is that coming from the river mouth. This is used as corroboration of the linear regression model and proof that riverine water reached the farm.

The distances are calculated as follow:

$$y = \sqrt{(TSM_1 - TSM_2)^2 + (SST_1 - SST_2)^2}$$

Where:

y = The distance in the TSM, SST space of either the shellfish-farm or the river mouth from the open ocean
TSM_1 = Total Suspended Matter of either the shellfish-farm or the river mouth
TSM_2 = Total Suspended Matter of the open sea

SST_1 = Sea Surface Temperature of either the shellfish-farm of the river mouth
SST_2 = Sea Surface Temperature of the open sea

The distances of the shellfish-farm and the river mouth are normalized and plotted against each other in a scatter plot where the events occurred in the same dates when the river flow percentile threshold is crossed are shown as red dots, while the others as blue. The normalization is performed as normal statistical standardization of a variable:

$$z = \frac{x - \mu_x}{\sigma_x}$$

Where:
z = the normalized variable
x = the original variable, distance value in this case
μ_x = the mean, or average, of the variable x
σ_x = the standard deviation of the variable x

3. APPLICATION OF THE METHODOLOGY TO THE VENETO REGION

The study area in which this methodology will be applied, and develop its focus is that of the Northern Adriatic Sea including part of the Veneto region, ranging from 44° 45' to 46° 05' latitude Nord and from 11° 50' to 13° 10' longitude East, which are the actual coordinates that will be used to collect precipitation and river flows data, and to extrapolate satellite images. This area lies in the northern section of the Adriatic Sea (see Fig. 1), located in the North-Central Mediterranean Sea, to which is connected through the Strait of Otranto where it exchanges its entire volume every 3-4 years. One important characteristic of the Adriatic Sea is that it takes up to one-third of the freshwater flow received by the entire Mediterranean Sea (***Danovaro et Al.. 2019***). In the area considered, the major inflows are given, from North-East to South-West, by the discharges of the Tagliamento, the Piave, the Brenta, the Adige and the Po rivers, carriers of terrigenous inputs, which are sources of nutrients for the growth of the shellfish located in the area but on the other hand they may contain important pollutants, particularly after urban stormwater runoff for flows exceeding the digesting capacity of the wastewater treatment plants (***Mallin. 2009***). The average flows of the rivers are respectively: $70m^3/s$, $125m^3/s$, $93m^3/s$, $235m^3/s$, $1540m^3/s$.

The circulation characterizing the whole Adriatic Sea is cyclonic superficial (see Fig. 3): from the Strait of Otranto water flows northwards along the eastern coast, forming the Eastern Adriatic Current (EAC) along the Croatian coast, turning southwards through the Italian west coast, Western Adriatic Current (WAC). In the northers Adriatic Sea, the circulation can be divided in two schemes: the winter one in which horizontal discontinuity layers divide the superficial waters from the deeper ones, the water column is highly stable between the overlapped layers and transport phenomena are usually weak. Even though, strong stratification phenomena may occur. On the other hand, during the summer circulation scheme, vertical discontinuity surfaces divide the superficial diluted water from the salty denser ones, the water column is unstable and shows strong horizontal transport phenomena (Fig. 4 shows the current trends respectively during summer and winter. ***Autorità di bacino del fiume Po, 2010).***

In the northern part of the Adriatic Sea, permanent tidal and wind currents moving at great speeds are found. Permanent currents represent a whirl with a counterclock direction, which is supposed to be a continuation of the general water circulation in the Ionian Sea (***Zohn et al., 2017***). Furthermore, the strong tidal activity, due to astronomical forcing (***ISPRA***) and strengthened by the wind activity, the Bora cold and dry downslope wind blowing northeasterly, and the Scirocco, warm and humid wind from the southeastern, makes the circulation complex and exposed to phenomena of alteration in the circulation and current velocities that may alter diffusion patterns through time (***Mihanović et Al., 2011***).

The Northern Adriatic Sea presents a shallower and broad shelf compared to the other parts of the Sea, with a depth ranging around 50m, and the accumulation of nutrients makes the area the most productive of the whole sea. with a high primary production. up to 350 $gC\ m^{-2}y^{-1}$ (***devotes-project.eu, 2012-2016***).

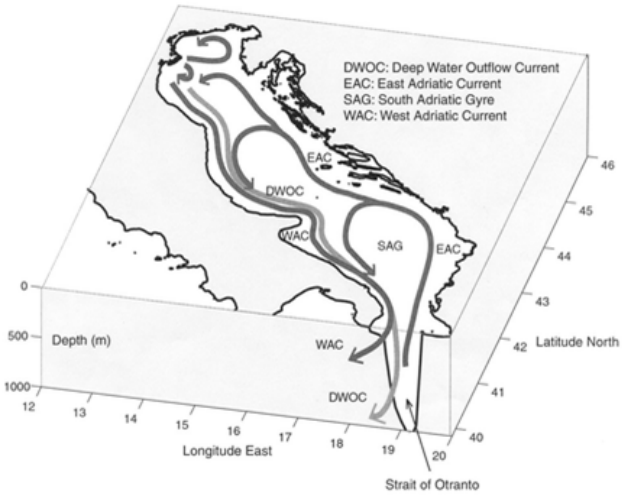

Figure 3: Adriatic Sea circulation (devotes-project.eu 2012-2016)

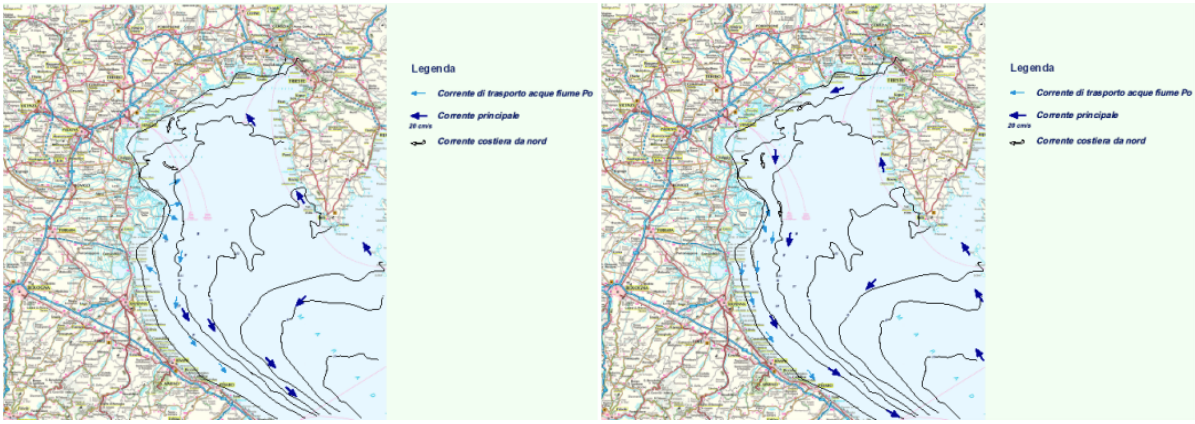

Figure 4: Summer and Winter circulation patterns in the northern Adriatic Sea (Autorità di bacino del fiume Po, 2010).

The Northern Adriatic Sea is characterized by cyclic seasonal eutrophication processes. Winter-spring large Diatomaceous flowering, with low salinity, and summer-autumn dinoflagellates flowering bring "red tides" in the coastal areas.

The high eutrophic condition is due to the large riverine inputs in the area and slightly lowered in the magnitude by the waves motion (***Autorità di bacino del fiume Po, 2010)***. The human development and the relative activity pressures that interested the area of the Veneto region in the recent years (***ugeo urbistat***), plays an important role upon the quality of the inland water (***Mallin, 2009***) that needs to be treated by the wastewater treatment plants, incrementing the FB loads that may be contained in the river plumes.

Recent changes, reductions, in the river flows regimes are lowering the river inputs in the coastal areas. As a matter of fact, a reduction in the growth of the shellfish have been registered in a study comparing the production of the years 2016 and 2017 (***Pastre,. 2017***).

The meteorological and the river flows data that are used in this study to evaluate the influence and relation to the episodes of river discharge in the sea, were taken from the Veneto Regional Environmental Agency, ARPAV, and the Emilia-Romagna Regional Environmental Agency, ARPAE. For what concerns the data collected from ARPAV the precipitation data are collected in the meteorological station close to the river flows station that are present over the region. Unfortunately, the agency presents one river flow station per river. For this reason, to evaluate the connection between extreme precipitation and river run-offs. or elevated flows, there was the need of

matching the closest precipitation station. The river flows analyzed for the Veneto region are the Adige river flow, ARPA river flow station No.284, located in Boara Pisani (coordinates: 1719069, 4998460). the Brenta river flow, ARPA river flow No. 283, station located in Barziza (coordinates: 1712306. 5072966) and the Piave river flow. ARPA river flow station No.327. located in Segusino (coordinates: 1728681, 5089687). All the river flows data are daily means expressed in [m^3/s]. The precipitation station close to the ones listed above are respectively: the station located in Concadirame Rovigo, station No. 98 (coordinates: 1714125, 4996919), the station in Bassano del Grappa, station No. 232 (coordinates: 1712249, 5073813), and the station in Quero, station No. 245 (coordinates: 1727966, 5089998). The precipitation is the cumulated precipitation of every single day expressed in [mm]. All coordinates are given in Gauss-Boaga West Time Zone (EPSG:3003). Figure 5 shows the location of the station given by the ARPAV website. In the case of the data collected from ARPAE website. the river analyzed is the Po river at the station of Pontelagoscuro. where both data of precipitation, millimeters cumulated per day, and data of river flow, daily mean, are available. The station lies at 11.60807 longitude degrees and 44.8883 latitude degrees. Figure 6 shows the location of the ARPAE station.

The data are collected in correspondence of the period in which there is the availability of the remotely sensed images, in the years spawning from the 1st January 2013 until the 31st July 2019. Over the same period are calculated, for both variables, precipitation and river flows, the 70th, 75th and 80th percentiles, for the precipitation the percentiles are calculated only for the rainy days (***World Meteorological Organization, 2018***). The cumulative distribution functions are shown in the result sections for the river flows, respectively Po, Adige, Brenta and Piave, in the plot is also shown the normalized cumulative distribution and the 75th percentile. The exceedance of the river flow percentile is used to select the images in the correspondent dates in order to evaluate the correlation between weather condition and the diffusion of the riverine plumes containing the FB and allowing their diffusion. If this is proven, an early warning system can be developed.

Precipitation data will be used only to evaluate whether there have been elevated precipitation regimes when the river flow percentiles are exceeded. This is because Adige, Brenta and Piave river are artificially controlled and deviated, therefore, a correlation of the early warning system against precipitation would have presented difficulties for this study.

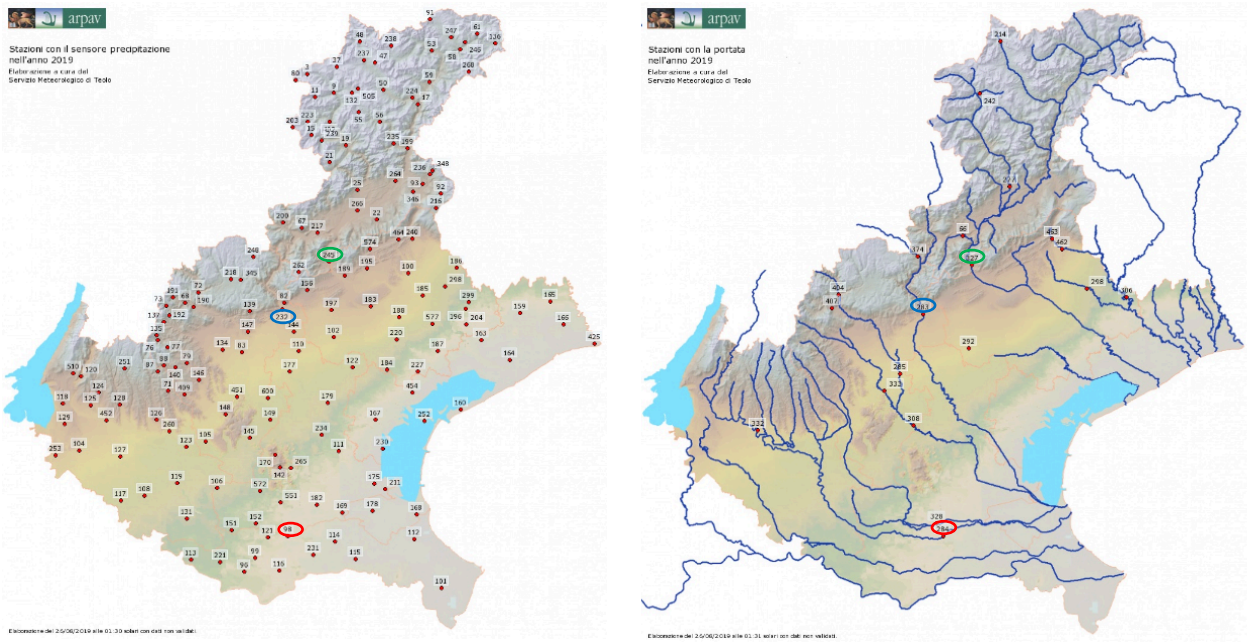

Figure 5: ARPAV maps of the stations located in the Veneto region: on the left the precipitation station. on the right the river flows station. The colored circle shows the location of green – station 245 and 327; blue – station 232 and 283; red – station 98 and 284.

Figure 6: ARPAE map of the station Pontelagoscuro (yellow circle).

The coordinates of the shellfish farms analyzed, and their AZA, are given by the IZSVe and, since during the study the shellfish farms have been renamed and, in some cases, joined for convenience. Table 4 shows the ID code corresponding to the name used in the study. Figure 7 instead represent the study area, with the shellfish farms. their respective allocated zone and the main rivers, Po, Adige, Brenta and Piave. Table 4 might be useful to better comprehend some of the results.

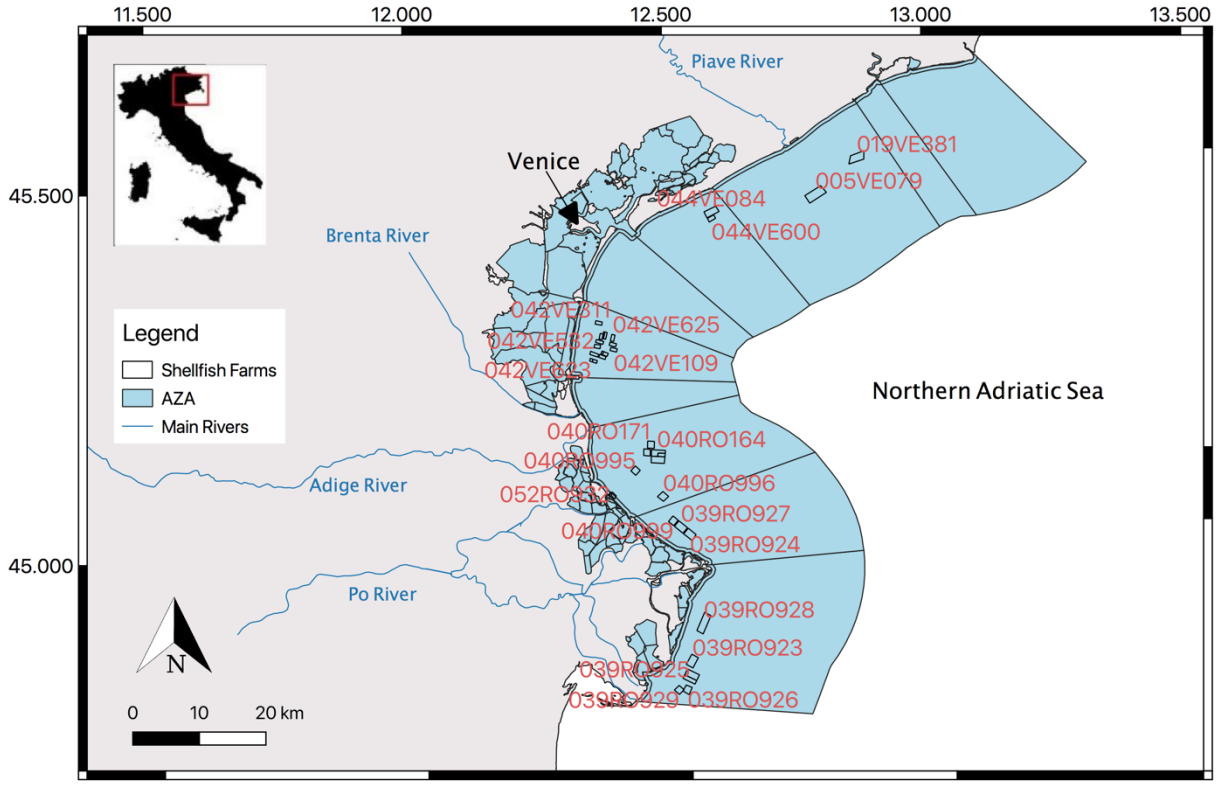

Figure 7: Study area with the Allocated Zones for Aquaculture (AZA), the single shellfish farms with their ID and the main rivers used in this study.

SHELLFISHFARM ID	NAME
044VE084	a
044VE600	b
042VE311	c
042VE477	d
042VE488	e
042VE625	f
042VE543	g
042VE064	h
042VE540	i
042VE109	l
042VE164	m
042VE160	m
042VE532	n
042VE571	o
042VE476	p

042VE623	p
040RO171	q
040RO180	r
040RO164	s
040RO191	s
040RO997	s
040RO995	t
052RO932	u
052RO931	v
040RO996	z
040RO999	a1
039RO927	b1
039RO924	c1
039RO928	d1
039RO923	f1
039RO922	g1
039RO925	g1
039RO926	h1
039RO929	i1
019VE381	l1
005VE079	m1

Table 4: Correspondences between shellfish-farms ID and name used in this study

4. RESULTS

First will be illustrated the time series resulting from the image processing and filtering method. This is followed by the river flows analysis results, with the common threshold found. The performances of the linear regression models and examples of Landsat 8 satellite images comparing a situation of likely contamination with a low river discharge one are illustrated. Finally, the results of the comparisons between the events s identified from remote sensing data and the ones of the controls provided by the *ISZVe*, courtesy of *Regione Veneto*, will be shown.

ENVIRONMENTAL VARIABLES OF SST AND TSM ANALYSIS

The images. covering the area of interest obtained through Landsat 8 satellite over the period spawning between 2013 and 2019, collected for TSM variable, first and last images dates respectively, are 250 for the TSM variable, 07/27/2013 and 12/09/2019, and 231 for the SST one, 07/27/2013 and 27/08/2019. After the processing method these are reduced to 68 images on average.

The variables time series of a single shellfish farm are displayed in contrast with the ones of the closest river mouth, along the preferential current direction crossing the farm, and a point in the open Adriatic Sea, chosen at a distance from coast such that the influence of riverine water never occurs. Figure 8, Figure 9 and Figure 10 are showing how these, SST and TSM, behave through time. The two variables are plotted for the shellfish farm, the closest river mouth and the open sea. It is clearly visible how the river mouth presents various peaks in TSM compared to that of the open sea. The peaks represent the discharge of fresh water into the sea. These peaks are also shown by the shellfish farms but reduced in magnitude, which is the prove that the riverine water is reaching the shellfish farm. SST variable time series instead are showing seasonal trends between summer and winter, and when river flow is discharged, drops in temperature is registered. Still shellfish farms related well during these events. Figure 8 particularly show a good relation between water quality in the shellfish farm (039RO924). Three events are evident, respectively 8th March 2014, 19th November 2014 and 4th March 2016 (red circles). In Figure 9 this correlation is weaker and some uncorrelated peaks in the shellfish farm (042VE064) TSM variable are evident, this is heightened in Figure 10 where TSM peaks of the shellfish farm (052RO931) are even more than the ones from the Adige river mouth. These results are only to introduce the time series analyses of the two variables SST and TSM, which have been chosen as efficient in detecting water quality.

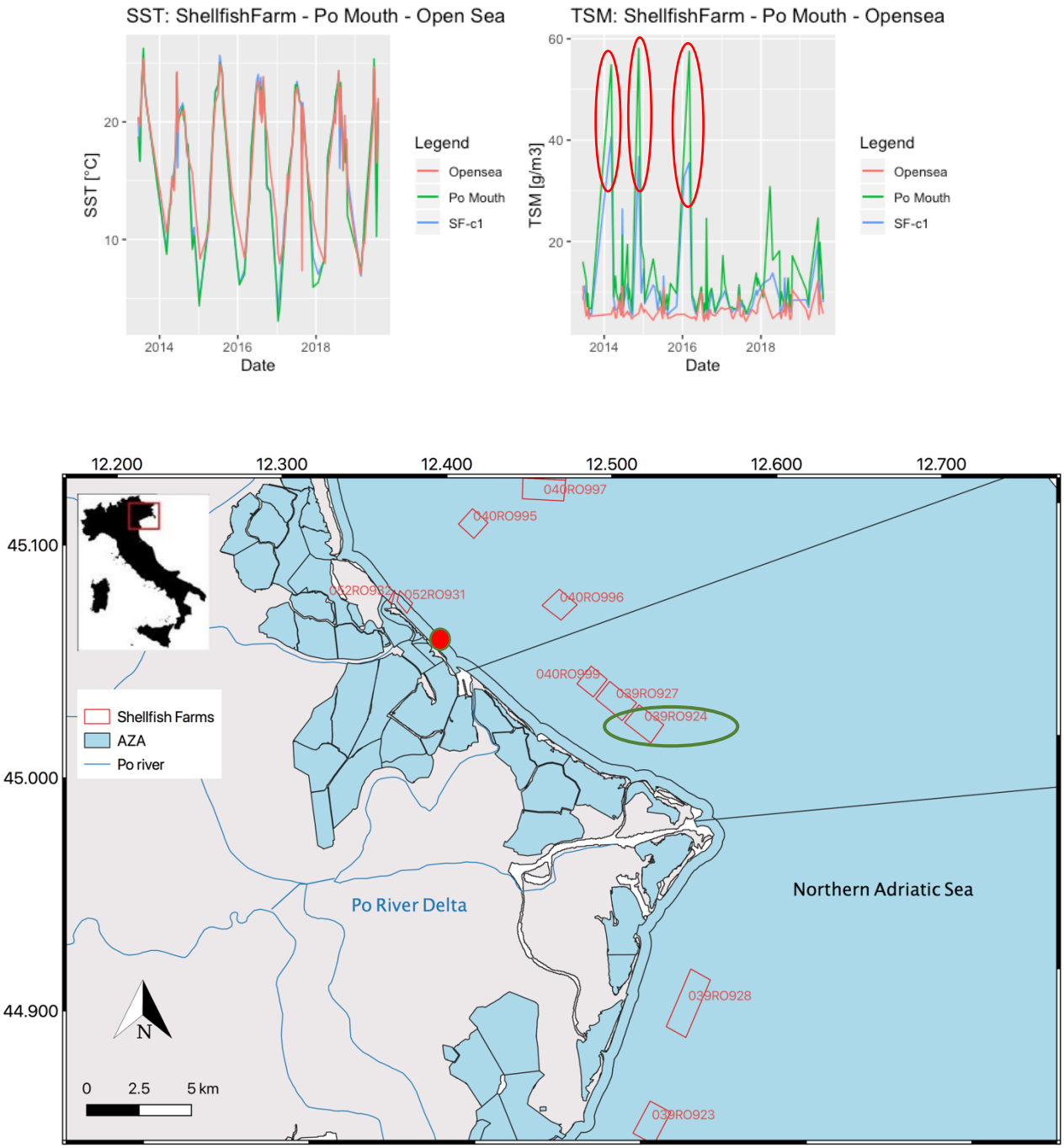

Figure 8: SST and TSM trends of the farm 039RO924 against Po river mouth and open sea. Underneath a map of the location of the farm, green circle, and the Po river mouth, red dot.

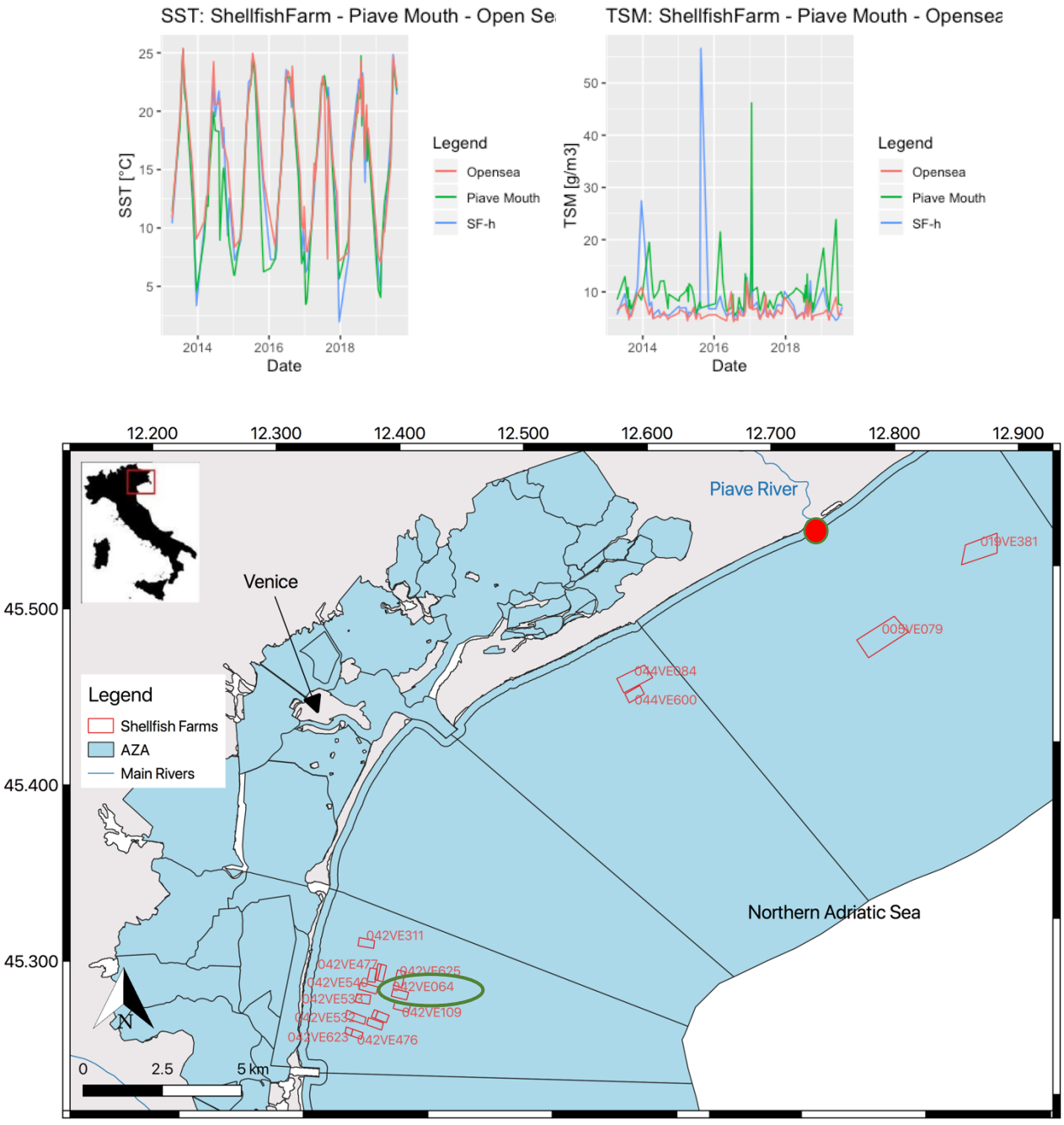

Figure 9: SST and TSM trends of the farm 042VE064 against Piave river mouth and open sea. Underneath a map of the location of the farm, green circle, and the Piave river mouth, red dot.

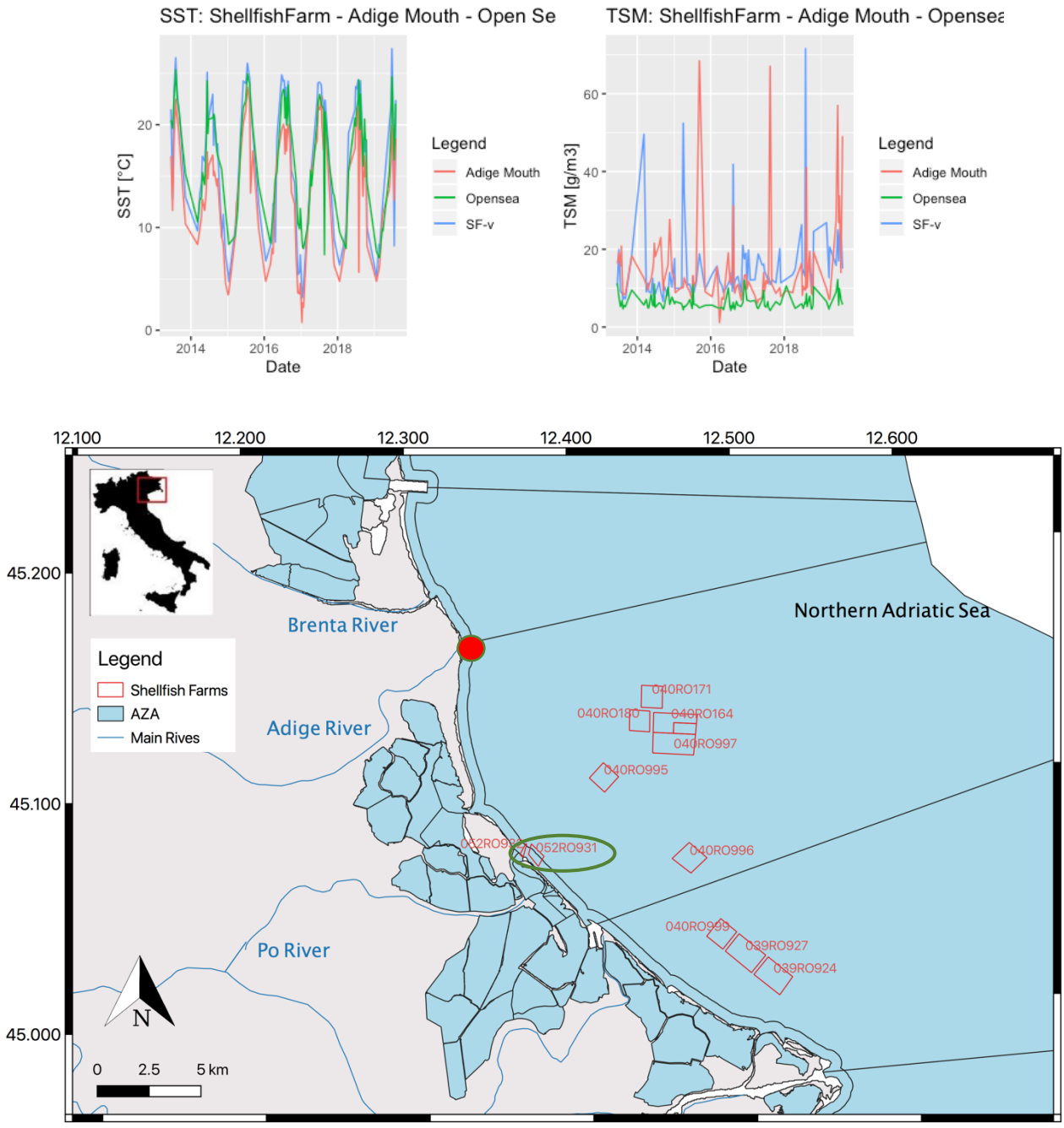

Figure 10: SST and TSM trends of the farm 052RO931 against Adige river mouth and open sea. Underneath a map of the location of the farm, green circle, and the Adige river mouth, red dot.

RIVER FLOWS EVALUATIONS

The retrieval of the TSM and SST time series is followed by the analysis of the main river flows. This analysis resulted in a set of dates in which was exceeded the 75th percentile of the flow. The choice of using the 75th percentile is due to a series of check on different values, starting from the 99th percentile and lowered down until a minimum number of matches (10) with Landsat-8 images where found. The number of river flow observations, presented in Table 5 for each river, are used to filter the dates in which anomalies in TSM and SST values are found for each different farm. In line with the aim of developing an early warning system. The cumulative distribution function of each river discharge is displayed in Fig. 11, shows river flows cumulative distribution function for each river, with the respective percentile and the normalized cumulative function. In Table 5 is shown that Piave and Po river are presenting the two lowest amounts of observations. This is due to gap in the data registered by the river flow station of ARPAV and ARPAE.

River	# Observations	Observations <75th Perc.	Observations >75th Perc.	Percentile [m^3/s]
Piave	1731	1298	433	53.2
Brenta	2401	1800	600	86.3
Adige	2401	1800	600	278
Po	2306	1729	577	1787

Table 5: River flows observations, their percentiles and the number of observations both exceeding and not the 75th percentile.

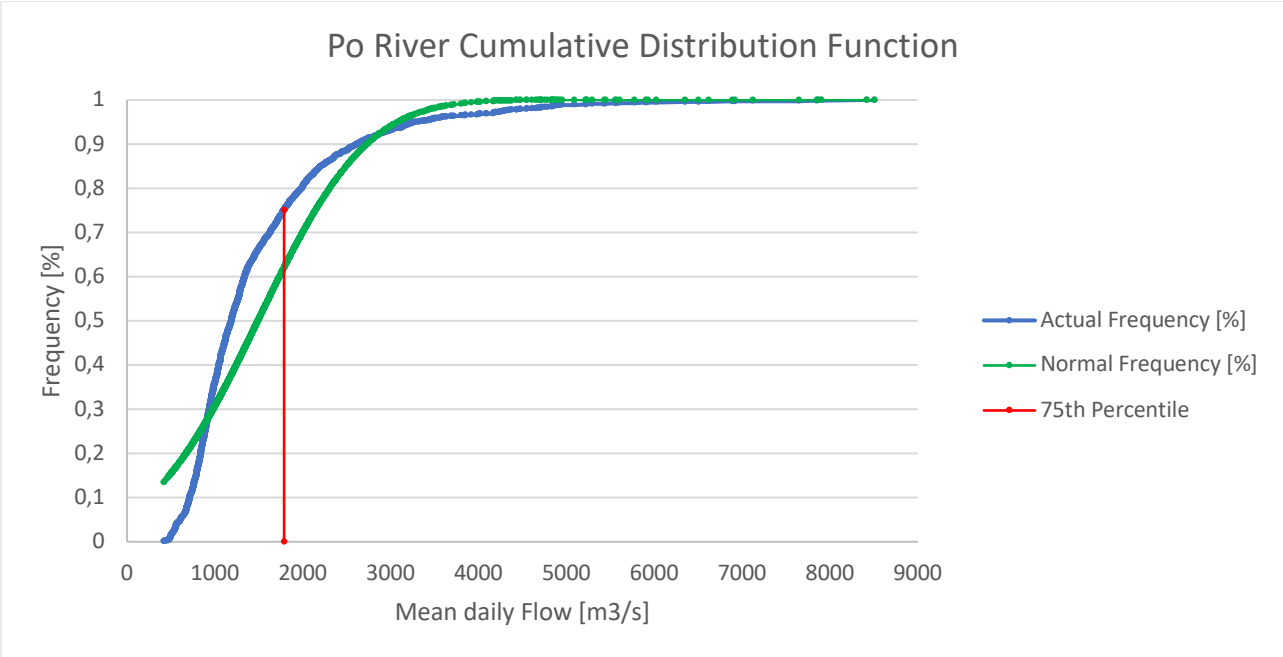

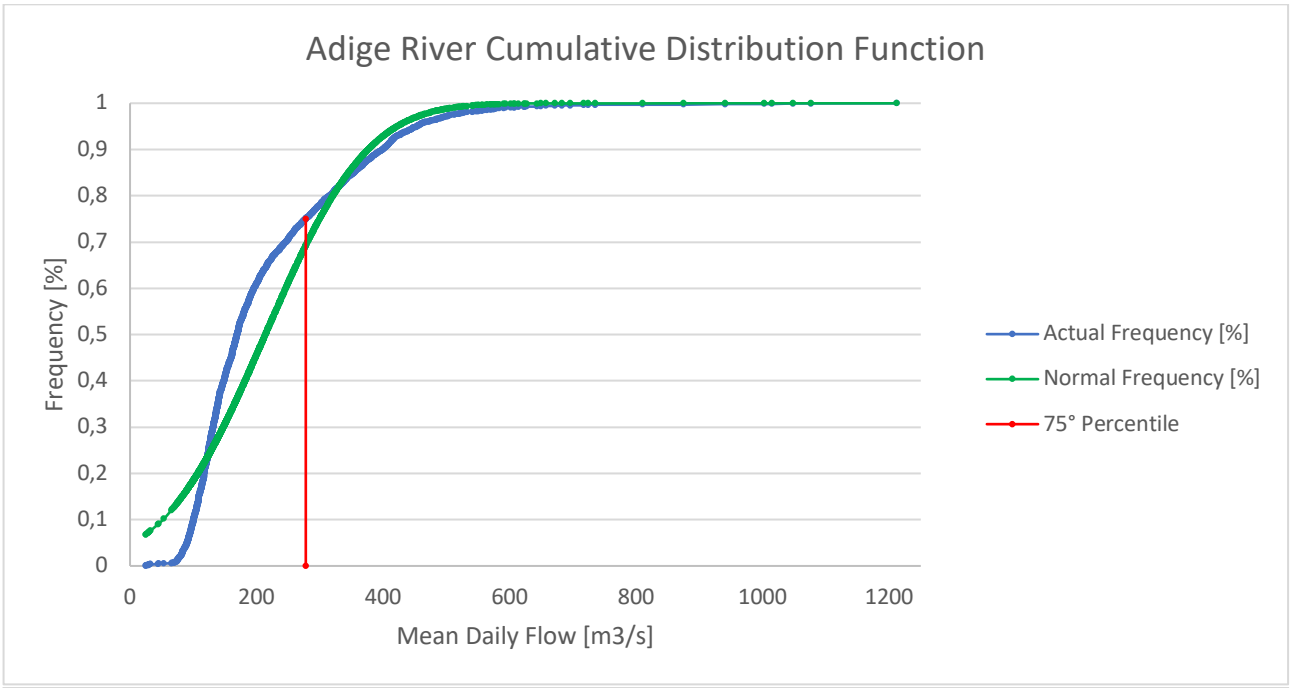
Adige River Cumulative Distribution Function
Frequency [%]
1
0,9
0,8
0,7
0,6
0,5
0,4
0,3
0,2
0,1
0
0
200
400
600
800
1000
1200
Mean Daily Flow [m3/s]
Actual Frequency [%]
Normal Frequency [%]
75° Percentile

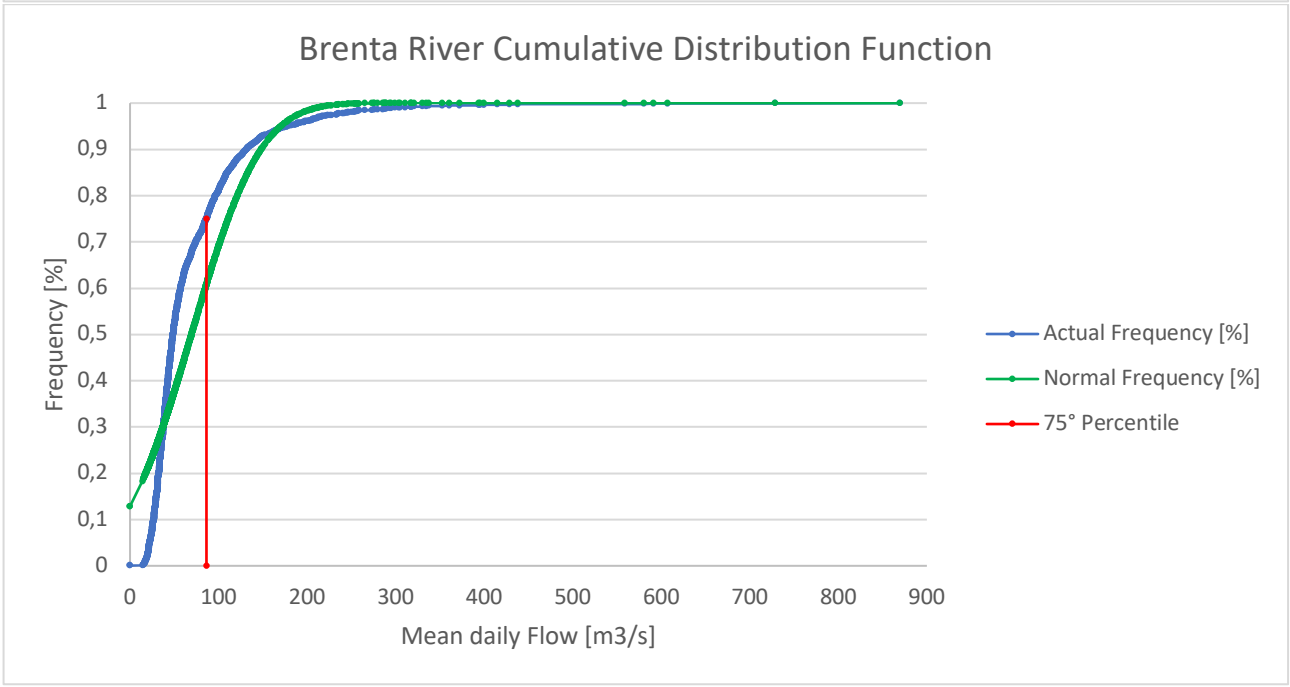
Brenta River Cumulative Distribution Function
Frequency [%]
1
0,9
0,8
0,7
0,6
0,5
0,4
0,3
0,2
0,1
0
0
100
200
300
400
500
600
700
800
900
Mean daily Flow [m3/s]
Actual Frequency [%]
Normal Frequency [%]
75° Percentile

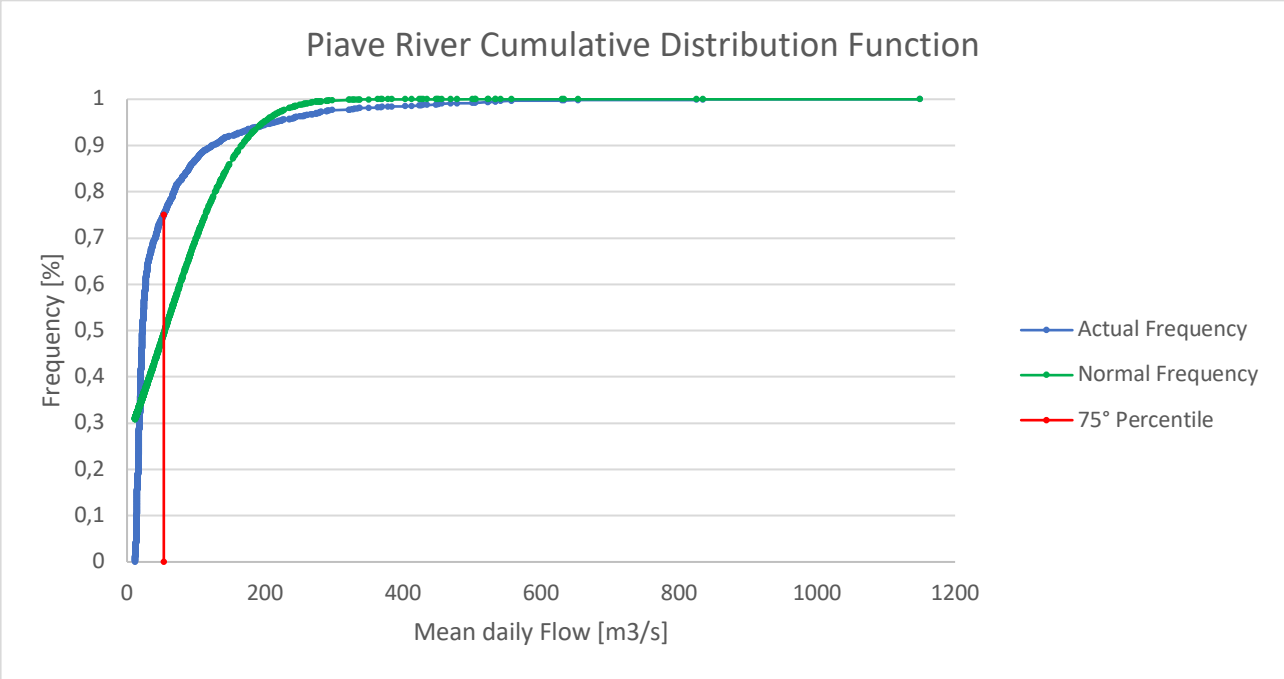

Figure 11: Top to bottom: Po, Adige, Brenta and Piave River Cumulative Distribution Function and 75th Percentile.

MULTIPLE LINEAR REGRESSION MODEL PERFORMANCES

The correlations, tested through t-test procedure, existing between the water flowing within a farm, the closest river mouth and the open sea point, analyzed for the dates both exceeding, or not, the 75th percentile of flow, provide a statistical evidence that the water quality at a given farm is strongly influenced by riverine water and, consequently, the risk of faecal bacteria contamination is higher than usual. As Table 6 shows, the stronger correlation is obtained for those farms collocated closest to the river mouth, along the current pattern line. All the Sea Surface Temperature regressions are statistically significant., as the p-values from the student t-test are lower than 0.05, the significance level for which the null hypothesis can be rejected. The linear model used is capable of predicting the values of temperature in the farm. The four regressions of the farms: 040RO999, 039RO927, 039RO924, 039RO928, 039RO922, 039RO925 and 039RO929 are all statistically significant. Therefore, the multiple linear model fitting the data is performing well in the estimation of both TSM and SST variables, showing how strongly the water for the exceeded river flows percentile relates to the river mouths. On the other hand, when the percentile is not exceeded it presents a more robust relation with that of the open sea. There are the farms presenting no statistical consistency for the regression corresponding to exceedances in the river flow percentile. These are the 042VE064, 042VE540, located in the area in front of the Venice lagoon, and the 040RO164, 040RO191, 040RO997 and 052RO931, situated in between the Venice lagoon and the delta of the Po river. The green color in the table is given when statistical consistency is found, for the whole model and also for each variable. The farms highlighted in green show consistency in all the four regressions performed: values of TSM over and below the river flow percentile, and values of SST over and below the SST.

Shellfish FARM ID	REGRESSION VARIABLES	α_1	α_2	β	p-value
040RO999	TSM over 75th	0.27	0.26	2.34	1.19E-04

	TSM below 75th	0.17	1.68	-3.91	2.09E-07
	SST over 75th	0.76	0.29	-0.49	1.08E-12
	SST below 75th	0.81	0.16	0.50	<2.2E-16
039RO927	TSM over 75th	0.41	0.30	0.81	9.48E-06
	TSM below 75th	0.47	2.26	-9.69	2.60E-07
	SST over 75th	0.74	0.31	-0.62	2.27E-12
	SST below 75th	0.82	0.15	0.43	<2.2E-16
039RO924	TSM over 75th	0.62	0.10	0.27	3.01E-18
	TSM below 75th	0.61	0.71	-2.00	<2.2E-16
	SST over 75th	0.87	0.18	-0.46	4.35E-15
	SST below 75th	0.85	0.13	0.34	<2.2E-16
039RO928	TSM over 75th	0.23	0.42	3.77	4.13E-03
	TSM below 75th	0.23	0.11	5.37	2.04E-03
	SST over 75th	0.73	0.29	-0.27	5.26E-13
	SST below 75th	0.67	0.38	-1.22	<2.2E-16
039RO992 & 039RO925	TSM over 75th	0.32	4.34	-24.35	7.69E-05
	TSM below 75th	0.10	0.58	3.23	7.10E-07
	SST over 75th	0.71	0.33	-0.50	1.71E-13
	SST below 75th	0.90	0.09	0.20	<2.2E-16
039RO929	TSM over 75th	0.21	0.56	3.23	1.19E-02
	TSM below 75th	0.05	0.60	3.57	4.77E-05
	SST over 75th	0.63	0.41	-0.40	1.16E-13
	SST below 75th	0.95	0.01	0.77	2.20E-16
042VE064	TSM over 75th	0.08	0.01	5.37	6.91E-01
	TSM below 75th	0.41	0.73	0.32	7.14E-02
	SST over 75th	0.30	0.77	-1.02	5.48E-07
	SST below 75th	0.37	0.68	-0.98	<2.2E-16
042VE540	TSM over 75th	0.08	-0.01	5.37	6.91E-01
	TSM below 75th	0.41	0.73	0.32	7.15E-02
	SST over 75th	0.23	0.78	-1.22	5.34E-07
	SST below 75th	0.55	0.43	-0.03	<2.2E-16
040RO164 & 040RO191 & 040RO997	TSM over 75th	0.10	0.54	4.28	5.44E-01
	TSM below 75th	-0.01	1.10	1.29	8.80E-02
	SST over 75th	0.60	0.52	-0.54	<2.2E-16
	SST below 75th	0.44	0.61	-0.01	<2.2E-16
052RO931	TSM over 75th	0.16	0.19	9.80	4.50E-01
	TSM below 75th	0.08	0.14	13.94	8.18E-01
	SST over 75th	1.17	0.08	0.18	<2.2E-16
	SST below 75th	0.70	0.45	-0.84	<2.2E-16

Table 6: Multiple Linear Regression Model results, α_1 the first parameter of correlation with the river mouth, α_2 the second parameter of correlation with the open sea, β the intercept coefficient for the regression and the p-value of the t-test. The green color is given to the regression that show statistical consistency, the whole model (p-value) and for the single coefficients (t-test on each coefficient).

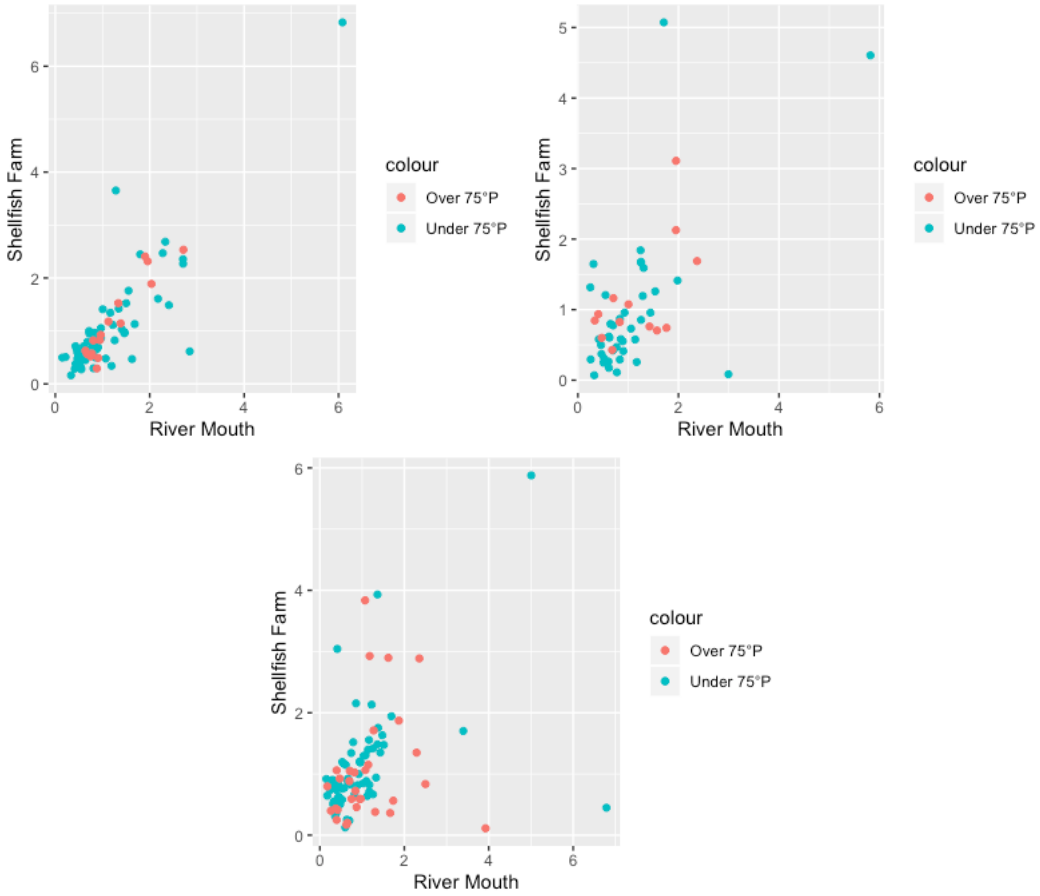

Figure 12: Scatter plots of the normalized distances, in the same order of the TSM and SST plots (039RO924, 042VE064 and 052RO931).

The linear regression results which proved evidence of that the water quality at a given shellfish farm is strongly influenced by riverine discharges is corroborated with the estimation of the distances of both: shellfish farm from the open sea and river mouth from the open sea. These distances are calculated through the two variables as presented in the methodology section. The values of both variables were used to represent, in a bidimensional plane, the normalized values of the distances from the open sea of both the River Mouth and the Shellfish farm, of the events exceeding the 75th percentile of flow of the river in red, and the ones within that threshold in blue. Each normalized value, each point in the graphs, corresponds to a satellite image. The points that align along the diagonal are prove that the water quality in a farm is strongly influenced by the water coming from the river mouth taken into account. The further from the origins the greater is the magnitude of the perturbation, the distance of TSM and SST values from the ones of the open sea is large. When few points are aligned and more spread around the bidimensional plane we have events where waters were of different quality from the open sea, but not very correlated between each other.

The satellite images corresponding to the images during the perturbation and during calm condition are shown below, for some illustrative events (Fig. 13 to 15). The images allow the understanding of the plume diffusion along the coastal area.

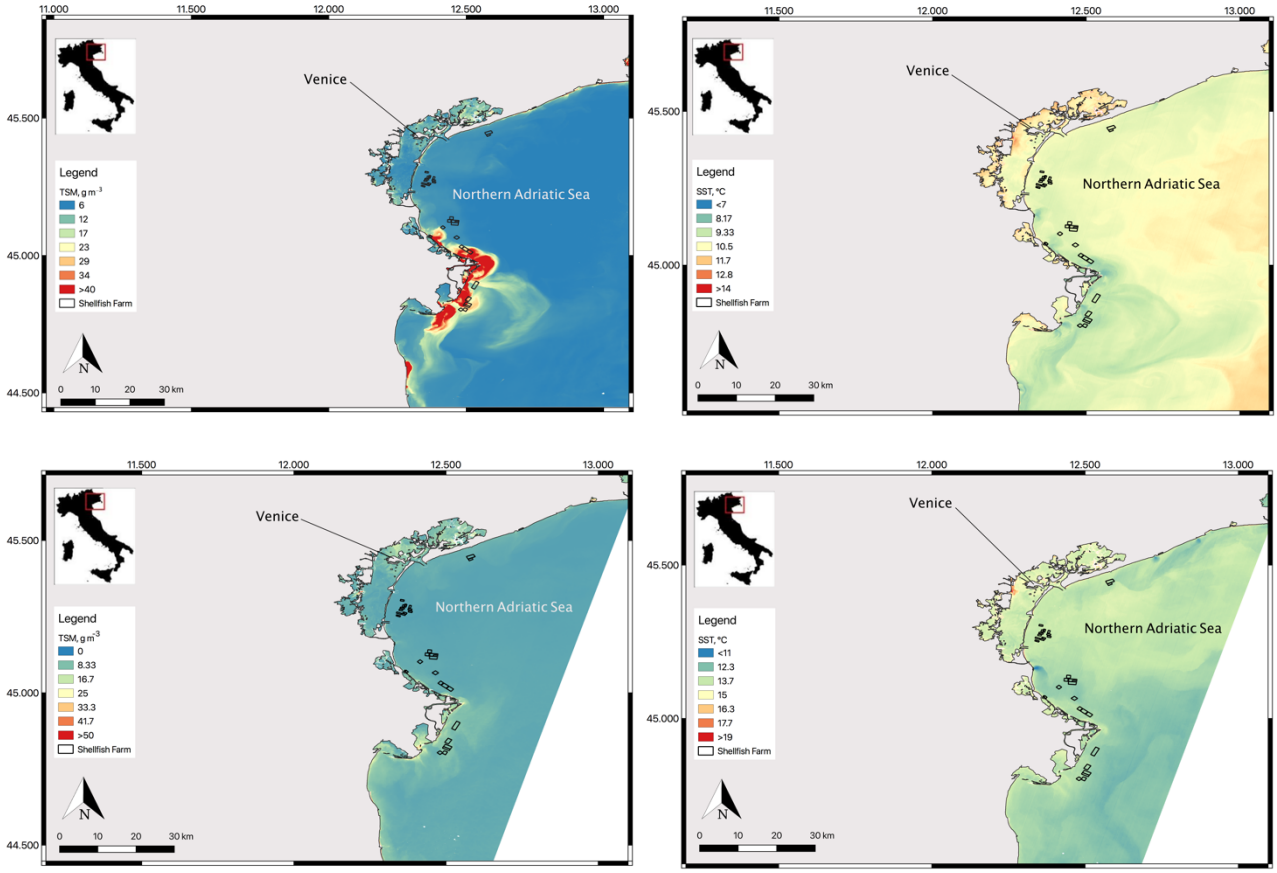

Figure 13: Comparison between TSM and SST, left to right, of the perturbation happened on March the 8th 2014 and a calm situation on April the 16th 2014, top to bottom.

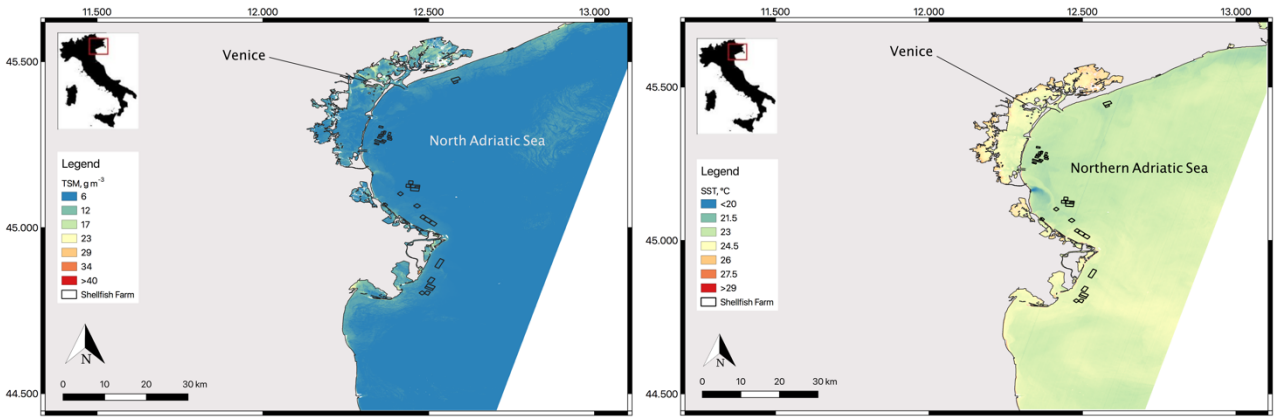

Figure 14: Comparison between TSM and SST, left to right, of the perturbation happened on March the 4th 2016 and a calm situation on July the 10th 2016, top to bottom.

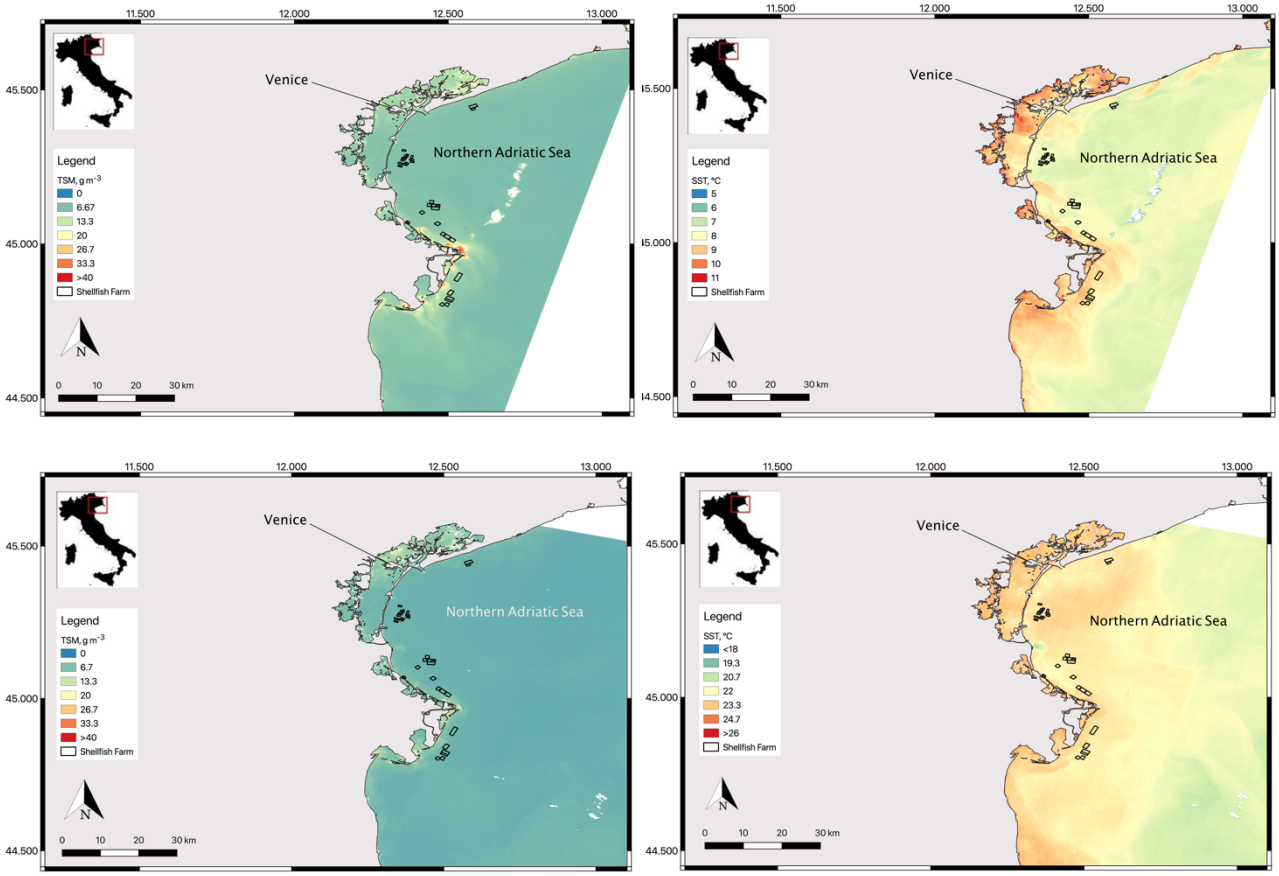

Figure 15: Comparison between TSM and SST, left to right, of the perturbation happened on March the 26th 2018 and a low discharge situation on July the 9th 2018, top to bottom.

CONTAMINATIONS CHECKS AND EARLY WARNING SYSTEM DELIVERY

The last results are given by the comparison between the events of likely contamination in the period April 2013- June 2019, (red points in fig. 12) and the actual contamination data, provided by the regional authorities of Veneto and Emilia Romagna regions. based on analysis performed by ISZVe. The total number of events found was 36, Every shellfish farm presented between the totality a number of events ranging between a maximum of 31 and a minimum of 15. These are reported as percentages in Table 7 below, only two farms with 15 observations while seven with 31.

Shellfish Farm ID	Occurence [%]
005VE079	39
042VE488	42
044VE084	42
044VE600	42
042VE311	42
042VE477	42
042VE625	42
042VE543	42
042VE064	42
042VE540	42
042VE109	42
042VE160 & 042VE164	42
042VE532	42
042VE571	42
042VE476 & 042VE623	42
040RO171	66
040RO180	66
040RO164 & 040RO191 & 040RO997	82
040RO995	82
052RO932	82
052RO931	82
040RO996	82
040RO999	42
039RO927	39
039RO924	42
039RO928	45
039RO923	42
039RO926	45
039RO929	42

Table 7: Number of images extracted for each shellfish farm, presented as percentage on the total of selected images. Green highlights the farms which presented the largest amounts of events through the methodology while red the lowest.

In Table 8, the total events (dates) selected that showed a control matching within 6 days the dates of the images are shown. These data are the checks that the authority carried out in specific months, reporting, where found, the number of *E. Coli* per 100 grams of flash and intravalvular liquid. The choice of the monthly range of controls dates is given on the basis of the ones selected through this study. In table 7 are presented the events of respectively the satellite images showing anomalies

and the authority control. The total amount of 38 observations is reduced to 18 given the data provided from November 2014 until June 2019. Of these 18, 3 dates have no matches within 6 days, the ones that are matching the same shellfish farm, a total of 8 coincidences are all showing presence of bacteria, 5 are perfect matches while 3 dates present controversial results. All the other dates have no coincidences between the exposed farms and the controls. More specifically, when the controls happened within the 6 days in other shellfish farms, we end up with 3 dates showing both presence and absence from laboratory analysis and 2 that found no presence of bacteria. Only one date presents contamination of bacteria but was not spotted by the method.

Shellfish Farm ID	Date of Capture	Date of Control	*E. coli* [MPN/100g]
005VE079	19th Nov 2014	20th Nov 2014	790
039RO928	03rd Apr 2015	09th Apr 2015	50
042VE476	04th Mar 2016	08th Mar 2016	940
039RO924	24th Jun 2016	23rd Jun 2016	330
040RO191	19th Jul 2016	20th Jul 2016	45
005VE079	22nd Jul 2017	22nd Jul 2017	-
044VE600		17th Jul 2017	45
005VE079	20th Apr 2018	17th Apr 2018	-
042VE543		24th Apr 2018	20
042VE543	1st Jun 2019	03rd Jun 2019	45
044VE600		04th Jun 2019	-

Table 8: Comparison between selected dates and regional controls. Deep green contamination with of E. coli; light red presence of E. coli while red is no bacteria found.

For each positive control was checked the TSM value corresponding to the shellfish farm controlled and the river flows in the same day, and in brackets the peak values within a week from the date. The precipitation is also shown as cumulative precipitation of the last rain event form the date for each river (see Table 9). The river flows are associated to different colours depending on the percentile threshold that have been trespassed, red represents the 99th, orange the 95th, yellow the 90th while green is the 75th. The river closest to the shellfish farm which showed bacteria presence is marked with a "*". For instance, each time the 75th percentile, at least, is exceeded bacteria is proven to be present.

Shellfish Farm ID	Date of Capture	TSM [g/m^3]	Po Flow (peak) [m^3/s]	Adige Flow (peak) [m^3/s]	Brenta Flow (peak) [m^3/s]	Piave Flow (peak) [m^3/s]	Precipitation [mm]
005VE079	19th Nov 2014	16.3	8510 (8510)	623.2 (671.5)	258.8 (437.6)	*268.4 (469.5)	12.8 – 13.6 – 85.4 – 98.6
039RO928	03rd Apr 2015	7.2	*1764.3 (3411)	134.1 (193.3)	62.3 (166.2)	22 (116.3)	27 – 39.8 – 82.2 – 73.4
042VE476	04th Mar 2016	8.68	2993.9 (3252.8)	182.1 (247.6)	68.6 (179.6)	*54.7 (193.8)	74.8 – 59.6 – 100.8 - 173
039RO924	24th Jun 2016	10.288	*1847.1 (2718.1)	394.5 (550.2)	55 (114.3)	29.9 (77)	4.8 – 5.8 – 15 – 16.8
040RO191	19th Jul 2016	6.9	635.2 (794)	*196.5 (291)	39.6 (69.1)	-	0 – 0 – 42.6 – 39

Table 9: TSM. flows and precipitation values of the confirmed contaminations or presences of E. coli. The different colours of the number are associated with different flow percentiles thresholds: red represent the 99th percentile, orange is the 95th percentile, yellow the 90th, while green is the 75th percentile.

This last result is the final prove needed to state that the 75th percentile between the different rivers examined in the present thesis can be used as threshold for delivering the early warning. When the value is exceeded by one of these rivers, the shellfish farm lying within the current pattern of the river are exposed to the risk of contamination.

All the results that are not shown above can be found in the Appendix section at the end of the present thesis. For issue of file dimension and upload limits some results have been omitted.

5. DISCUSSION

In this section some comments and reflections are made upon the results listed above, their displacement is followed. Therefore, before some further explanations about the SST and TSM time series, presented in the first section of the results, are shown. These are followed by comments upon the choice of the 75th percentile and the multiple linear regression model. The corroboration of the model with the distances plots are better explained and finally some discussion related to the success of the methodology and the early warning system.

In summing most of the results, 13 shellfish farms have been chosen as more significative: 040RO999, 039RO927, 039RO924,039RO928, 039RO922, 039RO925, 039RO929 042VE064. 042VE540, 040RO164, 040RO191, 040RO997 and 052RO931. These are the best, first 7, and worst, latter 6, performing in the correlation student t-test for the multiple linear regression models.

First of all, remarks need to be made regarding the remote sensing methodology applied. The satellites derived data are not verified by an in-situ campaign and regression analysis to evaluate the degree of accuracy yielded by the algorithm. Particularly the TSM algorithm taken was applied and verified over the Western Scheldt estuary, an area that present similar trophism state as the Adriatic. Therefore, the estimates are supposed to be acceptable but still not sustained by a statistical analysis which proves their precision. For the SST retrieval, even if the satellite collection providing the surface reflectance values is used. is always suggested and needed the in-situ data comparison, in every remote sensing study this is applied. In this case for time and budget issues this was not possible, but the yielded results still prove the efficacy of the method and leave space for further improvement. Using a third environmental variable for instance may increase the accuracy of the method and its robustness.

From what concerns the figures showing the SST and TSM time series of the most illustrative farms, it is clear that the trend of the variables values in the closest ones usually behave similarly with the one of the open sea. Peaks in TSM are due to large inflows of suspended solid when riverine water is discharged. These peaks are usually common between river mouth and shellfish farm (Fig. 8), shellfish farms presenting the best peaks matches are: 040RO999, 039RO927, 039RO924, 039RO928, 039RO922, 039RO925 and 039RO929. In some cases, the shellfish farm may present different peaks (Fig. 9 and Fig. 10), this is found particularly in the shellfish farms: 042VE064, 042VE540, 040RO164, 040RO191, 040RO997 and 052RO931. This is for those farms that are located at a distance from the river mouth, but close to the coastline or to resuspension of solids which may occur in the study area which is influenced by strong tidal activity. Furthermore, non-point source of contamination may be another possible explanation.

Surface temperature is showing seasonal trends in temperature, summer warmer and winter colder. For instance, riverine water inflows are usually colder, this is particularly evident during winter, when temperature differences observed are reaching up to 5°C.

Other important considerations to be made are relative to the rivers taken into account in this study. These were only the four major, Piave, Brenta, Adige and Po. while many other sources of discharge are present in the area. Furthermore, the amount of river observation of the river Piave is the lowest, missing more than one year of observations through the whole period. This is reflected in the amounts of events identified and collected based on methodology here presented. Also, Po flows are missing around three months of observations. The choice of using the 75th river flow percentile was due to: the desire of keeping a fixed threshold between the rivers but still weighted on their regime; different trials of image retrieval; and the regression analysis performances. Therefore, the

reduction of river flow percentile is also due to a lack of data. This might be improved with either longer time series or with the combination of another satellite products, such as Sentinel-2, covering the events in which Landsat-8 did not passed over the study area. Therefore, river flow thresholds may be adjusted in the light of new data and yield even better results.

This behavior is confirmed by the statistical significance of the multiple linear models run for each farm. All regressions concerning Sea Surface Temperature show statistically significant relations, this is because the differences between the temperatures of fresh water and saltwater are slight, usually no more than 5°C. Longer time series or the addition one extra variable may strengthen the multiple linear regression model, which may be able to obtain lower p-values, higher statistical consistency. The stronger correlation is obtained for those farms collocated closest to the river mouth, along the current pattern line. Particularly in the southern part of the study area. This can be explained by the different magnitude of the river discharges, in the southern area 3 out of the 4 examined river flows are located and here lays the largest river flow, which is the Po river one. These are: 040RO999, 039RO927, 039RO924, 039RO928, 039RO922, 039RO925 and 039RO929. As Table 6 showed, were the one with higher correlation scores.
The regressions where no statistical consistency was found between the farm and the chosen river, may highlight the fact that other sources of variations in the TSM variable are to be considered. E.g. other smaller river inflows or non-point sources that are dislocated in the area. In non-point sources boat traffic is to be considered, especially in a touristic area such that of the Venice Lagoon.
As a matter of fact, the farms presenting these anomalies are located in the area in front of the Venice Lagoon, 042VE064 and 042VE540, which can be explained by the distance that these lagoon have from the river correlated to them, which is the Piave river together with the fact that it is the river presenting the large gap in data as mentioned above. The other shellfish farms presenting anomalies are located in between the Venice lagoon and the delta of the Po river, 040RO164, 040RO191 and 040RO997, this may also be caused by the choice of the river that relates to them, either Adige or Brenta, or their combined influence.

The mussel farms, 042VE064 and 042VE540 (Fig. 9), in which the two TSM correlations, for the events over or under the river flow percentile, are presenting statistical anomalies that are to be intended as the prove that the increasing distance from the river mouth correspond to a reduction in its water influence within a shellfish farm.

Processes happening during the transport, together with other sources of pollutant, that are not taken into account in this study, reduce the influence of the water discharged by the river, without necessarily reducing the number of events in which anomalies might be found. The choice of using the dates of exceedance of the 75th percentile of the various rivers, resulted with the Piave river dataset being able to provide only 16 dates, therefore 16 samples to perform the linear regression model, which may be not enough to evaluate statistical significance.

This particularly for the farms 044VE084 and 044VE600, the closeness relates well to the river mouth, but the small amount of data for the regression performed over the 75th percentile, 16 dates for both farms, do not have statistical significance to relate the suspended solids of the water in the farm and the one flowing out of the Piave river. While, when the percentile is not exceeded, they still shows stronger correlation with the TSM values of the river mouth (seen the correlation coefficient and their significance).

Total suspended matter regressions together with the scatter plots (Fig. 12) show quite well how for some dates the distances between river water and ocean and shellfish farm water and ocean are close together, aligning along the diagonal of the scatter plot, and confirming that the plume riverine water reaches the farms with lowering amounts of suspended solids and always more homogeneous water to the surrounding area, this is for all of the shellfish farms with different magnitude of the phenomena. Landsat 8 displayed images give the chance to take a glance at the strong visibility of

some events in which the river plume diffuse largely in the adjacent areas, following the current patter from north to south, running along the coastline.

Finally, from the comparison of the images with the data of the controls carried out in the area, it is possible to say that the method gives 33.33% of perfect matches (5/15), 53.33% of matches, on the exact same location and presence or contamination found, and 6.67% of fails (1/15). If only the matching farms are counted. and the time gap with the date of the control is considered, then 8 are the total matches on which 7 found positive (87.5%) and 1 negative (12.5%).

Despite limitations in free available data, that could have enriched the information of the study area and the precisions of the results, the overall success yielded by the methodology highlight that there is a correlation between *E.coli* presence and river flows. Furthermore, the development of this methodology may lead to very precise and trustworthy results to be implemented in the management of shellfish farms, and more generally aquaculture practices. It is therefore confirmed by the study the choice of adopting the 75th as a preliminary Early Warning System.

Some remarks on the possible improvements of the methodology will be shown in the following conclusions section.

6. CONCLUSIONS

The first important logical remark is that the methodology applied, even though data limitation, yielded good results and was able to deliver its objectives. Due to the fact that here only Landsat 8 products were used, providing a total of 240 (average between TSM and SST variables) images which, after filtering processes and outliers removal, are scaled down to roughly 100 pictures, or observations, constrained the efficacy of the correlations. Waving together Landsat 8 and Sentinel 2 products, for example, could largely increase the number of observations. The implementation of the observations provided by a second satellite could fill the gap in the data provided by Landsat-8. The river flows also played as limitation, since more than a year of observation is missing in the flows of the Piave river and around three months in the Adige river may alter the definition of the percentile and the data missing could have highlighted other important events. As a matter of fact, in the scatter plots created with the Piave river large number of events presenting large distances from the sea are not highlighted in red, this reasonable can be due to the absence of the observation. Furthermore, the length of the study period is roughly 6 years. a study of over 10 years may yield more satisfactory results and permit to define a more precise early warning system. Augmented amount of data would increase the precision in identifying the exact threshold for each river flow. This in particular could be further improved connecting the found river flow thresholds, though a corrivation-model in the Veneto and Emilia Romagna regions to heavy rain events. The corrivation-model would identify the amount of cumulated precipitation needed to reach a certain river flow for each river taken into account.

Finally, this work had as objective the delivery of an early warning system, this dynamic application can be used in a static way producing risk-associated map. These map can be elaborated on a statistical basis and can provide an efficient tool to be implemented in the spatial planning of aquaculture and help with site selection. This approach and resulting map can be corrivated with a mechanistic approach to properly describe FB transport and diffusion dynamics, taking into account physical phenomena such as wind and current direction and velocity, tidal activity and other environmental variables vitals for the FB loads. This consideration further explains the importance of the results obtained through the methodology applied in this thesis.

REFERENCES

Ansper, A., Alikas. K. (2018). Retrieval of Chlorophyll a from Sentinel-2 MSI Data for the European Union Water Framework Directive Reporting Purposes. Remote Sensing 11(1): 64

Autorità di bacino del fiume Po (2010). Caratterizzazione dei tipi di acque marino costiere e di transizione del bacino del fiume Po. Piano di gestione del distretto idrografico del fiume Po: allegato 1.3 all'Elaborato 1

Bresciani, M., Cazzaniga, I., Austoni, M., Sforzi, T., Buzzi, F., Morabito, G., Giardino, C. (2018). Mapping phytoplankton blooms in deep subalpine lakes from Sentinel-2A and Landsat-8. HYDROBIOLOGIA 824(1): 197-214

Brigolin, D., Pastres, R., Tonino, M., Camuffo, M., Soriani, S. (2011). BHAM: A modelling tool for bathing water management. Proceedings of the Tenth International Conference on the Mediterranean Coastal Environment. MEDCOAST 11.

Brigolin, D., Porporato, E. M. D., Prioli, G., Pastres, R. (2017). Making space for shellfish farming along the Adriatic coast. ICES journal of marine science 74(6): 1540-1551.

Chander, G., Markham, B. L., Helder, D. (2009). Summary of current radiometric calibration coefficients for Landsat MSS, TM, ETM+, and EO-1 ALI sensors. Remote Sensing of Environment 113: 893-903.

Chauhan, A. S., Sharma, R., Kumar, A., Malik, K., Dagar, H. (2018). Applications of remote sensing in agriculture. Agricultural, Allied Sciences & Biotechnology for Sustainability of Agriculture, Nutrition & Food Security (chapter: Agriculturural meteorology).

Chen, J., Zhu, W., Tian, Y. Q., Yu, Q. (2017). Estimation of Colored Dissolved Organic Matter From Landsat-8 Imagery for Complex Inland Water: Case Study of Lake Huron. IEEE Transactions on Geosciences and Remote Sensing PP(99): 1-12.

Chen, J., Zhu, W., Tian, Y. Q., Yu, Q., Zheng, Y., Huang, L. (2017). Remote estimation of colored dissolved organic matter and chlorophyll-a in Lake Huron using Sentinel-2 measurements. Journal of Applied Remote Sensing 11(03): 1.

Cho, K. H., Cha, S. M., Kang, J. H., Lee, S. W., Park, Y., Kim, J. W., Kim, J. H. (2010). Meterological effect on the levels of fecal indicator bacteria in an urban stream: a modeling approach. Water Res. 44(7): 2189-202.

CEFAS (2014). Microbiological Monitoring of Bivalve Molluscs Harvesting Areas. Guide to Good Practice: Technical Application. EU Working Group on the Microbiological Monitoring of Bivalve Molluscs Harvesting Areas.

Doxani, G., Vermote, E., Roger, J-C., Gascon, F., Adriaensen, S., Frantz, D., Hagolle, O., Hollstein, A., Kirches, G., Li, F., Louis, J., Mangin, A., Pahlevan, N., Pflug, B., Venhellemont, Q. (2018). Atmospheric Correction Inter-Comparison Exercise. Remote Sensing 10(2): 352.

Faour, G., Mario, M., Najem, S. A. (2015). Regional Landsat-Based Drought Monitoring from 1982 to 2014. Climate 3: 563-577.

Giardino, C., Brando, V. E., Gege, P., Pinnel, N., Hochberg, E., Knaeps, E., Reusen, I., Doerffer, R., Bresciani, M., Braga, F., Foerster, S., Champollion, N., Dekker, A. (2019). Imaging Spectrometry of Inland and Coastal Waters: State of the Art, Achievements and Perspectives. Surveys in Geophysics 40(3): 401-429.

Gordon, H., Brown, J. W., Brown, O. B., Evans, R. H., Smith. R. C. (1988). A semianalytic radiance model of ocean color. Journal of Geophysical Research Atmospheres 93(10).

Grant, J., Bacher. C., Ferreira, J. G., Groom, S., Morales, J., Benito, C. V. R., Saitoh, S. I., Sathyendranath, S., Stuart, V. (2008). Remote Sensing applications in marine aquaculture. Remote sensing in fisheries and aquaculture (chapter: 6).

Hopkins J., Lucas, M., Dufau, C., Sutton, M., Stum, J., Lauret, O., Channelliere, C. (2013). Detection and variability of the Congo River plume from satellite derived sea surface temperature, salinity, ocean colour and sea level. Remote Sensing of Environment 139: 365-385.

Huizeng, L., Qingquan, L., Tiezhu, S., Shuibo, H., Guofeng, W., Qiming, Z. (2017). Application of Sentine 2 MSI Images to Retrieve Suspended Particulate Matter Concentrations in Poyang Lake. Remote Sensing 9(7).

Jaelani, L. M., Alfatinah, A. (2017). Sea Surface Temperature Mapping at Medium Scale Using Landsat 8 – TIRS Satellite Image. Regional Conference in Civil Engineering (RCCE). The Third International Conference on Civil Engineering Research (ICCER)

Lahet, F., Stramski, D. (2010). MODIS imagery of turbid plumes in San Diego coastal waters during rainstorm events. Remote Sensing of Environment 114: 332-344.

Laureano-Rosario, A. E., Symonds, E. M., Rueda-Roa, D., Otis, D., Muller-Karger, F. E. (2017). Environmental Factors Correlated with Culturable Enterococci Concentrations in Tropical Recreational Waters: A Case Study in Escambron Beach, San Juan, Puerto Rico. Int J Environ Res Public Health 14(12).

Lesar, T. T., Filipčić, A. (2017). Multiple Linear Regression (MLR) model simulation of hourly PM10 concentrations during sea breeze events in the Split area. Naše More 64(3): 77-85

Mallin, M. A. (2009). Effect of Human Land Development on Water Quality. Handbook of Water Purity and Quality: 67-90.

Mihanović, H., Cosoli, S., Vilibić, I., Ivanković, D., Dadić, V., Gačić, M. (2011). Surface current patterns in the northern Adriatic extracted from high-frequency radar data using self-organizing map analysis. Journal of Geophysical Research: Oceans 116: C8.

Mishra, S., Mishr,a, D. (2012). Normalized difference chlorophyll index: A novel model for remote estimation of chlorophyll-a concentration in turbid productive waters. Remote Sensing of Environment 117: 394-406.

Nezlin, N. P., DiGiacomo, P. M., Stein, E. D., Ackerman. D. (2005). Stormwater runoff plumes observed by SeaWiFS radiometer in the Southern California Bight. Remote Sensing of Environment 98(4): 494-510.

Pastres, R. (2017). Primavera-estate 2017: eccezione o assaggio del clima che verrà. VI Convegno SIRAM.

Radiarta, N., Saitoh, S.I. Miyazono, A. (2008). GIS-based multicriteria evaluation models for identifying suitable sites for Japanese scallop (Mizuhopecten yessoensis) aquaculture in Funka Bay, southwestern Hokkaido, Japan. Aquaculture 284(1-4): 127-135.

Shi, W., Zhang, Y., Wang, M. (2018). Deriving Total Suspended Matter Concentration from the Near-Infrared-Based Inherent Optical Properties over Turbid Waters: A Case Study in Lake Taihu. Remote Sensing 10: 333.

Sillmann, J., Roeckner, E. (2007). Indices for extreme events in projections of anthropogenic climate change. Climatic Change 86(1): 83-104.

Song, K., Li, L., Wang, Z., Liu, D., Zhang, B., Xu, J., Du, J., Li, L., Li, S., Wang, Y. (2011). Retrieval of total suspended matter (TSM) and chlorophyll-a (Chl-a) concentration from remote sensing data for drinking water resources. Environmental Monitoring and Assessment 184(3): 1449-1470.

Thomas, Y., Mazurié, J., Alunno-Bruscia, M., Bacher, C., Bouget, J., Gohin, F., Pouvreau, S., Struski, C. (2011). Modelling spatio-temporal variability of Mytilus edulis (L.) growth by forcing a dynamic energy budget model with satellite-derived environmental data. Journal of Sea Research 66(4): 308-317.

Thomas, Y., Cassou, C., Gernez, P., Pouvreau, S. (2018). Oysters as sentinels of climate variability and climate change in coastal ecosystems. Environmental Research Letters.

Van Rijn, L. C. (2010). Tidal Phenomena in the Scheldt Estuary. Deltares Project.

Vermote, E., Justice, C., Claverie, M., Franch, B. (2016). Prelminary analysis of the performance of the Landsat 8/OLI land surface reflectance product. Remote Sensing of Environment 185: 45-56.

Wang, C., Chen, S., Li, D., Wang, D., Liu, W., Yang, J. (2017). A Landsat-based model for retrieving total suspended solids concentration of estuaries and coasts in China. Geosci. Model Dev. 10: 4347-4365.

World Meteorological Organization (2018). Guidelines on the definition and monitoring of extreme weather and climate events 13:10.

Yang, Z. (2016). Estimating Chlorophyll-A Concentration in a Freshwater Lake Using Landsat 8 Imagery. Journal of Environment and Earth Science 6:4. ISSN 2224-3216 (Paper).

Zhao, J., Temimi, M., Ghedira, H. (2017). Remotely sensed sea surface salinity in the hyper-saline Arabian Gulf: Application to landsat 8 OLI data. Estuarine. Coastal and Shelf Science 187: 168-177.

Zhaojun, S., Haifeng L., Zhenyan, W., Xiaoming, L. (2010). Remote sensing retrieval of total suspended matter near tidal sand ridges off the coast of Jiangsu. The 2nd Conference on Environmental Science and Information Application Technology.

Zonn, I. S., Kostrianoy, G. (2017). The Adriatic Sea. The Boka Kotorska Bay Environment. Hbd. Env. Chem. 54: 19-42.

Corrigendum to Regulation (EC) No 854/2004 of the European Parliament and of the Council of 29 April 2004 laying down specific rules for the organisation of official controls on products of animal origin intended for human consumption.

Commission Regulation (EC) No 2073/2005 of 15 November 2005 on microbiological criteria for foodstuffs.

Commission Regulation (EU) 2015/2285 of 8 December 2015 amending Annex II to Regulation (EC) No 854/2004 of the European Parliament and of the Council laying down specific rules for the organisation of official controls on products of animal origin intended for human consumption as regards certain requirements for live bivalve molluscs. echinoderms. tunicates and marine gastropods and Annex I to Regulation (EC) No 2073/2005 on microbiological criteria for foodstuffs

Websites:

Devotes: http://www.devotes-project.eu/adriatic-sea/
Eumofa: http://www.eumofa.eu/it/web/eumofa/ad-hoc-queries3
Eurostat: https://ec.europa.eu/eurostat/statistics-explained/index.php?title=Aquaculture_statistics&oldid=356961
Fao: http://www.fao.org/fishery/countrysector/naso_italy/en
NASA: https://landsat.gsfc.nasa.gov/landsat-data-continuity-mission/
Ugeo Urbistat: https://ugeo.urbistat.com/AdminStat/en/it/demografia/popolazione/veneto/5/2

GEE SCRIPTS

TOTAL SUSPENDED MATTER

```
//Mapping Venetian Lagoon: tidal areas and suspended sediment
//=====================================
var cloudcov = 20; // remove scenes with more than ## percent cloud
var years    = [2013,2019]; // [from. to]
// get data ===========================================
var ls8_toa       = ee.ImageCollection("LANDSAT/LC08/C01/T1_TOA"); // Landsat Image
collection
var venezia = ee.Geometry.Point(12.30.45.25); // center  of general area of interest
var laguna = ee.Geometry.Polygon(
                    [[[13.10. 46.05],
                    [13.10. 44.45],
                    [11.50. 44.45],
                    [11.50. 46.05]]]);

// filter the landsat 8 collection and rename bands
var ls8_toa = ls8_toa
       .filterBounds(laguna)
       .filterDate( years[0]+'-01-01', years[1]+'-12-31' )
       .filter(ee.Filter.lte('CLOUD_COVER'.cloudcov))
       .map(function(x){
         return x.select(['B2','B3','B4','B5','B6','BQA','B10','B11'])
                .rename(['blue','green','red','nir','swir1','bqa','b10','b11'])
});

print(ls8_toa)

//=====================================

// apply cloud mask on per-image basis and add Normalized Difference Water Index band
var lsmasked = ls8_toa.map(function(x){                    // loop over image collection
// Cloud and Shade Masking
  // cloud mask bit from QA band (bit 4)
  var cloudBitPattern = ee.Number(2).pow(4).int();
  // shadow mask bits from QA band (bit 7 and 8)
  var shadeBitsPattern = ee.Number(2).pow(7).add(ee.Number(2).pow(8)).int();
  //combine cloud and shade into single binary mask band
  var mask = x.select('bqa').bitwiseAnd(cloudBitPattern).rightShift(4).eq(0).and(
           x.select('bqa').bitwiseAnd(shadeBitsPattern).rightShift(7).lte(1))
  var masked = x.updateMask(mask)                          // apply mask to the image

// Water index calculation
  var index   = x.normalizedDifference(['green', 'nir'])     // calculate NDWI
               .rename('index')
  var invindex = ee.Image.constant(0).subtract(index)        // change sign of the index
               .rename('invindex')
```

```
  var tsm = x.expression(
    '2.7 * exp(19.0 * RED)'.
      { 'RED': x.select('red') }
    )
    .rename('tsm')

  // return masked image incl. the two index bands
  return masked.addBands(index).addBands(invindex).addBands(tsm).addBands(Temp) })

// Find and map tidal areas ========================================
var indexperc = lsmasked.select(['index']).reduce(ee.Reducer.percentile([20.95]. ['lo','hi']))    // get
image with low and high percentile NDWI
var lsmasked  = lsmasked.map(function(x){                          // loop over image collection
  var selector = x.select('index').subtract(indexperc).abs()        // get absolute difference of the
percentiles with the NDWI
  var invsel   = ee.Image.constant(1).divide(selector)              // invert to let the min diff be the
largest value
  return x.addBands(invsel.rename(['selector_lo','selector_hi']))    // add inverted difference band to
the image and name properly
})

// Quality mosaic and ading
var minwat  = lsmasked.qualityMosaic('selector_lo')
var maxwat  = lsmasked.qualityMosaic('selector_hi')
Map.addLayer(minwat, {min:0. max:0.3. bands:['nir','red','green']}, 'LT composite v2', false)
Map.addLayer(maxwat.,{min:0. max:0.3. bands:['nir','red','green']}, 'HT composite v2', false)


// Calculate suspended matter content for water area
========================================

var TSM = meanwat.expression(
    '2.7 * exp(19.0 * RED)'.
      { 'RED': meanwat.select('red') }
    )
  .updateMask(minwat2.select('index').gte(0.09))
Map.addLayer(TSM, {min:0, max:50, palette: ['blue'.'yellow'.'red']}, 'TSM', true)

// Export a cloud-optimized GeoTIFF
Export.image.toDrive({
  image: TSM,
  description: 'TSMtoGeoTIFF',
  scale: 30,
  region: laguna,
  fileFormat: 'GeoTIFF',
  formatOptions: {
    cloudOptimized: true
  }
});
```

SEA SURFACE TEMPERATURE

```
//8. Mapping the Venetian Lagoon: sea surface temperature
//=====================================
var cloudcov = 20; // remove scenes with more than ## percent cloud
var years    = [2013,2019]; // [from, to]
var tempVis =
{"opacity":1,"bands":["B10"],"min":7.748000000000034,"max":12.452000000000012,"palette":["2
33eff","34b4ff","42f6ff","6bff46","e6ff1f","ff9e27","ff661d"]};
// get data ====================================
var ls8_toa      = ee.ImageCollection("LANDSAT/LC08/C01/T1_SR"); // Landsat Image collection
var venezia = ee.Geometry.Point(12.30,45.25); // center  of general area of interest
var laguna = ee.Geometry.Polygon(
                  [[[13.10, 46.05].
                  [13.10, 44.45].
                  [11.50, 44.45].
                  [11.50, 46.05]]]);

// filter the landsat 8 collection and rename bands
var ls8_toa = ls8_toa
      .filterBounds(laguna)
      .filterDate( years[0]+'-01-01', years[1]+'-12-31' )
      .filter(ee.Filter.lte('CLOUD_COVER'.cloudcov))
      .map(function(x){
        return x.select(['B2','B3','B4','B5','B6','pixel_qa','B10',’B11’])
              .rename([‘blue’,’green’,’red’,’nir’,’swir1’,'bqa','b10','b11'])
});

print(ls8_toa)

//=====================================

// apply cloud mask on per-image basis and add Normalized Difference Water Index band
var lsmasked = ls8_toa.map(function(x){                    // loop over image collection
// Cloud and Shade Masking
  // cloud mask bit from QA band (bit 4)
  var cloudBitPattern = ee.Number(2).pow(4).int();
  // shadow mask bits from QA band (bit 7 and 8)
  var shadeBitsPattern = ee.Number(2).pow(7).add(ee.Number(2).pow(8)).int();
  //combine cloud and shade into single binary mask band
  var mask = x.select('bqa').bitwiseAnd(cloudBitPattern).rightShift(4).eq(0).and(
           x.select('bqa').bitwiseAnd(shadeBitsPattern).rightShift(7).lte(1))
  var masked = x.updateMask(mask)                          // apply mask to the image

// Water index calculation
  var index   = x.normalizedDifference(['green','nir'])     // calculate NDWI
              .rename('index')
  var invindex = ee.Image.constant(0).subtract(index)        // change sign of the index
```

```
                .rename('invindex')
  var Temp = x.expression(
    '(B10 * 0.1) - 273.15',
      { 'B10': x.select('b10') }
      )
    .rename('Temp')
  var Temp1 = x.expression(
    '(B11 * 0.1) - 273.15',
      { 'B11': x.select('b11') }
      )
    .rename('Temp1')
  // return masked image incl. the two index bands
  return
masked.addBands(index).addBands(invindex).addBands(tsm).addBands(Temp).addBands(Temp1)
})

// Calculate sea surface temperature for the two thermal bands b10, b11
=======================================

var Temp = meanwat.expression(
    '(B10 * 0.1) - 273.15',
      { 'B10': meanwat.select('b10') }
    )
  .updateMask(minwat2.select('index').gte(0.09))
Map.addLayer(Temp, {min:0, max:30, palette: ['blue','yellow','red']}, 'Temp', true)

var Temp1 = meanwat.expression(
    '(B11 * 0.1) - 273.15',
      { 'B11': meanwat.select('b11') }
    )
  .updateMask(minwat2.select('index').gte(0.09))
Map.addLayer(Temp1, {min:0, max:30, palette: ['blue','yellow','red']}, 'Temp1', true)

// Export a cloud-optimized GeoTIFF.
Export.image.toDrive({
  image: Temp,
  description: 'TemptoGeoTIFF',
  scale: 30,
  region: laguna,
  fileFormat: 'GeoTIFF',
  formatOptions: {
    cloudOptimized: true
  }
});
Export.image.toDrive({
  image: Temp1,
  description: 'Temp1toGeoTIFF',
  scale: 30,
  region: laguna,
  fileFormat: 'GeoTIFF',
```

```
  formatOptions: {
    cloudOptimized: true
  }
});
```

R SCRIPTS

SST & TSM ANALYSIS (Shellfishfarm – River Mouth – Opensea)

```
setwd("~/Desktop/CSV-Molcol+Rivers")
library(lubridate)
library(dplyr)
library(tidyr)
library(tidyverse)
library(chron)
library(date)
library(data.table)
library(sqldf)
library(wesanderson)
library(magrittr)
library(metR)
library(gghighlight)

#### Sea Surface Temperature Comparison: ####

sst_MC <- read.csv("LandsatMC30Tempb10.csv",sep=",",row.names = NULL)
sst_MC <- edit(sst_MC)
sst_MC <- sst_MC %>% separate(row.names, c("m", "d"), " ")
sst_MC$NewCol <- paste(sst_MC$d, sst_MC$m, sst_MC$system.time_start, sep="-")

sst_Foce <- read.csv("LandsatDeltaPo2Tempb10.csv",sep=",",row.names = NULL)
sst_Foce <- edit(sst_Foce)
sst_Foce <- sst_Foce %>% separate(row.names, c("m", "d"), " ")
sst_Foce$NewCol <- paste(sst_Foce$d, sst_Foce$m, sst_Foce$system.time_start, sep="-")

sst_Opensea <- read.csv("LandsatOpenseaTempb10.csv",sep=",",row.names = NULL)
sst_Opensea <- edit(sst_Opensea)
sst_Opensea <- sst_Opensea %>% separate(row.names, c("m", "d"), " ")
sst_Opensea$NewCol <- paste(sst_Opensea$d, sst_Opensea$m, sst_Opensea$system.time_start,
sep="-")

data_sstMC <- sst_MC$NewCol
write.csv(data_sstMC,"data_sstMC.csv")
#converti le date su excel in formato dd/mm/yyyy#
data_sstMC <- read.csv("data_sstMC.csv")
data_sstMC <- as.Date(data_sstMC$x, format = "%d/%m/%Y")

data_sstFoce <- sst_Foce$NewCol
write.csv(data_sstFoce,"data_sstFoce.csv")
#converti le date su excel#
data_sstFoce <- read.csv("data_sstFoce.csv")
data_sstFoce <- as.Date(data_sstFoce$x, format = "%d/%m/%Y")

data_sstOpensea <- sst_Opensea$NewCol
```

```
write.csv(data_sstOpensea,"data_sstOpensea.csv")
#converti le date su excel#
data_sstOpensea <- read.csv("data_sstOpensea.csv")
data_sstOpensea <- as.Date(data_sstOpensea$x, format = "%d/%m/%Y")

newSST_MC <- cbind.data.frame(sst_MC$Temp, data_sstMC)
setnames(newSST_MC, "data_sstMC", "data")
setnames(newSST_MC, "sst_MC$Temp", "Temp")

newSST_Foce <- cbind.data.frame(sst_Foce$Temp, data_sstFoce)
setnames(newSST_Foce, "data_sstFoce", "data")
setnames(newSST_Foce, "sst_Foce$Temp", "Temp")

newSST_OS <- cbind.data.frame(sst_Opensea$Temp, data_sstOpensea)
setnames(newSST_OS, "data_sstOpensea", "data")
setnames(newSST_OS, "sst_Opensea$Temp", "Temp")

# Ottieni le SST sulle stesse date #
newdata_sst <- sqldf("
                SELECT *
                FROM newSST_MC MC JOIN newSST_Foce FC
                ON MC.data = FC.data
                ")
newdata_sst1 <- sqldf("
                SELECT *
                FROM newdata_sst ND JOIN newSST_OS OS
                ON ND.data = OS.data
                ")
newdata_sst1 <- newdata_sst1[!duplicated(newdata_sst1$data), ]

# Elimina Outliers #
newdata_sst1 <- subset(newdata_sst1,newdata_sst1$Temp>0)
newdata_sst1 <- subset(newdata_sst1,newdata_sst1$Temp..3>0)
newdata_sst1 <- subset(newdata_sst1,newdata_sst1$Temp..5>0)

# Calcolo dei percentili e probabilità di superamento #
QQtemp <- quantile(newdata_sst1$Temp..3,probs = 0.95)
ntemp_greater_QQ <- nrow(newdata_sst1[newdata_sst1$Temp>QQtemp, ])
perctemp <- (ntemp_greater_QQ/nrow(newdata_sst1))*100
QQtemp1 <- quantile(newdata_sst1$Temp..3,probs = 0.05)
ntemp_smaller_QQ1 <- nrow(newdata_sst1[newdata_sst1$Temp<QQtemp1, ])
perctemp1 <- (ntemp_smaller_QQ1/nrow(newdata_sst1))*100

# Plotta il risultato #
ggplot(newdata_sst1) + geom_line(aes(x=data, y=Temp, col="SF-t")) +
  geom_line(aes(x=data, y=Temp..3, col="Po Mouth"))+
  geom_line(aes(x=data, y=Temp..5, col="Opensea"))+
  labs(x="Date", y="SST [°C]") +
  scale_color_discrete(name="Legend") + labs(title="SST: ShellfishFarm - Po Mouth - Open Sea")
# plot multiple time series using 'geom_line's
```

```
#### Total Suspended Matter Comparison: ####

tsm_MC <- read.csv("LandsatMC30TSM.csv",sep=",",row.names = NULL)
tsm_MC <- edit(tsm_MC)
tsm_MC <- tsm_MC %>% separate(row.names, c("m", "d"), " ")
tsm_MC$NewCol <- paste(tsm_MC$d, tsm_MC$m, tsm_MC$system.time_start, sep="-")

tsm_Foce <- read.csv("LandsatDeltaPo2TSM.csv",row.names = NULL)
tsm_Foce <- edit(tsm_Foce)
tsm_Foce <- tsm_Foce %>% separate(row.names, c("m", "d"), " ")
tsm_Foce$NewCol <- paste(tsm_Foce$d, tsm_Foce$m, tsm_Foce$system.time_start, sep="-")

tsm_Opensea <- read.csv("LandsatOpenseaTSM.csv",row.names = NULL)
tsm_Opensea <- edit(tsm_Opensea)
tsm_Opensea <- tsm_Opensea %>% separate(row.names, c("m", "d"), " ")
tsm_Opensea$NewCol <- paste(tsm_Opensea$d, tsm_Opensea$m,
tsm_Opensea$system.time_start, sep="-")

data_tsmMC <- tsm_MC$NewCol
write.csv(data_tsmMC,"data_tsmMC.csv")
#converti data su excel#
data_tsmMC <- read.csv("data_tsmMC.csv")
data_tsmMC <- as.Date(data_tsmMC$x, format = "%d/%m/%Y")

data_tsmFoce <- tsm_Foce$NewCol
write.csv(data_tsmFoce,"data_tsmFoce.csv")
#converti data su excel#
data_tsmFoce <- read.csv("data_tsmFoce.csv")
data_tsmFoce <- as.Date(data_tsmFoce$x, format = "%d/%m/%Y")

data_tsmOpensea <- tsm_Opensea$NewCol
write.csv(data_tsmOpensea,"data_tsmOpensea.csv")
#converti data su excel#
data_tsmOpensea <- read.csv("data_tsmOpensea.csv")
data_tsmOpensea <- as.Date(data_tsmOpensea$x, format = "%d/%m/%Y")

newTSM_MC <- cbind.data.frame(tsm_MC$tsm, data_tsmMC)
setnames(newTSM_MC, "data_tsmMC", "data")
setnames(newTSM_MC, "tsm_MC$tsm", "TSM")

newTSM_Foce <- cbind.data.frame(tsm_Foce$tsm, data_tsmFoce)
setnames(newTSM_Foce, "data_tsmFoce", "data")
setnames(newTSM_Foce, "tsm_Foce$tsm", "TSM")

newTSM_Opensea <- cbind.data.frame(tsm_Opensea$tsm, data_tsmOpensea)
setnames(newTSM_Opensea, "data_tsmOpensea", "data")
setnames(newTSM_Opensea, "tsm_Opensea$tsm", "TSM")
```

```
# Ottieni la TSM sulle stesse date #
newdata_tsm <- sqldf("
                SELECT *
                FROM newTSM_MC MCt JOIN newTSM_Foce FCt
                ON MCt.data = FCt.data
                ")
newdata_tsm1 <- sqldf("
                SELECT *
                FROM newdata_tsm NDt JOIN newTSM_Opensea OSt
                ON NDt.data = OSt.data
                ")
newdata_tsm1 <- newdata_tsm1[!duplicated(newdata_tsm1$data), ]

# Elimina Outliers #
newdata_tsm1 <- subset(newdata_tsm1,newdata_tsm1$TSM<100)
newdata_tsm1 <- subset(newdata_tsm1,newdata_tsm1$TSM..3<200)
newdata_tsm1 <- subset(newdata_tsm1,newdata_tsm1$TSM..5<50)

# Calcolo dei percentili e probabilità di superamento #
QQtsm <- quantile(newdata_tsm1$TSM..3,probs = 0.90)
ntsm_greater_QQ <- nrow(newdata_tsm1[newdata_tsm1$TSM>QQtsm, ])
perctsm <- (ntsm_greater_QQ/nrow(newdata_tsm1))*100

# Plotta il risultato #
ggplot(newdata_tsm1) + geom_line(aes(x=data, y=TSM, col="SF-t")) +
  geom_line(aes(x=data, y=TSM..3, col="Po Mouth"))+
  geom_line(aes(x=data, y=TSM..5, col="Opensea"))+
  labs(x="Date", y="TSM [g/m3]") +
  scale_color_discrete(name="Legend") + labs(title="TSM: ShellfishFarm - Po Mouth - Opensea")
# plot multiple time series using 'geom_line's


#### Crea CSV per estrapolare SST e TSM sopra e sotto 80 perc. di portata ####
write.csv(newdata_sst1,"newdatasst.csv")
write.csv(newdata_tsm1,"newdatatsm.csv")


#### CALCOLO DELLE DIFFERENZE TRA TSM E TEMP - MARE APERTO COME
RIFERIMENTO ####
difftsm <- cbind.data.frame(newdata_tsm1$data, newdata_tsm1$TSM - newdata_tsm1$TSM..5,
newdata_tsm1$TSM..3 - newdata_tsm1$TSM..5)
diffsst <- cbind.data.frame(newdata_sst1$data, newdata_sst1$Temp - newdata_sst1$Temp..5,
newdata_sst1$Temp..3 - newdata_sst1$Temp..5)
setnames(difftsm, "newdata_tsm1$data", "data")
setnames(diffsst, "newdata_sst1$data", "data")

differenze <- sqldf("
                SELECT *
                FROM  difftsm TS JOIN diffsst ST
                ON TS.data = ST.data
```

```
                ")
differenze <- differenze[!duplicated(differenze$data), ]
differenze$data..4 <- NULL
setnames(differenze, "newdata_tsm1$TSM - newdata_tsm1$TSM..2", "TSM_SF")
setnames(differenze, "newdata_tsm1$TSM..3 - newdata_tsm1$TSM..3", "TSM_RM")
setnames(differenze, "newdata_sst1$Temp - newdata_sst1$Temp..5", "SST_SF")
setnames(differenze, "newdata_sst1$Temp..3 - newdata_sst1$Temp..6", "SST_RM")

diffSF <- sqrt((differenze$TSM_SF)^2 + (differenze$SST_SF)^2)
diffRM <- sqrt((differenze$TSM_RM)^2 + (differenze$SST_RM)^2)

differenzeSF <- cbind.data.frame(differenze$data, differenze$TSM_SF, differenze$SST_SF)
setnames(differenzeSF, "differenze$TSM_SF", "TSM_SF")
setnames(differenzeSF, "differenze$SST_SF", "SST_SF")
differenzeRM <- cbind.data.frame(differenze$data, differenze$TSM_RM, differenze$SST_RM)
setnames(differenzeRM, "differenze$TSM_RM", "TSM_RM")
setnames(differenzeRM, "differenze$SST_RM", "SST_RM")

#### CALCOLO STANDARD DEVIATION E NORMALIZZAZIONE CAMPIONE ####
stdfSFtsm <- sd(differenzeSF$TSM_SF)
stdfSFsst <- sd(differenzeSF$SST_SF)
stdfRMtsm <- sd(differenzeRM$TSM_RM)
stdfRMsst <- sd(differenzeRM$SST_RM)
TSMnormSF <- differenzeSF$TSM_SF/stdfSFtsm
SSTnormSF <- differenzeSF$SST_SF/stdfSFsst
TSMnormRM <- differenzeRM$TSM_RM/stdfRMtsm
SSTnormRM <- differenzeRM$SST_RM/stdfRMsst

diffSFnorm <- sqrt((TSMnormSF)^2 + (SSTnormSF)^2)
diffRMnorm <- sqrt((TSMnormRM)^2 + (SSTnormRM)^2)
DiffSFnorm <- cbind.data.frame(differenze$data, diffSFnorm)
DiffRMnorm <- cbind.data.frame(differenze$data, diffRMnorm)
setnames(DiffSFnorm, "differenze$data", "data")
setnames(DiffRMnorm, "differenze$data", "data")

Diffnorm <- sqldf("
                SELECT *
                FROM  DiffSFnorm DS JOIN DiffRMnorm DR
                ON DS.data = DR.data
                ")
Diffnorm <- Diffnorm[!duplicated(Diffnorm$data), ]
Diffnorm$data..3 <- NULL

QQnormSF <- quantile(DiffSFnorm$diffSFnorm,probs = 0.80)
nSF_greater_QQ <- nrow(DiffSFnorm[DiffSFnorm$diffSFnorm>QQnormSF, ])
percSF <- (nSF_greater_QQ/nrow(DiffSFnorm))*100
QQnormRM <- quantile(DiffRMnorm$diffRMnorm,probs = 0.80)
nRM_greater_QQ <- nrow(DiffRMnorm[DiffRMnorm$diffRMnorm>QQnormRM, ])
percRM <- (nRM_greater_QQ/nrow(DiffRMnorm))*100
```

```
Diffreg <- cbind.data.frame(Diffnorm$diffSFnorm, Diffnorm$diffRMnorm)

DNsub <- subset(Diffnorm, diffSFnorm > 1.01 & diffRMnorm > 2.05)
write.csv(DNsub,"Diffnorm.csv")

corr <- cor.test(x=Diffnorm$diffRMnorm, y=Diffnorm$diffSFnorm, method = 'spearman')

regression <- combn(names(Diffreg), 2, function(x){coefficients(lm(Diffreg[, x]))}, simplify =
FALSE)
vars <- combn(names(Diffreg), 2)
names(regression) <- vars[1 , ] # adding names to identify variables in the reggression
regression

Campionenormale <- cbind.data.frame(TSMnormSF, SSTnormSF, TSMnormRM, SSTnormRM)

# PLOT DEI RISULTATI #
q <- ggplot()
q + geom_point(aes(x=diffRMnorm, y=diffSFnorm, colour = diffRMnorm > 2.05 & diffSFnorm >
1.01), shape=19, size=1) +
  scale_color_manual(values = c("blue", "red")) +
  theme(legend.position = "none") +
  labs(x = "Dist RM") +
  labs(y = "Dist SF") +
  labs(title="Norm Dist")
```

APPENDIX

SEA SURFACE TEMPERATURE AND TOTAL SUSPENDED MATTER TIME SERIES

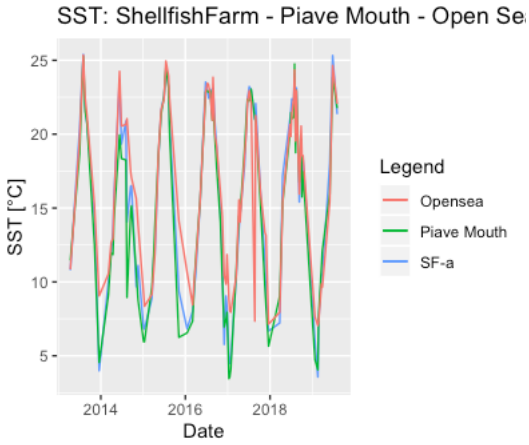

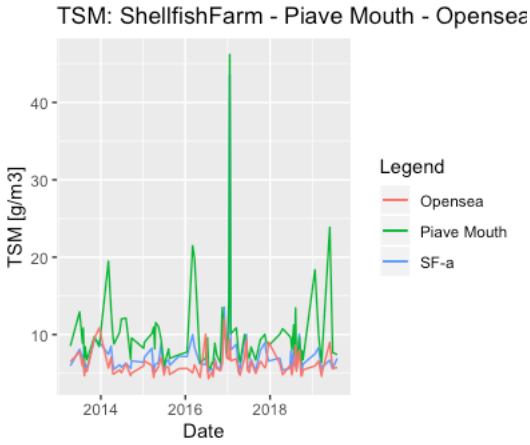

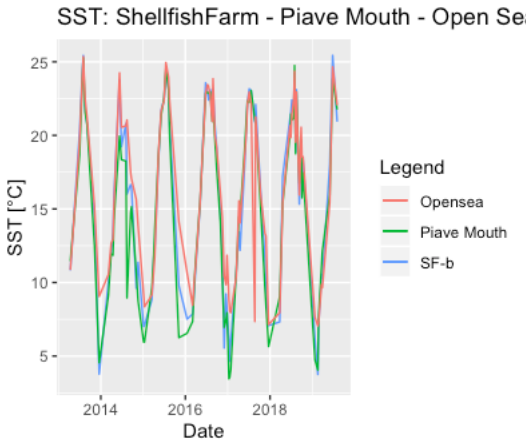

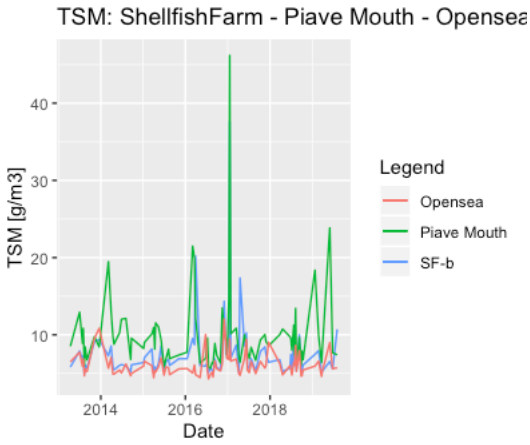

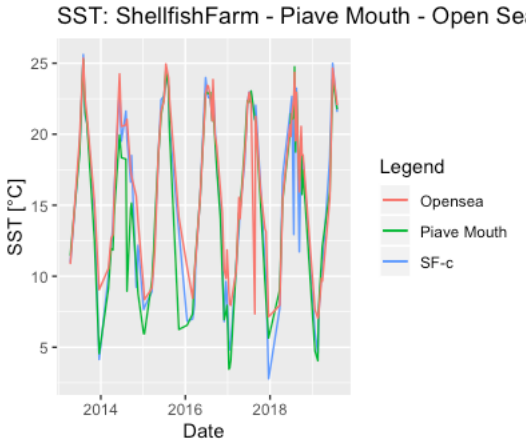

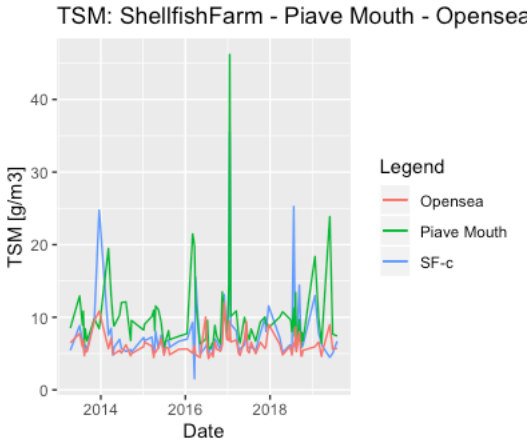

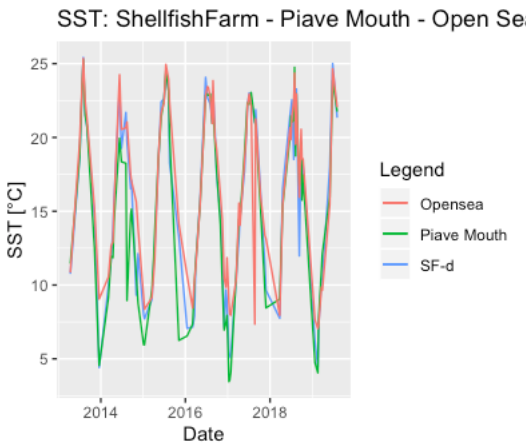
SST: ShellfishFarm - Piave Mouth - Open Se
SST [°C]
25
20
15
10
5
2014
2016
2018
Date
Legend
Opensea
Piave Mouth
SF-d

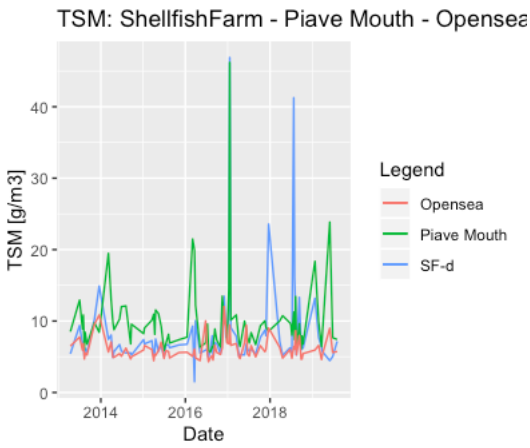
TSM: ShellfishFarm - Piave Mouth - Opensea
TSM [g/m3]
40
30
20
10
0
2014
2016
2018
Date
Legend
Opensea
Piave Mouth
SF-d

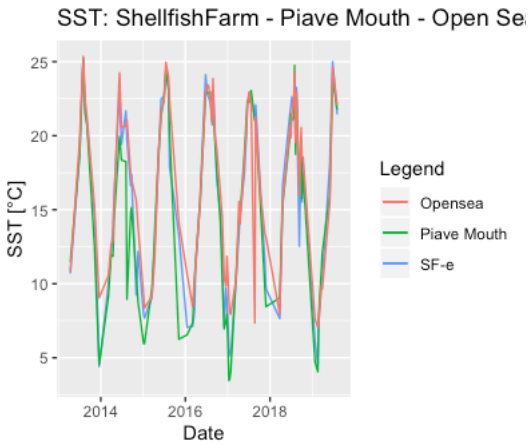
SST: ShellfishFarm - Piave Mouth - Open Se
SST [°C]
25
20
15
10
5
2014
2016
2018
Date
Legend
Opensea
Piave Mouth
SF-e

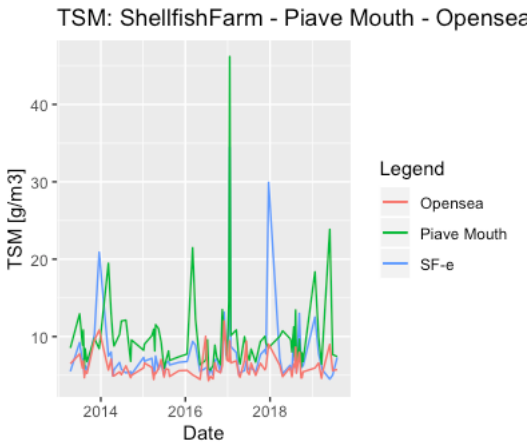
TSM: ShellfishFarm - Piave Mouth - Opensea
TSM [g/m3]
40
30
20
10
2014
2016
2018
Date
Legend
Opensea
Piave Mouth
SF-e

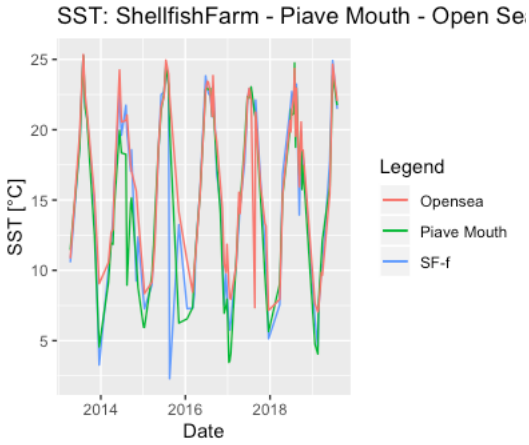
SST: ShellfishFarm - Piave Mouth - Open Se
SST [°C]
25
20
15
10
5
2014
2016
2018
Date
Legend
Opensea
Piave Mouth
SF-f

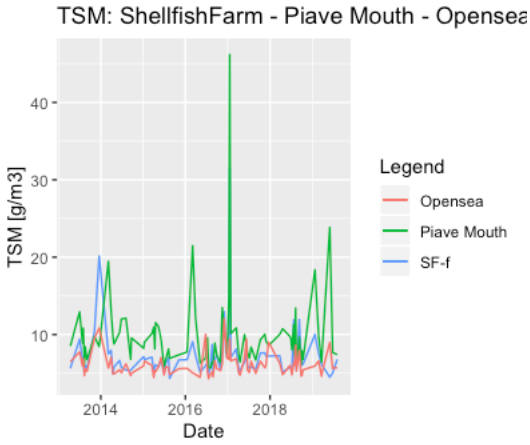
TSM: ShellfishFarm - Piave Mouth - Opensea
TSM [g/m3]
40
30
20
10
2014
2016
2018
Date
Legend
Opensea
Piave Mouth
SF-f

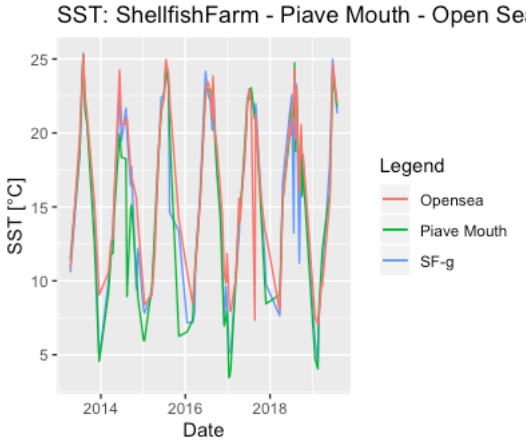
SST: ShellfishFarm - Piave Mouth - Open Se
SST [°C]
25
20
15
10
5
2014
2016
2018
Date
Legend
Opensea
Piave Mouth
SF-g

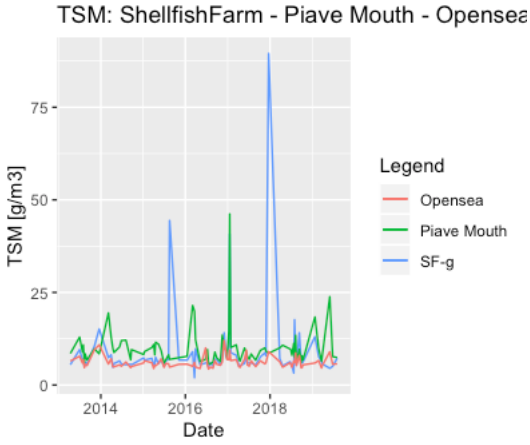
TSM: ShellfishFarm - Piave Mouth - Opensea
TSM [g/m3]
75
50
25
0
2014
2016
2018
Date
Legend
Opensea
Piave Mouth
SF-g

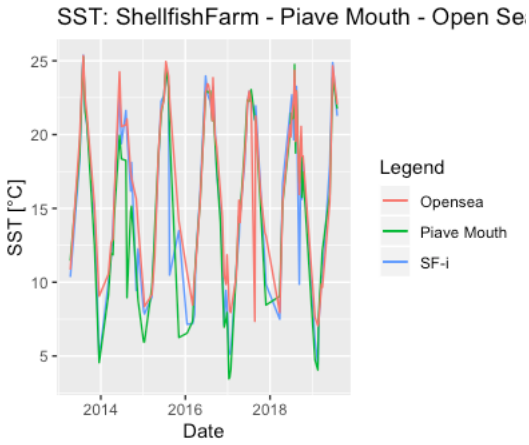
SST: ShellfishFarm - Piave Mouth - Open Se
SST [°C]
25
20
15
10
5
2014
2016
2018
Date
Legend
Opensea
Piave Mouth
SF-i

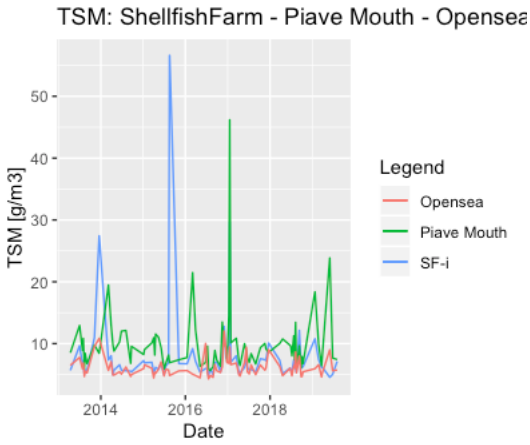
TSM: ShellfishFarm - Piave Mouth - Opensea
TSM [g/m3]
50
40
30
20
10
2014
2016
2018
Date
Legend
Opensea
Piave Mouth
SF-i

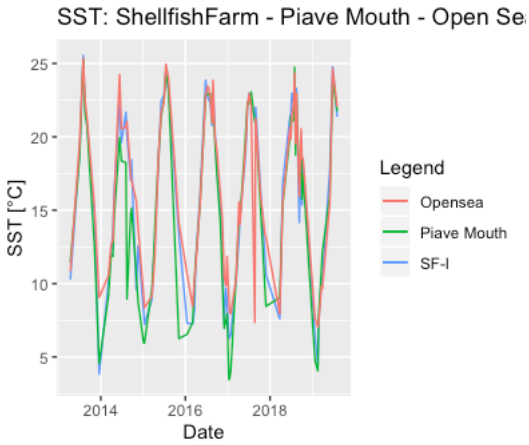
SST: ShellfishFarm - Piave Mouth - Open Se
SST [°C]
25
20
15
10
5
2014
2016
2018
Date
Legend
Opensea
Piave Mouth
SF-I

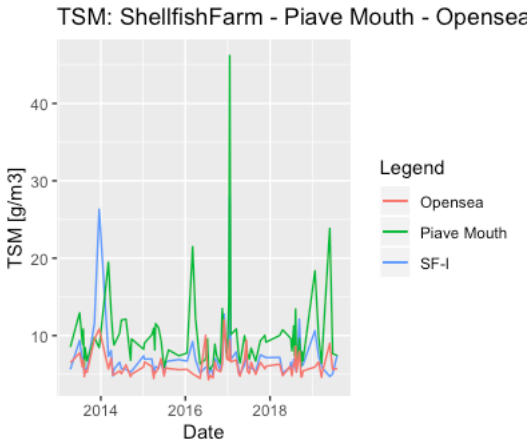
TSM: ShellfishFarm - Piave Mouth - Opensea
TSM [g/m3]
40
30
20
10
2014
2016
2018
Date
Legend
Opensea
Piave Mouth
SF-I

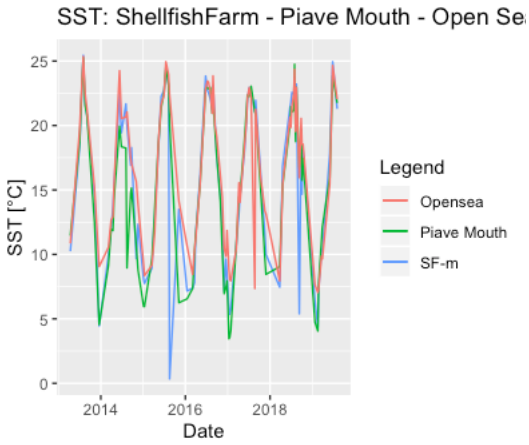
SST: ShellfishFarm - Piave Mouth - Open Se
SST [°C]
25
20
15
10
5
0
2014
2016
2018
Date
Legend
Opensea
Piave Mouth
SF-m

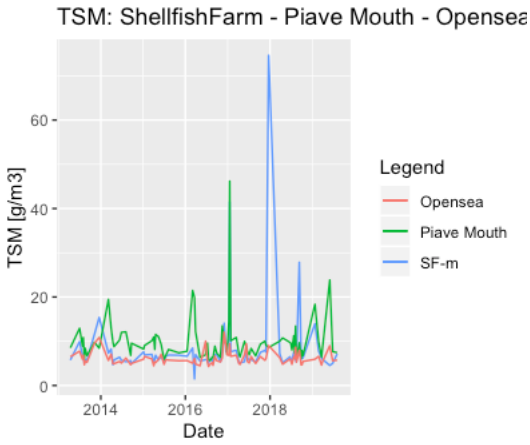
TSM: ShellfishFarm - Piave Mouth - Opensea
TSM [g/m3]
60
40
20
0
2014
2016
2018
Date
Legend
Opensea
Piave Mouth
SF-m

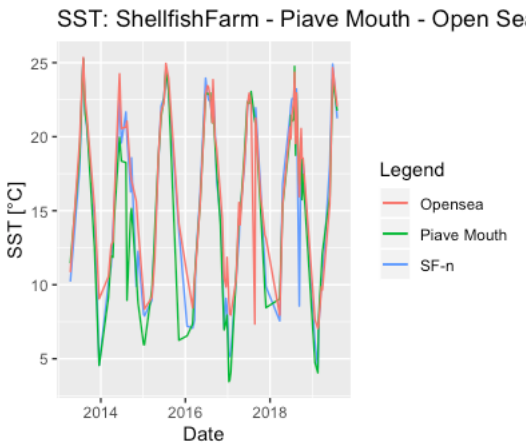
SST: ShellfishFarm - Piave Mouth - Open Se
SST [°C]
Date
Legend
Opensea
Piave Mouth
SF-n

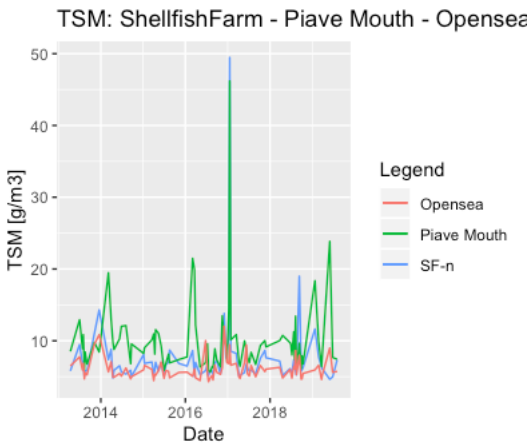
TSM: ShellfishFarm - Piave Mouth - Opensea
TSM [g/m3]
Date
Legend
Opensea
Piave Mouth
SF-n

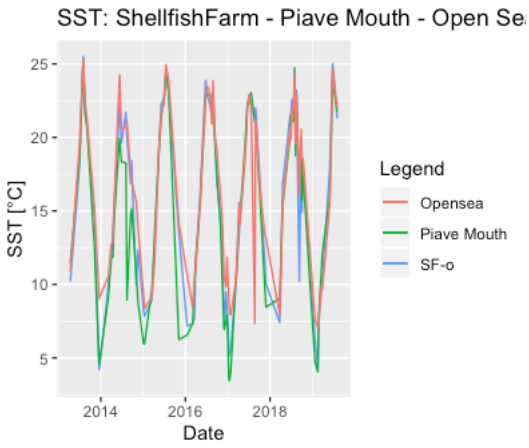
SST: ShellfishFarm - Piave Mouth - Open Se
SST [°C]
Date
Legend
Opensea
Piave Mouth
SF-o

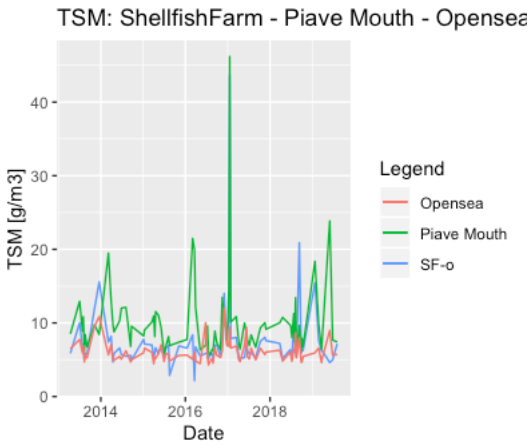
TSM: ShellfishFarm - Piave Mouth - Opensea
TSM [g/m3]
Date
Legend
Opensea
Piave Mouth
SF-o

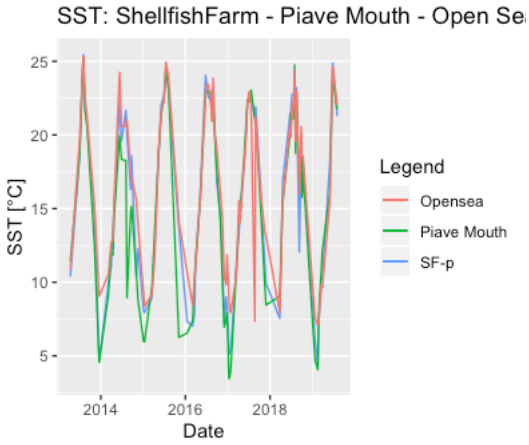
SST: ShellfishFarm - Piave Mouth - Open Se
SST [°C]
Date
Legend
Opensea
Piave Mouth
SF-p

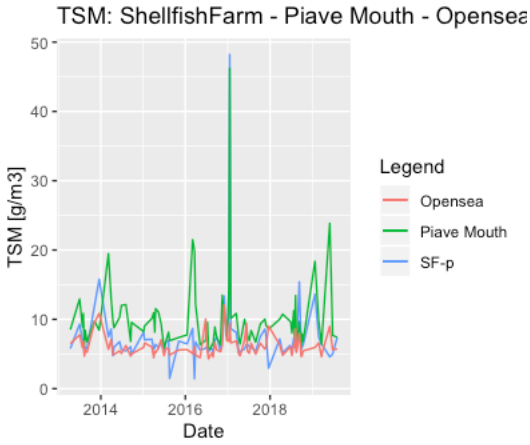
TSM: ShellfishFarm - Piave Mouth - Opensea
TSM [g/m3]
Date
Legend
Opensea
Piave Mouth
SF-p

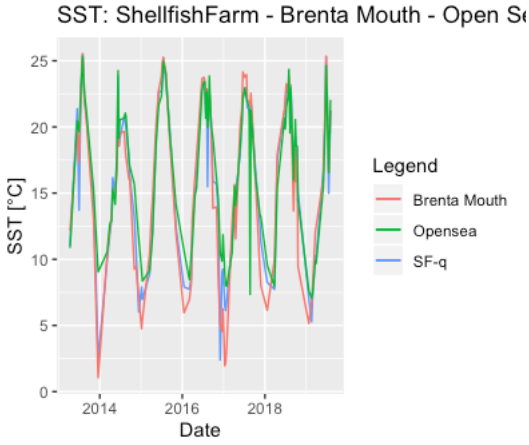
SST: ShellfishFarm - Brenta Mouth - Open Se
SST [°C]
Date
Legend
Brenta Mouth
Opensea
SF-q

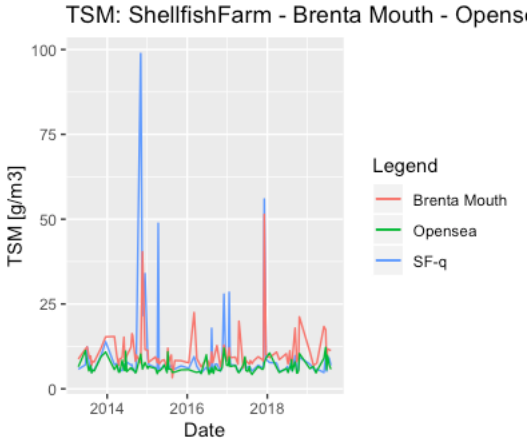
TSM: ShellfishFarm - Brenta Mouth - Opens
TSM [g/m3]
Date
Legend
Brenta Mouth
Opensea
SF-q

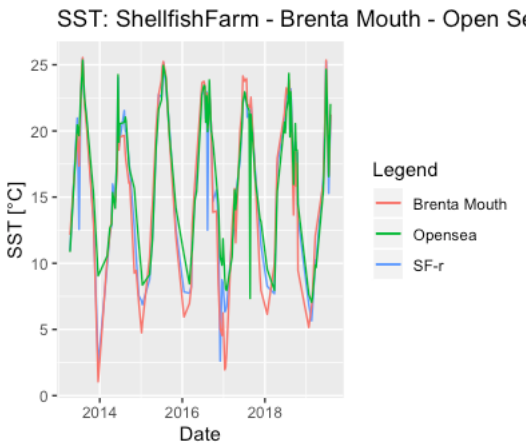
SST: ShellfishFarm - Brenta Mouth - Open Se
SST [°C]
Date
Legend
Brenta Mouth
Opensea
SF-r

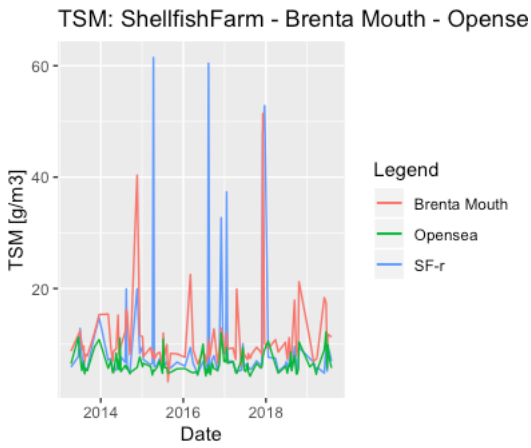
TSM: ShellfishFarm - Brenta Mouth - Opense
TSM [g/m3]
Date
Legend
Brenta Mouth
Opensea
SF-r

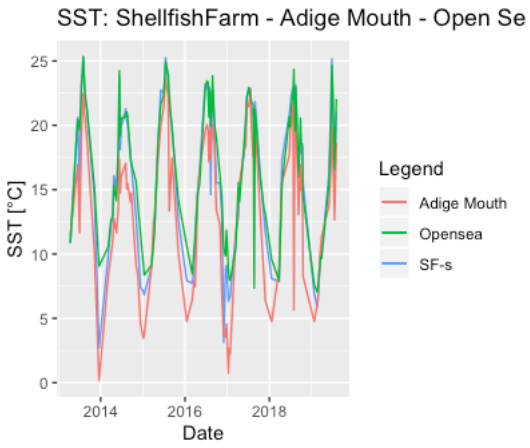
SST: ShellfishFarm - Adige Mouth - Open Se
SST [°C]
Date
Legend
Adige Mouth
Opensea
SF-s

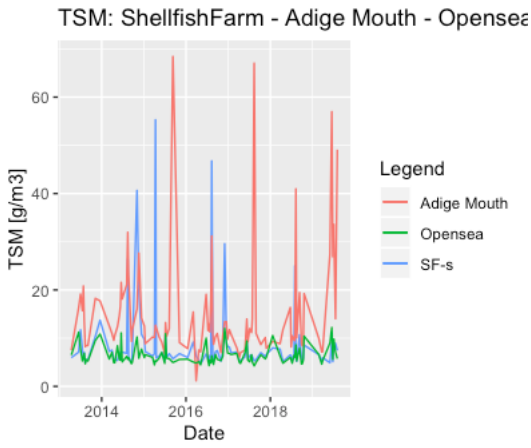
TSM: ShellfishFarm - Adige Mouth - Opensea
TSM [g/m3]
Date
Legend
Adige Mouth
Opensea
SF-s

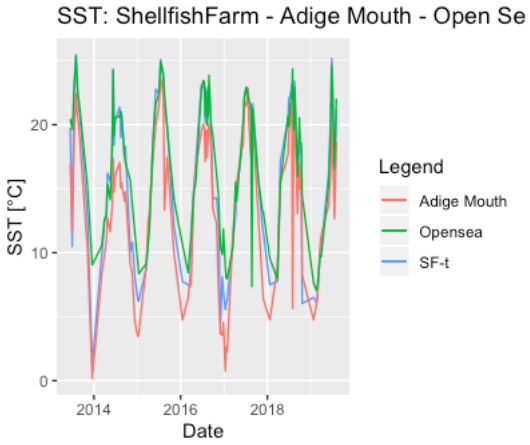
SST: ShellfishFarm - Adige Mouth - Open Se
SST [°C]
Date
Legend
Adige Mouth
Opensea
SF-t

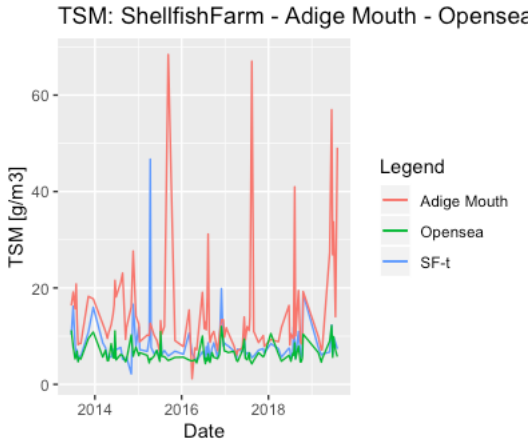
TSM: ShellfishFarm - Adige Mouth - Opensea
TSM [g/m3]
Date
Legend
Adige Mouth
Opensea
SF-t

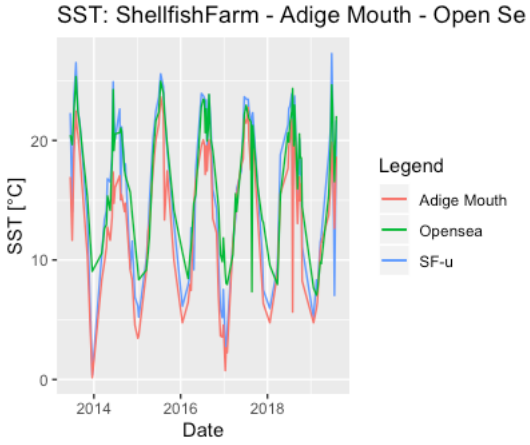
SST: ShellfishFarm - Adige Mouth - Open Se
SST [°C]
Date
Legend
Adige Mouth
Opensea
SF-u

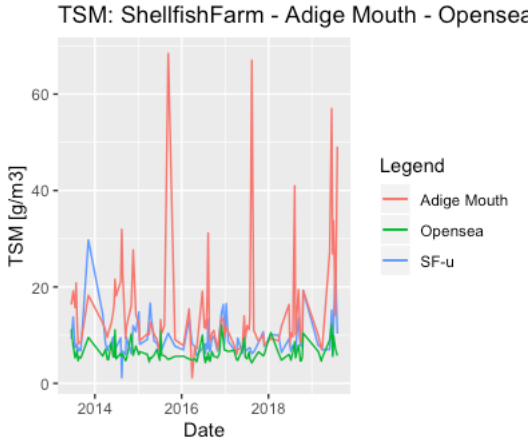
TSM: ShellfishFarm - Adige Mouth - Opensea
TSM [g/m3]
Date
Legend
Adige Mouth
Opensea
SF-u

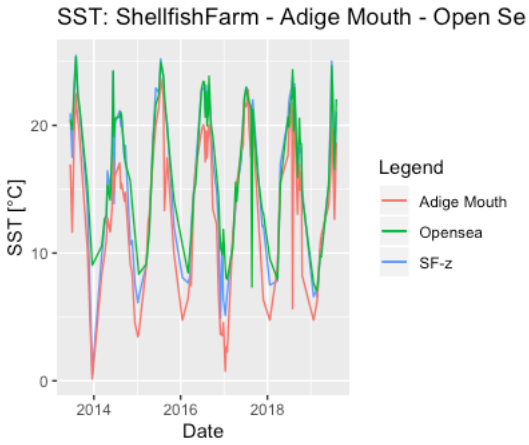
SST: ShellfishFarm - Adige Mouth - Open Se
SST [°C]
0
10
20
2014
2016
2018
Date
Legend
Adige Mouth
Opensea
SF-z

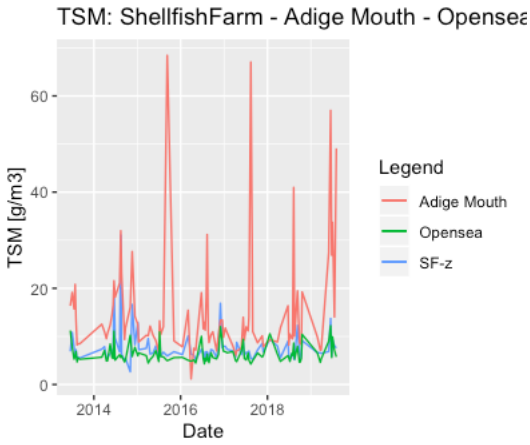
TSM: ShellfishFarm - Adige Mouth - Opensea
TSM [g/m3]
0
20
40
60
2014
2016
2018
Date
Legend
Adige Mouth
Opensea
SF-z

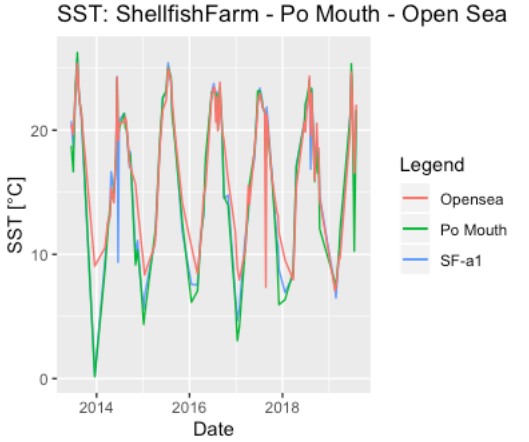
SST: ShellfishFarm - Po Mouth - Open Sea
SST [°C]
0
10
20
2014
2016
2018
Date
Legend
Opensea
Po Mouth
SF-a1

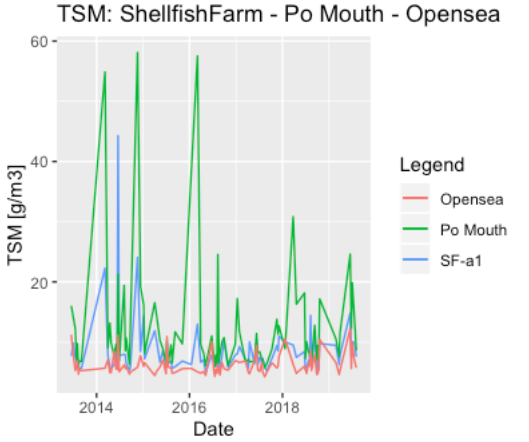
TSM: ShellfishFarm - Po Mouth - Opensea
TSM [g/m3]
20
40
60
2014
2016
2018
Date
Legend
Opensea
Po Mouth
SF-a1

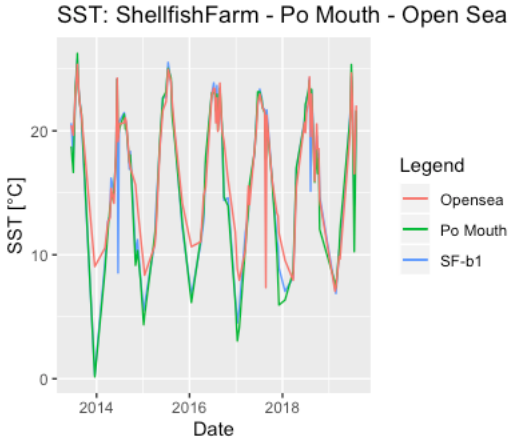
SST: ShellfishFarm - Po Mouth - Open Sea
SST [°C]
0
10
20
2014
2016
2018
Date
Legend
Opensea
Po Mouth
SF-b1

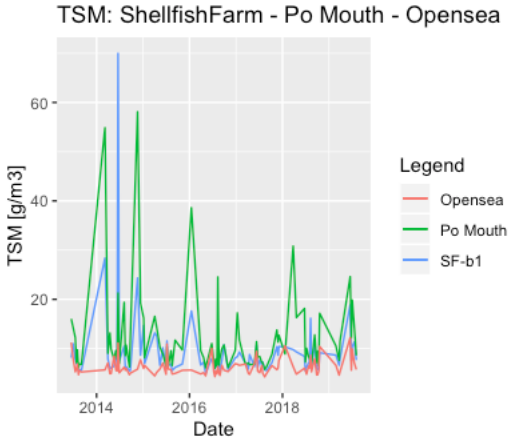
TSM: ShellfishFarm - Po Mouth - Opensea
TSM [g/m3]
20
40
60
2014
2016
2018
Date
Legend
Opensea
Po Mouth
SF-b1

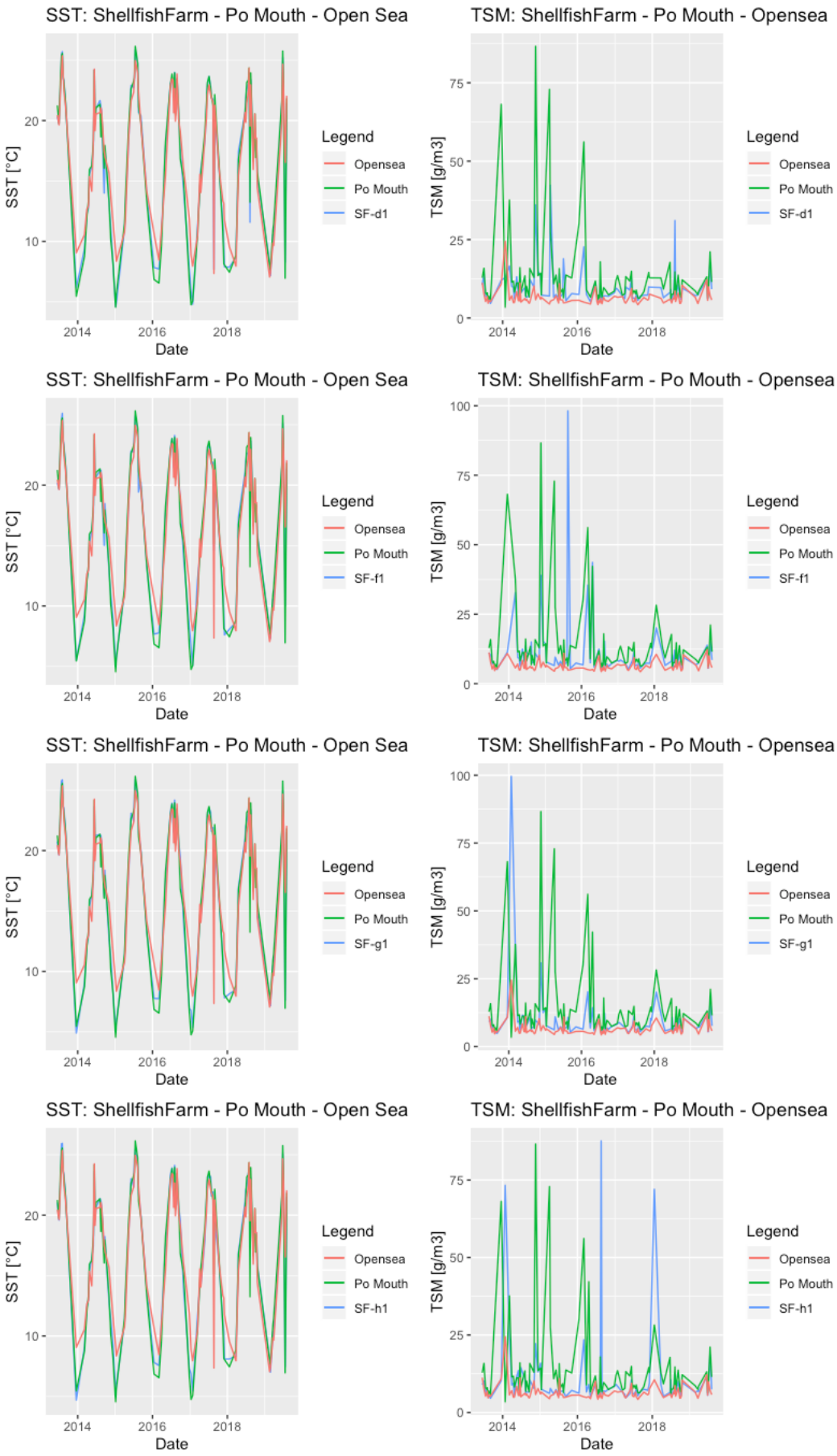
SST: ShellfishFarm - Po Mouth - Open Sea
SST [°C]
Date
Legend
Opensea
Po Mouth
SF-d1
TSM: ShellfishFarm - Po Mouth - Opensea
TSM [g/m3]
SST: ShellfishFarm - Po Mouth - Open Sea
SF-f1
TSM: ShellfishFarm - Po Mouth - Opensea
SST: ShellfishFarm - Po Mouth - Open Sea
SF-g1
TSM: ShellfishFarm - Po Mouth - Opensea
SST: ShellfishFarm - Po Mouth - Open Sea
SF-h1
TSM: ShellfishFarm - Po Mouth - Opensea

MULTIPLE LINEAR REGRESSION MODEL

		a1	a2	b	p-value	res. Error
a	coeff. Value	0.15057	0.03556	4.61215	0.1249	1.205 (10)
tsm over	signif [P(>|t|)	0.0677	0.9061	0.0222		
		a1	a2	b	p-value	res. Error
a	coeff. Value	0.7426	0.3663	-0.8932	3.53E-09	1.21 (13)
sst over	signif [P(>|t|)	6.85E-06	0.00364	0.44736		
		a1	a2	b	p-value	res. Error
a	coeff. Value	0.81717	0.62945	-3.9949	<2.2e-16	1.87 (39)
tsm under	signif [P(>|t|)	<2e-16	0.00057	0.0006		
		a1	a2	b	p-value	res. Error
a	coeff. Value	0.63187	0.42247	-1.188	<2.2e-16	0.6887 (39)
sst under	signif [P(>|t|)	2.90E-14	7.90E-08	0.0022		
		a1	a2	b	p-value	res. Error
b	coeff. Value	0.13025	0.06499	4.60049	0.1645	1.169 (10)
tsm over	signif [P(>|t|)	0.0978	0.8244	0.0195		
		a1	a2	b	p-value	res. Error
b	coeff. Value	0.6161	0.4933	-1.0497	1.26E-08	1.333 (13)
sst over	signif [P(>|t|)	0.000115	0.000822	0.418263		
		a1	a2	b	p-value	res. Error
b	coeff. Value	0.68686	0.41913	-1.1485	6.10E-11	3.131 (40)
tsm under	signif [P(>|t|)	1.83E-10	0.139	0.523		
		a1	a2	b	p-value	res. Error
b	coeff. Value	0.55834	0.48603	-1.0584	<2.2e-16	0.8453 (39)
sst under	signif [P(>|t|)	2.94E-10	2.95E-07	0.0224		
		a1	a2	b	p-value	res. Error
c	coeff. Value	0.09801	-0.10564	5.79049	0.6449	1.69 (10)
tsm over	signif [P(>|t|)	0.3644	0.8031	0.0361		
		a1	a2	b	p-value	res. Error
c	coeff. Value	0.36	0.7362	-1.2349	5.37E-07	1.814 (13)
sst over	signif [P(>|t|)	0.036501	0.000384	0.48278		
		a1	a2	b	p-value	res. Error
c	coeff. Value	0.55074	1.14496	-4.6741	4.87E-10	3.343 (40)
tsm under	signif [P(>|t|)	1.46E-07	0.0004	0.0184		
		a1	a2	b	p-value	res. Error
c	coeff. Value	0.46114	0.58852	-1.0427	<2.2e-16	1.074 (39)
sst under	signif [P(>|t|)	2.99E-06	7.41E-07	0.0726		
		a1	a2	b	p-value	res. Error

d	coeff. Value	0.0911	-0.06767	5.66902	0.6777	1.698 (10)
tsm over	signif [P(>|t|)	0.3998	0.8735	0.0401		
		a1	a2	b	p-value	res. Error
d	coeff. Value	0.3285	0.7609	-1.3063	4.33E-07	1.774 (13)
sst over	signif [P(>|t|)	0.048652	0.000237	0.448478		
		a1	a2	b	p-value	res. Error
d	coeff. Value	0.83077	0.82059	-5.577	1.79E-14	3.027 (40)
tsm under	signif [P(>|t|)	3.51E-13	0.00396	0.0024		
		a1	a2	b	p-value	res. Error
d	coeff. Value	0.46378	0.56581	-0.7806	<2.2e-16	1.082 (39)
sst under	signif [P(>|t|)	3.11E-06	1.77E-06	0.178		
		a1	a2	b	p-value	res. Error
e	coeff. Value	0.09899	-0.09191	5.68487	0.633	1.68 (10)
tsm over	signif [P(>|t|)	0.357	0.827	0.038		
		a1	a2	b	p-value	res. Error
e	coeff. Value	0.338	0.7515	-1.2342	4.71E-07	1.785 (13)
sst over	signif [P(>|t|)	0.04455	0.00028	0.47616		
		a1	a2	b	p-value	res. Error
e	coeff. Value	0.61285	0.93681	-4.0557	5.80E-16	2.098 (39)
tsm under	signif [P(>|t|)	2.33E-13	1.22E-05	0.0016		
		a1	a2	b	p-value	res. Error
e	coeff. Value	0.45372	0.57063	-0.7055	<2.2e-16	1.114 (39)
sst under	signif [P(>|t|)	7.32E-06	2.54E-06	0.236		
		a1	a2	b	p-value	res. Error
f	coeff. Value	0.0866	-0.04591	5.56361	0.6892	1.673 (10)
tsm over	signif [P(>|t|)	0.4161	0.9127	0.0408		
		a1	a2	b	p-value	res. Error
f	coeff. Value	0.3215	0.7568	-1.1282	4.66E-07	1.768 (13)
sst over	signif [P(>|t|)					
		a1	a2	b	p-value	res. Error
f	coeff. Value	0.53151	0.99661	-3.9075	3.38E-16	1.89 (39)
tsm under	signif [P(>|t|)	7.04E-13	6.83E-07	0.0008		
		a1	a2	b	p-value	res. Error
f	coeff. Value	0.594	0.3376	0.654	4.20E-14	3.15 (39)
sst under	signif [P(>|t|)	0.0216	0.2567	0.6954		
		a1	a2	b	p-value	res. Error
g	coeff. Value	0.07899	0.0154	5.29017	0.7132	1.71 (10)
tsm over	signif [P(>|t|)	0.4664	0.9713	0.0538		
		a1	a2	b	p-value	res. Error
g	coeff. Value	0.3091	0.7685	-1.2053	4.63E-07	1.767 (13)

sst over	signif [P(>|t|)	0.06066	0.00021	0.48205		
		a1	a2	b	p-value	res. Error
g	coeff. Value	0.6504	0.4998	-0.9396	0.000582	6.74 (40)
tsm under	signif [P(>|t|)	0.000599	0.40786	0.8076		
		a1	a2	b	p-value	res. Error
g	coeff. Value	0.5064	0.5011	-0.4192	<2.2e-16	1.453 (39)
sst under	signif [P(>|t|)	7.56E-05	0.00065	0.5866		

		a1	a2	b	p-value	res. Error
l	coeff. Value	0.094341	-0.003082	5.210897	0.6147	1.651 (10)
tsm over	signif [P(>|t|)	0.371	0.994	0.05		
		a1	a2	b	p-value	res. Error
l	coeff. Value	0.2959	0.7705	-0.9485	4.56E-07	1.749 (13)
sst over	signif [P(>|t|)	0.068371	0.000187	0.574706		
		a1	a2	b	p-value	res. Error
l	coeff. Value	0.40906	1.27035	-4.4249	1.29E-10	2.662 (38)
tsm under	signif [P(>|t|)	1.40E-06	4.93E-06	0.0065		
		a1	a2	b	p-value	res. Error
l	coeff. Value	0.36973	0.67537	-0.9328	<2.2e-16	1.069 (38)
sst under	signif [P(>|t|)	1.00E-04	6.94E-08	0.111		

		a1	a2	b	p-value	res. Error
m	coeff. Value	0.05416	0.13079	4.89019	0.7599	1.73 (10)
tsm over	signif [P(>|t|)	0.619	0.7631	0.0739		
		a1	a2	b	p-value	res. Error
m	coeff. Value	0.2904	0.773	-1.0019	4.36E-07	1.738 (13)
sst over	signif [P(>|t|)	0.071449	0.000171	0.551178		
		a1	a2	b	p-value	res. Error
m	coeff. Value	0.68761	0.99124	-5.4882	1.09E-13	2.78 (39)
tsm under	signif [P(>|t|)	9.41E-12	0.00028	0.0015		
		a1	a2	b	p-value	res. Error
m	coeff. Value	0.6407	0.2765	0.9016	6.08E-13	3.424 (39)
sst under	signif [P(>|t|)	0.0226	0.391	0.6197		

		a1	a2	b	p-value	res. Error
n	coeff. Value	0.06026	0.1017	5.05103	0.7508	1.707 (10)
tsm over	signif [P(>|t|)	0.5756	0.812	0.0631		
		a1	a2	b	p-value	res. Error
n	coeff. Value	0.2809	0.7898	-1.2213	5.07E-07	1.775 (13)
sst over	signif [P(>|t|)	0.085834	0.000171	0.478182		
		a1	a2	b	p-value	res. Error
n	coeff. Value	0.8967	0.816	-6.067	3.21E-16	2.858 (40)
tsm under	signif [P(>|t|)	5.74E-15	0.00254	0.0006		

		a1	a2	b	p-value	res. Error
n	coeff. Value	0.42617	0.62238	-1.0316	<2.2e-16	1.097 (38)
sst under	signif [P(>|t|)	1.93E-05	5.92E-07	0.0864		

		a1	a2	b	p-value	res. Error
o	coeff. Value	0.04945	0.1494	4.88722	0.7599	1.713 (10)
tsm over	signif [P(>|t|)	0.6463	0.7283	0.0717		

		a1	a2	b	p-value	res. Error
o	coeff. Value	0.2783	0.7857	-1.0835	3.93E-07	1.726 (13)
sst over	signif [P(>|t|)	0.080691	0.000139	0.516833		

		a1	a2	b	p-value	res. Error
o	coeff. Value	0.74079	0.99665	-5.9978	1.40E-14	2.818 (40)
tsm under	signif [P(>|t|)	1.24E-12	0.00027	0.0006		

		a1	a2	b	p-value	res. Error
o	coeff. Value	0.4132	0.63817	-1.0602	<2.2e-16	1.092 (38)
sst under	signif [P(>|t|)	2.86E-05	3.35E-07	0.0771		

		a1	a2	b	p-value	res. Error
p	coeff. Value	0.0636	0.05051	5.32903	0.7676	1.672 (10)
tsm over	signif [P(>|t|)	0.547	0.9039	0.0482		

		a1	a2	b	p-value	res. Error
p	coeff. Value	0.2835	0.7916	-1.2487	2.03E-07	1.648 (13)
sst over	signif [P(>|t|)	0.0644	8.41E-05	0.4357		

		a1	a2	b	p-value	res. Error
p	coeff. Value	0.84246	0.96053	-6.6683	3.57E-14	3.205 (40)
tsm under	signif [P(>|t|)	1.24E-12	0.00162	0.0007		

		a1	a2	b	p-value	res. Error
p	coeff. Value	0.42807	0.61922	-0.9638	<2.2e-16	1.07 (38)
sst under	signif [P(>|t|)	1.22E-05	4.03E-07	0.0999		

		a1	a2	b	p-value	res. Error
q	coeff. Value	-0.04118	2.70394	-5.56042	0.3088	18.95 (22)
tsm over	signif [P(>|t|)	0.941	0.13	0.704		

		a1	a2	b	p-value	res. Error
q	coeff. Value	0.625	0.4002	-0.578	1.35E-10	1.692 (22)
sst over	signif [P(>|t|)	0.0012	0.0386	0.6935		

		a1	a2	b	p-value	res. Error
q	coeff. Value	0.9305	0.4902	-3.8107	3.32E-11	5.922 (78)
tsm under	signif [P(>|t|)	2.98E-10	0.208	0.124		

		a1	a2	b	p-value	res. Error
q	coeff. Value	0.56758	0.40062	0.5488	<2.2e-16	1.325 (77)
sst under	signif [P(>|t|)	<2e-16	6.81E-09	0.258		

		a1	a2	b	p-value	res. Error
r	coeff. Value	0.3061	-0.2272	7.7373	0.6741	11.77 (21)
tsm over	signif [P(>|t|)	0.389	0.842	0.402		
		a1	a2	b	p-value	res. Error
r	coeff. Value	0.547957	0.431262	-0.002052	2.87E-08	2.151 (22)
sst over	signif [P(>|t|)	0.0178	0.0756	0.9991		
		a1	a2	b	p-value	res. Error
r	coeff. Value	0.7195	1.3061	-6.0534	6.12E-06	8.753 (78)
tsm under	signif [P(>|t|)	3.08E-04	0.02489	0.0991		
		a1	a2	b	p-value	res. Error
r	coeff. Value	0.58848	0.38145	0.4294	<2.2e-16	1.291 (77)
sst under	signif [P(>|t|)	<2e-16	1.29E-08	0.363		

		a1	a2	b	p-value	res. Error
t	coeff. Value	0.04493	0.3597	4.25742	0.1307	2.95 (28)
tsm over	signif [P(>|t|)	0.3046	0.1396	0.0219		
		a1	a2	b	p-value	res. Error
t	coeff. Value	0.9678	0.2064	-0.1531	<2.2e-16	1.333 (29)
sst over	signif [P(>|t|)	9.36E-08	0.147	0.898		
		a1	a2	b	p-value	res. Error
t	coeff. Value	0.02811	1.0607	1.3213	1.92E-02	5.261 (65)
tsm under	signif [P(>|t|)	7.14E-01	0.00751	0.5957		
		a1	a2	b	p-value	res. Error
t	coeff. Value	0.50345	0.57415	-0.6405	<2.2e-16	1.722 (70)
sst under	signif [P(>|t|)	2.60E-13	5.59E-13	0.302		

		a1	a2	b	p-value	res. Error
u	coeff. Value	-0.002255	0.790635	3.750551	0.1008	4.556 (29)
tsm over	signif [P(>|t|)	0.973	0.037	0.175		
		a1	a2	b	p-value	res. Error
u	coeff. Value	1.12334	0.07799	0.70883	1.90E-15	1.626 (29)
sst over	signif [P(>|t|)	2.32E-07	0.648	0.627		
		a1	a2	b	p-value	res. Error
u	coeff. Value	0.05317	0.84485	3.5043	1.22E-03	3.167 (63)
tsm under	signif [P(>|t|)	2.53E-01	0.001	0.0285		
		a1	a2	b	p-value	res. Error
u	coeff. Value	0.74651	0.38911	-0.8627	<2.2e-16	1.793 (70)
sst under	signif [P(>|t|)	<2e-16	2.23E-07	0.183		

		a1	a2	b	p-value	res. Error
z	coeff. Value	0.10833	0.31699	4.03112	0.2255	5.345 (28)
tsm over	signif [P(>|t|)	0.169	0.472	0.216		
		a1	a2	b	p-value	res. Error

z	coeff. Value	0.6336	0.5304	-1.1671	<2.2e-16	1.17 (29)
sst over	signif [P(>|t|)	1.24E-05	0.000147	0.270379		
		a1	a2	b	p-value	res. Error
z	coeff. Value	-0.0094	0.75692	2.6167	4.30E-07	1.608 (63)
tsm under	signif [P(>|t|)	0.68904	7.76E-08	0.0016		
		a1	a2	b	p-value	res. Error
z	coeff. Value	0.4194	0.6587	-0.5452	<2.2e-16	1.617 (70)
sst under	signif [P(>|t|)	1.92E-11	<2e-16	0.349		
		a1	a2	b	p-value	res. Error
f1	coeff. Value	0.29449	0.52098	4.4932	2.19E-02	8.492 (13)
tsm over	signif [P(>|t|)	0.00764	0.61028	0.59917		
		a1	a2	b	p-value	res. Error
f1	coeff. Value	0.67818	0.33514	-0.06134	7.86E-13	0.6861 (13)
sst over	signif [P(>|t|)	1.56E-05	0.0128	0.9205		
		a1	a2	b	p-value	res. Error
f1	coeff. Value	0.2507	-0.4704	9.8531	3.37E-01	11.79 (67)
tsm under	signif [P(>|t|)	1.45E-01	0.6229	0.0737		
		a1	a2	b	p-value	res. Error
f1	coeff. Value	0.80863	0.18518	0.0958	<2.2e-16	0.6581 (68)
sst under	signif [P(>|t|)	<2e-16	5.05E-05	0.732		
		a1	a2	b	p-value	res. Error
h1	coeff. Value	0.23197	3.10689	-15.11199	6.57E-05	8.739 (14)
tsm over	signif [P(>|t|)	0.0264	1.57E-05	0.0152		
		a1	a2	b	p-value	res. Error
h1	coeff. Value	0.63261	0.41425	-0.49395	7.38E-15	0.4885 (13)
sst over	signif [P(>|t|)	8.49E-07	0.000242	0.270595		
		a1	a2	b	p-value	res. Error
h1	coeff. Value	0.09345	1.42675	-0.1069	1.59E-01	12.29 (67)
tsm under	signif [P(>|t|)	5.99E-01	0.155	0.985		
		a1	a2	b	p-value	res. Error
h1	coeff. Value	0.954691	0.00386	0.7628	<2.2e-16	0.9542 (68)
sst under	signif [P(>|t|)	<2e-16	9.51E-01	0.0632		
		a1	a2	b	p-value	res. Error
l1	coeff. Value	-0.05796	0.87748	2.68932	0.6256	3.656 (10)
tsm over	signif [P(>|t|)	0.8	0.349	0.615		
		a1	a2	b	p-value	res. Error
l1	coeff. Value	0.3297	0.6088	0.9996	2.72E-07	1.462 (13)

sst over	signif [P(>|t|)	0.020104	0.000308	0.481042		
		a1	a2	b	p-value	res. Error
l1	coeff. Value	0.30911	0.43946	1.3221	5.44E-10	1.707 (40)
tsm under	signif [P(>|t|)	1.91E-08	0.00596	0.1807		
		a1	a2	b	p-value	res. Error
l1	coeff. Value	0.47624	0.53726	-0.4218	<2.2e-16	1.005 (39)
sst under	signif [P(>|t|)	4.96E-07	1.18E-06	0.43		
		a1	a2	b	p-value	res. Error
m1	coeff. Value	0.1316	0.278	3.7533	0.4383	2.263 (10)
tsm over	signif [P(>|t|)	0.363	0.626	0.269		
		a1	a2	b	p-value	res. Error
m1	coeff. Value	0.63953	0.40676	-0.22439	2.79E-10	0.9267 (13)
sst over	signif [P(>|t|)	1.94E-06	0.000193	0.801216		
		a1	a2	b	p-value	res. Error
m1	coeff. Value	0.8892	0.2769	-2.2123	2.95E-08	4.992 (40)
tsm under	signif [P(>|t|)	2.76E-08	0.535	0.44		
		a1	a2	b	p-value	res. Error
m1	coeff. Value	0.39223	0.67334	-1.6711	<2.2e-16	0.9295 (39)
sst under	signif [P(>|t|)	4.06E-06	1.86E-09	0.0015		

NORMALIZED DIFFERENCES SCATTER PLOTS

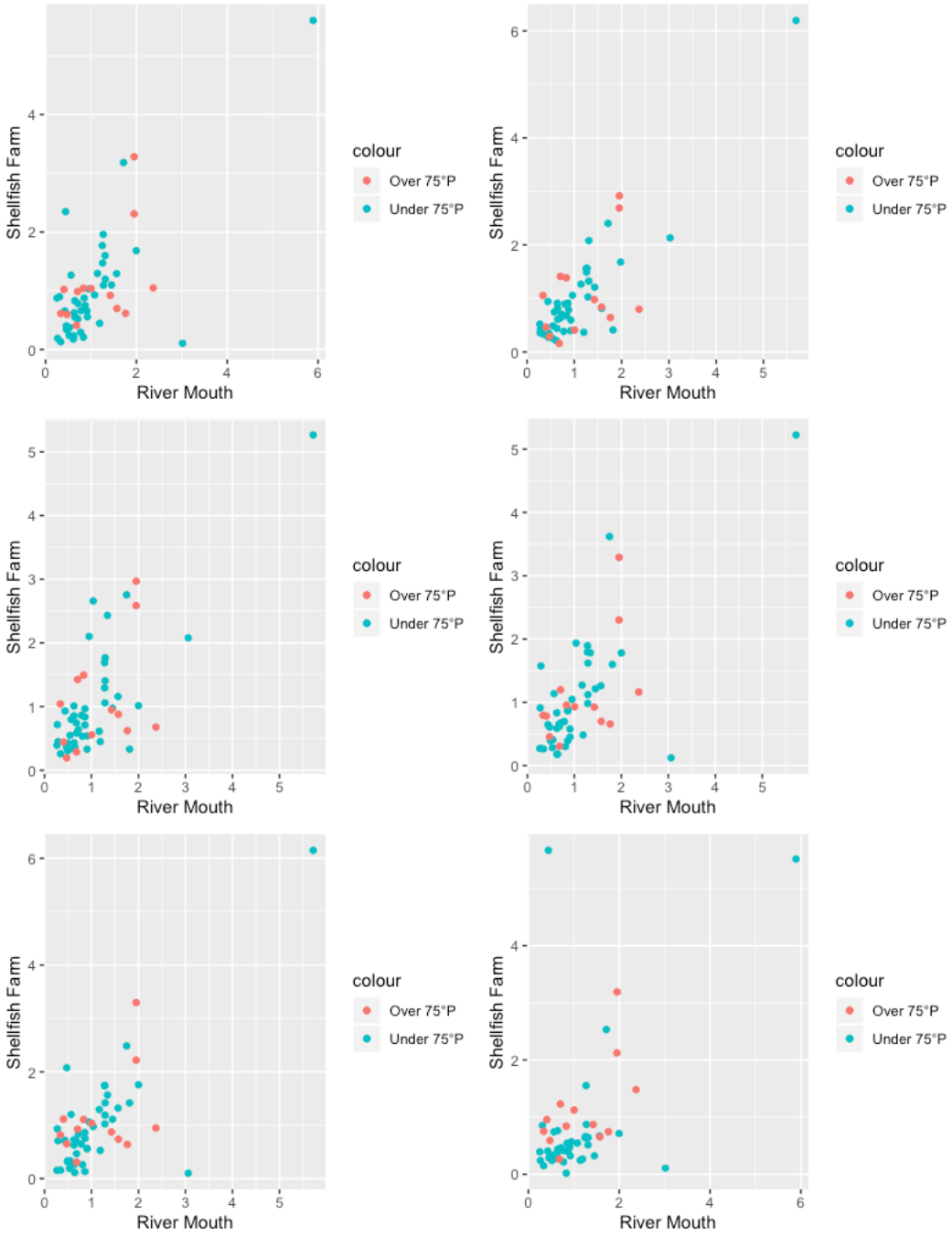

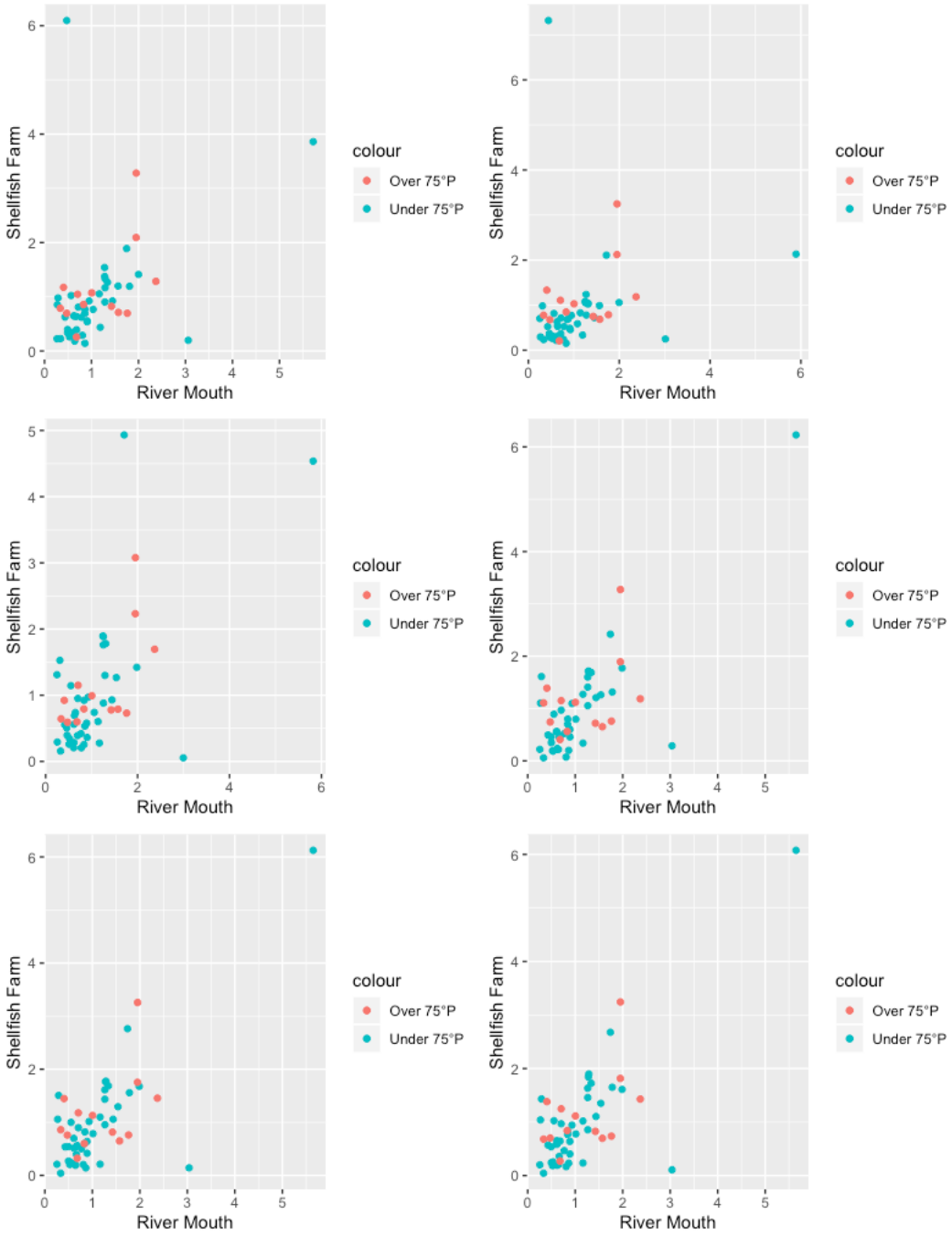
Shellfish Farm
River Mouth
colour
Over 75°P
Under 75°P

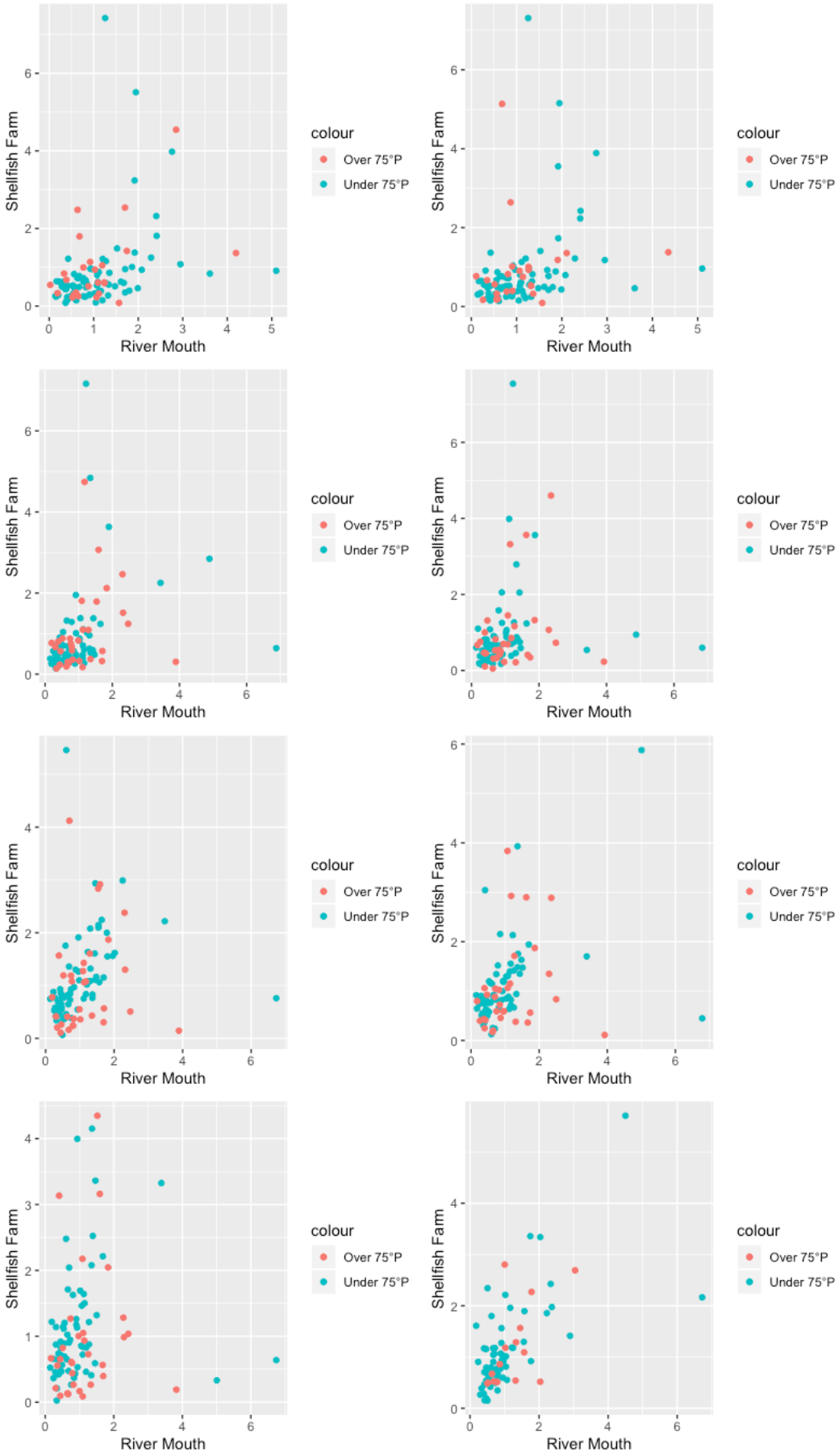
Shellfish Farm
River Mouth
colour
Over 75°P
Under 75°P

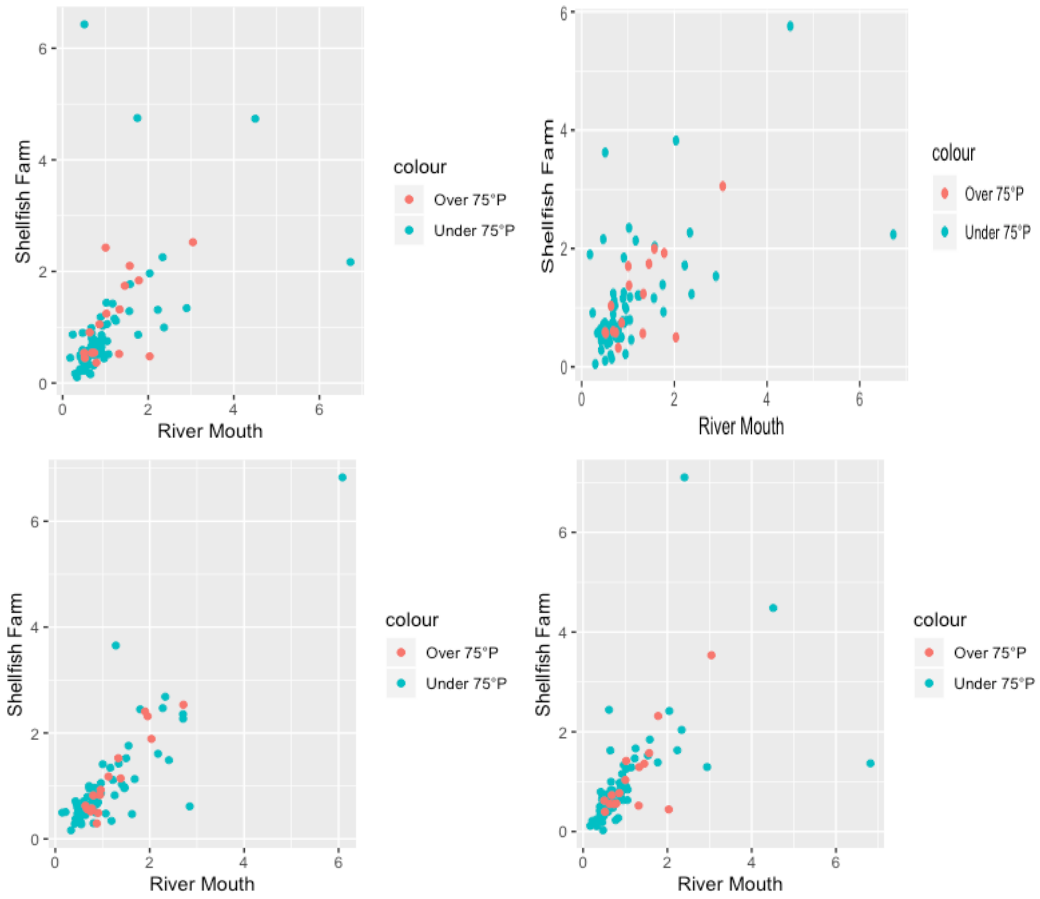

COMPLETE LIST OF EVENTS OF PROBABLE CONTAMINATION

13/04/2013	16/09/2014
16/06/2013	03/11/2014
02/07/2013	19/11/2014
18/07/2013	12/12/2014
07/11/2013	03/04/2015
26/01/2014	14/05/2015
08/03/2014	04/03/2016
31/03/2014	24/06/2016
16/04/2014	10/07/2016
25/04/2014	19/07/2016
18/05/2014	04/08/2016
03/06/2014	11/08/2016
12/06/2014	22/07/2017
19/06/2014	14/08/2017
28/06/2014	26/03/2018
06/08/2014	20/04/2018
15/08/2014	01/06/2019
22/08/2014	17/06/2019